Abel Alvarez Bustos

Systems of balance laws in fluid dynamics problems: mathematical modeling and numerical approximation

Sistemas de leis de balanço em problemas de dinâmica de fluidos: modelagem matemática e aproximação numérica

CAMPINAS
2015

Universidade Estadual de Campinas

Instituto de Matemática, Estatística
e Computação Científica

Abel Alvarez Bustos

Systems of balance laws in fluid dynamics problems: mathematical modeling and numerical approximation

Sistemas de leis de balanço em problemas de dinâmica de fluidos: modelagem matemática e aproximação numérica

Thesis presented to the Institute of Mathematics, Statistics and Scientific Computing of the University of Campinas in partial fulfillment of the requirements for the degree of Doctor in applied mathematics.

Tese apresentada ao Instituto de Matemática, Estatística e Computação Científica da Universidade Estadual de Campinas como parte dos requisitos exigidos para a obtenção do título de Doutor em matemática aplicada.

Orientador: Eduardo Cardoso de Abreu

Este exemplar corresponde à versão final da tese defendida pelo aluno Abel Alvarez Bustos, e orientada pelo Prof. Dr. Eduardo Cardoso de Abreu.

Assinatura do Orientador

Campinas
2015

Agência de fomento: FAPESP
Nº processo: 2011/23628-0

Ficha catalográfica
Universidade Estadual de Campinas
Biblioteca do Instituto de Matemática, Estatística e Computação Científica
Maria Fabiana Bezerra Muller - CRB 8/6162

AL86s

Alvarez Bustos, Abel, 1980-
Systems of balance laws in fluid dynamics problems : mathematical modeling and numerical approximation / Abel Alvarez Bustos. – Campinas, SP : [s.n.], 2015.

Orientador: Eduardo Cardoso de Abreu.
Tese (doutorado) – Universidade Estadual de Campinas, Instituto de Matemática, Estatística e Computação Científica.

1. Equações diferenciais hiperbólicas. 2. Euler, Equações de. 3. Método dos volumes finitos. 4. Expansões assintóticas. 5. Onda viajante. I. Abreu, Eduardo Cardoso de,1974-. II. Universidade Estadual de Campinas. Instituto de Matemática, Estatística e Computação Científica. III. Título.

Informações para Biblioteca Digital

Título em outro idioma: Sistema de leis de balanço em problemas de dinâmicas de fluidos : modelagem matemática e aproximação numérica
Palavras-chave em inglês:
Hyperbolic differential equations
Euler equations
Finite volume method
Asymptotic expansions
Traveling wave
Área de concentração: Matemática Aplicada
Titulação: Doutor em Matemática Aplicada
Banca examinadora:
Eduardo Cardoso de Abreu [Orientador]
Frederico da Cunha Furtado
Grigori Chapiro
Aparecido Jesuino de Souza
Maria Cristina de Castro Cunha
Data de defesa: 23-07-2015
Programa de Pós-Graduação: Matemática Aplicada

Tese de Doutorado defendida em 23 de julho de 2015 e aprovada

Pela Banca Examinadora composta pelos Profs. Drs.

Eduardo Cardoso de Abreu

Prof(a). Dr(a). EDUARDO CARDOSO DE ABREU

Prof(a). Dr(a). MARIA CRISTINA DE CASTRO CUNHA

Aparecido Jesuino de Souza

Prof(a). Dr(a). APARECIDO JESUINO DE SOUZA

Frederico Furtado

Prof(a). Dr(a). FREDERICO DA CUNHA FURTADO

Prof(a). Dr(a). GRIGORI CHAPIRO

My parents.
Ana and Abel for giving me life
My sister Diana
my support in the more difficult moments

Acknowledgments

Foremost, I want to thank God.

I would like to express my sincere gratitude to my advisor Prof. Dr. Eduardo Abreu for the continuous support of my Ph.D study and research, for your patience, motivation, enthusiasm, and immense knowledge and good advice
I would like to thank, Prof. Dr. Wanderson Lambert, for your invaluable advice and guidance during my scientific investigation, who with your long conversations and dedication performed large contributions in my work.

I would like to thank three important groups of people, without whom this these would not have been possible: first I thank my fellow reaches group, Paola, Arthur, Juan, John, Ciro, Felipe and Jardel by many interesting conversations and their encouragement, insightful comments, and hard questions.

I also want to thank that Colombian community of the UNICAMP, in special my dear friends Margui, Miller, Patty, Adrian and Yovany by continuous moral support.
I would like to thank my family: my parents Ana and Abel, for giving birth to me at the first place and supporting me spiritually throughout my life. My sister Diana that in all times was aware and support me in the difficult moments. My brother Carlos and Harold that always present.
I would like to thanks in special Paola, Arthur and Ciro that help me with my English.

I thanks The UNICAMP-IMECC and all your functionaries by support in my reaches.

Last but not the least, I would like to thank the funding agencies CAPES (in the very beginning, first 6 months) and FAPESP grant for the remaining 42 months of financial support: graduate fellowship through grant $2011/23628-0$; I also thank for financial support: the FAPESP $2014/03204-9$ and CNPq $445758/2014-7$.

Resumo

Nesta tese, estamos preocupados com o comportamento limite de sistemas hiperbólicos de leis de conservação com termos de relaxamento *stiff* para os sistemas locais de leis de conservação, com particular interesse na questão da estabilidade e limites singulares dessas soluções no tempo zero de relaxão. O relaxamento é importante em muitas situações físicas, tais como, em teoria cinética, dinâmica de gases fora do equilíbrio termodinâmico local, em elasticidade com memória (histerese), transição de fase em fluxo multifásico e problemas lineares e não lineares de progação de ondas. Embora a teoria matemática para modelos não lineares de leis equilíbrio com relaxamento tem apresentado algum significativo progresso na boa colocação no contexto de modelos em termodinâmica e teoria cinética, uma compreensão completa sobre o comportamento assintótico para sistemas maiores que 2×2, sobre os quais soluções evoluem a partir de um determinado dado inicial com regularidade, permanece indefinida, notadamente para soluções fracas de sistemas hiperbólicos. Assim, devido à complexidade inerente a esta classe de modelos, existem poucas soluções para tais leis de equilíbrio de relaxamento por meio de métodos analíticos. Então, uma análise abstrata, bem como a computação numérica prática por meio de algoritmos de aproximação, constituem ferramentas importantes para estudar tal classe de modelos, bem como para obter novas perspectivas para ampliar o conhecimento geral de sistemas de leis de balanço, ou de leis de equilíbrio. Portanto, foi também desenvolvido um novo método de volumes finitos de tipo *unsplitting*, localmente conservativo, via construção formal. Este método foi capaz de computar para sistemas de Euler tanto novas soluções não monótonas como também de reproduzir soluções qualitativamente corretas em regime de fricção alta e gravidade, recentemente publicados na literatura. De fato, os novos algoritmos de aproximação *unsplitting* também foram usados para ajudar a compreender um problema de injeção de nitrogênio e de vapor em meios poroso. Outro ponto de vista fundamental perseguido nesta tese é a comparação entre duas metodologias para abordar a questão da resolução de leis equilíbrio com termos fonte de relaxamento: uma metodologia baseia-se do pressuposto que o fenômeno físico está sob equilíbrio termodinâmico (equilíbrio instantâneo), que é modelado por sistemas de leis de conservação hiperbólicas, e a outra metodologia é baseada no relaxamento de tal equilíbrio, que por sua vez dá origem à utilização dos sistemas de leis de equilíbrio na modelagem do processo de relaxamento, como por exemplo, em modelos de transição de fase. Neste momento, uma série de perguntas naturais surgem: quão diferentes são essas soluções de ambas as soluções obtidas por meio destas duas abordagens? A este respeito, uma pergunta mais rigorosa - e mais fundamental - é: como é o comportamento de tais soluções durante o processo de relaxamento e qual é o seu limite? A fim de entender melhor essas metodologias, vamos considerar dois formalismos matemáticos distintos. Nesta tese, nós damos um exemplo de modelagem utilizando esta nova metodologia para a injeção de nitrogênio e de vapor de água em meios porosos. Nós não fomos capazes de dar uma resposta assertiva a todas as perguntas acima, mas um sólido ponto de partida é um estudo aprofundado do caso unidimensional para um problema concreto, que é feito nesta tese. Acreditamos que temos um campo muito interessante (e promissor) de trabalho pela frente, que temos a intenção de continuar a estudar, a fim de entender melhor, via análises abstrata e numérica, tais perguntas importantes e que permanecem indefinidas. Esta tese é uma pequena tentativa de obter uma nova compreensão sobre tais modelos de leis de balanço.

Palavras-chave: Leis de balanço, onda viajante, Equações de Euler, expansão assintótica, Método de volume finito, problemas de Riemann, injeção de vapor e nitrogênio em meios porosos.

Abstract

In this thesis, we are concerned with the limit behaviour of hyperbolic systems of conservation laws with stiff relaxation terms to the local systems of conservation laws, particularly the question of stability and singular limits of such solutions to the zero relaxation time. Relaxation is important in many physical situations, as such, in kinetic theory, gases not in local thermodynamic equilibrium, elasticity with memory (hysteresis), multiphase and phase transition and linear and nonlinear waves. Although the mathematical theory of nonlinear balance law with relaxation has presented significant progress on well-posedness linked to extended thermodynamics and kinetic theory, a complete understanding for systems larger than 2×2 about how solutions evolve from a given initial data and their regularity and asymptotic behaviour remains elusive, mainly for weak solutions of hyperbolic systems. Thus, due to the complexity inherent to this class of models, there are few solutions for such relaxation balance laws by means of analytical methods. Then, abstract analysis as well as practical computing via approximation algorithms are both significant mathematical tools to tackle as well as to get further insights to enlarge the knowledge for systems of balance laws. Therefore, it was also developed a new unsplitting finite volume methods, which in turn is locally conservative by formal construction. This method was able to corroborate the new solutions for Euler systems with a non-monotonic character as well as to reproduce correct qualitatively solutions of the Euler models with high friction regime and gravity, recently published in the literature. Indeed, the novel unsplitting approximation algorithms were also used to address injection problems of nitrogen and steam in porous media. Another crucial viewpoint pursued in this thesis is the comparison between two methodologies to tackle the issue of solving balance laws with relaxation source terms: one methodology is based by assuming that the physical phenomenon is under thermodynamic equilibrium (instantaneous equilibrium), which is modelled by systems of conservation laws, and the other methodology is based in the relaxation of such equilibrium, which in turn gives rise to the use of systems of balance laws in the modelling of the relaxation process, for instance, in the modelling of phase transition. At this moment a natural questions is: how different are these both solutions obtained by means of two approaches? In this regard, a more stringent – and more fundamental – question is: how is the behaviour of such solutions during the relaxation process and how is its limit? In order to better understand these methodologies we will consider two distinct mathematical formalisms. In thesis, we give an example of modelling using this novel methodology for the injection of nitrogen and steam in porous media. We were not able to give assertive answers to the above questions, but a solid starting point is a thorough study of the one-dimensional case for a concrete problem, which is done in this thesis. We believe we have a very interesting (and promising) field of work ahead of us, which we intend to continue studying in order to better understand abstract and numerical analysis for these important questions that remains elusive. This thesis is a small attempt to get new insights in this direction.

Keywords: Balance Laws, travelling wave, Euler equations, asymptotic expansion, central finite volume, Riemann problem, Nitrogen and steam injection in porous media.

Contents

1 An unsplitting finite volume method for models with stiff relaxation source terms 11

1.1 Balance law shock-fitting numerical algorithms . . . 12
1.1.1 Hyperbolic system with relaxation . . . 13
1.1.2 The design of an unspliting method for balance laws . . . 13
1.2 Numerical experiments . . . 19
1.2.1 Euler equations with gravity and friction . . . 19
1.2.2 Shallow water flow down in an inclined open channel model . . . 22
1.2.3 A Cauchy problem for the inviscid Burgers equation with source term for multiple equilibria . . . 23
1.2.4 Steady-state equilibrium solutions linked with shallow water equations . 23

2 An analysis of the existence of a non-monotonic travelling wave for Euler equations with relaxation 31

2.1 Thermal relaxation Euler equation as a model problem . . . 31
2.1.1 A local approximate analytic solution for the isothermal Euler system . . 32
2.2 Outer expansion analysis for the solution . . . 35
2.2.1 Asymptotic analysis around constant states, shock and rarefactions . . . 36
2.3 Conditions for the existence of travelling wave solutions . . . 39
2.4 Numerical experiments linked to the order expansion approach for a Euler system model . . . 43

3 A physical, mathematical and computational modelling for a nitrogen and steam injection in porous media 50

3.1 Injection of nitrogen and steam in porous media . . . 50
3.2 Physical models and equations of state for steam and nitrogen injetion problems in porous media . . . 51
3.2.1 Thermodynamical equilibrium and physical situations . . . 54
3.3 Hyperbolic system . . . 60
3.3.1 Characteristic speeds of system (3.14)-(3.17) . . . 63
3.4 Hugoniot locus . . . 66

4 Numerical Simulation for the injection 70

4.1 An unsplitting approximate algorithm for relaxation balance laws . . . 70
4.1.1 Numerical scheme for a compositional model for oil recovery . . . 72
4.2 Numerical experiments with applications to stiff differential models with relaxation 73
4.2.1 A simple example . . . 73

4.2.2 A Riemann problem for an injection of steam and nitrogen in a porous medium . . . 74
4.2.3 Mathematical analysis . . . 80

5 Concluding remarks and perspectives for the future 84
5.1 Concluding remarks . . . 84
5.2 Perspectives for future work . . . 86

A An analysis of the qualitative behaviour of the non-monotone travelling wave of the reduced Euler system 90
A.1 Proof of proposition 2.1.1 . . . 90

B Calculations for the eingenpairs linked to thermodynamic balance law system 93
B.1 Eingenpairs for the thermodynamic balance law system (3.14)-(3.17) . . . 93

C Physical quantities, the equations of state and the laws of thermodynamics 100
C.1 Primary and secondary variables and properties of fluids in injection problems . 100

D An approximation of the pressure-velocity problem by hybrid mixed finite elements linked to a thermodynamic balance law system 103
D.1 A thermodynamic balance law system coupled with a pressure-velocity problem to the Darcy's equation . . . 103
D.2 A computational physics-based operator splitting modelling for the thermal equations . . . 105
D.3 An approximation of the pressure-velocity model by hybrid mixed finite element 106
D.3.1 Mixed methods for nonlinear parabolic problems . . . 106

E The secondary variable u 112

Bibliography 115

Chapter 1

An unsplitting finite volume method for models with stiff relaxation source terms

In this chapter we use a locally conservative finite volume to approximate conservation law with a stiff source term. We developed a cheap scheme that account the nonlinear balance between the hyperbolic flux function and the source term. The method is conservative by construction and relatively easy to understand and implement, wich does not need some splitting strategies.

We are interested in designing a locally conservative scheme to account the balance between numerical approximations of the hyperbolic flux function and the source term linked to steady solutions. The method is based on central difference schemes see [2, 47, 110] or [85], which in turn exhibits some desirable stability and entropy properties for the approximation of hyperbolic conservation laws and balance laws [21, 22, 21, 32, 68, 70, 123]. The new numerical scheme is also used to reproduce consistency solutions for the more general problem of Euler equations with gravity and friction recently published in *F. Bouchut et al.* [33], *C. Chalons et al.* [38, 39], *F. Coquel et al.* [49] and *M. Dumbser et al.* [61]. We explain our findings along with a representative set of numerical examples in order to describe the interplay of theory and numerics methods with disciplinary models and their applications. There are many relevant studies of approximate methods and numerical analysis for balance laws with relaxation terms. This novel approach is a tentative to contribute in order to tackle the mentioned class of differential equation. As a possible continuation of this work is the application of the new findings that account the nonequilibrium effects in models of three-phase flow in porous media [2] and for thermal injection problems [92] as those found in the modelling of many groundwater flow and solute transport problems in groundwater aquifers systems as well as oil recovery problems in porous media.

For the oil recovery problems model, a proof of stability and convergence of approximate solutions remains elusive. There are several other methods to construct approximate solutions to balance law models as discussed here. Some methods are naturally derived from physical considerations, others lead to more efficient numerical algorithms; see also [113] and the references cited therein. Indeed, for balance laws, we mention [32, 70] for a modern description of numerical methods for relaxation systems of conservation laws. No matter what is the approximation algorithm, the same natural questions arise (see [70]). Does the total variation

of the approximate solutions remain uniformly bounded for all times $t > 0$? In general, the source term might not be decreasing and some semi-implicit and fully implicit scheme are not applicable, at least in a straightforward manner. Additionally, it is possible to design well-balanced schemes which are also asymptotically consistent for a particular system of parabolic equations [32, 70], but the resulting scheme is stable under a very restrictive CFL condition. Another issue is: the approximate solutions depend continuously on the initial data, in the L_1 norm? As the approximation parameters (in dicrete space and in dicrete time) tend to zero, does the approximate solutions converge to the unique entropy weak solution of the hyperbolic Cauchy problem with relaxation? All such questions must be addressed carefully as a possible continuation of this work.

1.1 Balance law shock-fitting numerical algorithms

Well-balanced and asymptotic preserving schemes have been proposed in the last years for solving balance laws, see, e.g., [32, 33, 70]. Such class of methods are receiving an increasing amount of interest in the scientific community, which arises from a mathematically oriented approach to a computational point of view, due to many real world applications for this kind of methods (see, e.g., [31, 33, 38, 54, 61, 71, 73, 83, 107, 112]). The property of well-balance can be formally enunciated as follows. Consider the balance law, $U = U(x,t)$,

$$U_t + F_x(U) = S(U), \tag{1.1}$$

we denote U^e by the stationary solution, which satisfies the equation,

$$F_x(U^e) = S(U^e). \tag{1.2}$$

We say that a numerical scheme is well-balanced with respect to problem (1.1), if it fully satisfies a discrete version of the equilibrium equation (1.2). If a method is not well-balanced, the truncation error of solutions near of equilibrium state may be larger than $|U(x,t) - U^e(x)|$.

Asymptotic-Preserving schemes, or AP-schemes – were introduced first by S. Jin [82] with the aim to cope with singularly perturbed problems, particularly in the framework of *kinetic models in a diffusive regime*. In the construction of these AP-schemes is necessary the existence of a well-posed limit problem P^0, which has to be identified beforehand. The main feature of these schemes is that they permit a precise, ϵ-independent, resolution of the problem P^ϵ as well as of its limit problem P^0, with no huge computational effort. The main idea for the construction of AP-schemes, is based on asymptotic arguments and consists in a mathematical reformulation of the singular perturbed problem P^ϵ into an equivalent problem $(AP)^\epsilon$, which is a regular perturbation of the limit problem P^0. The essential properties of AP-schemes are:

i. let $\epsilon > 0$ fixed the AP-scheme is a consistent discretization of the continuous problem $(P)^\epsilon$, where $h = (\Delta t, \Delta x)$,

ii. the stability condition is independent of ϵ,

iii. for fixed discretization parameters $h = (\Delta t, \Delta x)$ the AP-scheme $(P)^\epsilon_h$ provides in the limit $\epsilon \to 0$ a consistent discretization of the limit problem $(P)^0$.

Thus, the asymptotic-preserving approach consists in trying to mimic on the discrete level the asymptotic behaviour of the singularly perturbed problem solutions. Our numerical experiments have shown some numerical evidence of such properties; for more details on this subject we refer to the monographs [32, 70].

1.1.1 Hyperbolic system with relaxation

In this work, we are focused in the computation of accurate approximate solutions for the nonlinear hyperbolic systems of conservation laws with stiff relaxation source terms:

$$U_t + F_x(U) = \epsilon^{-1} Q(U), \quad t > 0, \quad -\infty < x < \infty, \tag{1.3}$$

with a rexalation time factor $\epsilon > 0$, for a given initial data $U(x, 0)$ (possibly with bounded jump discontinuity), where the variables unknown $U : \mathbb{R} \times \mathbb{R}^+ \to \Omega$ takes its values in an open convex set $\Omega \in \mathbb{R}^n$. The associated conservation law counterpart of model (1.3), i.e. $Q(U) \equiv 0$, is supposed to be strictly hyperbolic in the following sense: the Jacobian of the flux function $F(U)$ has real eigenvalues and a complete set of right eigenvectors. Moreover, we make the assumption that there is a $m \times n$ constant matrix R, with $rank(R) < n$

$$RQ(U) = 0, \text{ for all } U \in \mathbb{R}.$$

This gives m independent conserved quantities $v = RU$. Such conserved quantities uniquely determine a local equilibrium value $\mathcal{E}$,

$$\mathcal{E} = \{U : v = QU, R(v) = 0\}.$$

Note that $\mathcal{E}$ represents the *manifold of local equilibrium* of the relaxation operator Q [133]. Over the manifold of local equilibrium, we can reduce the balance law (1.3) in the system

$$\partial_t v + \partial_x G(v) = 0$$

where $G(v) = RF(U)$ and $U \in \mathcal{E}$. In this work, we are focusing only when the Jacobian matrix of G have real eigenvalues.

1.1.2 The design of an unspliting method for balance laws

There are many studies on approximation methods and numerical analysis devoted to balance laws, along with advantages and disadvantages since it is a very difficult problem due to the lack of a general mathematical theory (see [70]). Thus, the purpose of this work is to give an alternative approach for the numerical approximation of the differential equation (1.3) based on central differencing. The flexibility of the central scheme framework [2, 47, 112] makes it appealing to a further straightforward extension for multidimensional problems.

Here we will concentrate on the one-dimensional Euler equations model with gravity and friction terms since it has been used as a proper prototype model [31, 33, 38, 49, 61]. The design of robust general-purpose numerical schemes for balance laws with a relaxation stiff source term is clearly a difficult task [38, 61, 70, 71, 73, 83, 107]. The key issues are the well-balanced discretizations in order to achieve the proper nonlinear balance between fluxes and source term linked to the original differential system. The mathematical nature of the underlying differential balance system can be the best indicator for the design of new scheme.

For the sake of simplicity, we will give a formal construction of the methods for a scalar balance law of the form,

$$u_t + f_x(u) = \frac{1}{\epsilon} g(u), \quad t > 0, \quad -\infty < x < \infty; \qquad u(x, 0) = \eta(x), \quad -\infty < x < \infty. \tag{1.4}$$

Essentially, we will use a central differencing framework in a staggered mesh grid as in [47, 112] for the construction of our new scheme. First, we define the grid points $x_j = j\Delta x$, $x_{j+1/2} = x_j + \frac{1}{2}\Delta x$, for $j = \cdots, -2, -1, 0, 1, 2, \cdots$, Δx is *constant*, and the local average of quantity $u = u(x,t)$ for fixed time $t = t^n$ over the interval $[x_j, x_{j+1}]$ as,

$$u^n_{j+1/2} = \frac{1}{\Delta x}\int_{x_j}^{x_{j+1}} u(x,t^n)dx.$$

Integration of (1.4) over the local finite control volume $[x_j, x_{j+1}] \times [t^n, t^{n+1}]$ reads,

$$\begin{aligned} u^{n+1}_{j+1/2} = \frac{1}{\Delta x}\int_{x_j}^{x_{j+1}} u(x,t^n)\,dx + \frac{1}{\Delta x}\int_{t^n}^{t^{n+1}} [f(u(x_j,t)) - f(u(x_{j+1},t))]\,dt \\ + \frac{1}{\epsilon\Delta x}\int_{t^n}^{t^{n+1}}\int_{x_j}^{x_{j+1}} g(u(x,t))\;dx\,dt. \end{aligned} \tag{1.5}$$

The key-point in (1.5) is clearly to perform a discretization that account a well-balancing between the nonlinear numerical flux function $f(u)$ and the nonlinear source term $\epsilon^{-1}g(U)$. Different quadrature rules will lead to a family of schemes, thus, at each time level $t^n = n\,\Delta t$, we reconstruct first-order piecewise linear of $u(x,t)$ (see [47, 112], but any other high-order approximation is acceptable), over the staggered mesh grid $x_{j-1/2} < x < x_{j+1/2}$, given by,

$$L_j(x,t) = u_j(t) + (x - x_j)\frac{(u_x)^n_j}{\Delta x}, \quad \text{such that} \quad \frac{(u_x)^n_j}{\Delta x} \equiv u_x(x,t^n)|_{x=x_j} + O(\Delta x), \tag{1.6}$$

where $u_j(t)$ denotes a piecewise constant approximate solution over cells of width $\Delta x = x_{j+1/2} - x_{j-1/2}$, which is of the form, $\overline{u}(x,t) = u_j(t)$, $x_{j-1/2} < x < x_{j+1/2}$, and $(u_x)^n_j$ is a numerical approximation of the partial derivative u_x at point (x_j, t^n). Indeed, quantity $(u_x)^n_j$ is a degree of freedom since there are many slope limiter options for its approximation. These limiters effectively switch between monotonicity mode to prevent spurious oscillations and artificial increase gradient magnitudes, wich minimize damping of high frequency solution components. This is a key issue in the central difference framework (see elsewhere, e.g., [38, 47, 61, 70, 112]). Here we use the Upstream Non-Oscillatory (UNO) limiter approach, where for fixed $t = t^n$, it is given by,

$$(u_x)^n_j = MM\left\{\Delta u_{j-1/2} + \tfrac{1}{2}MM(\Delta^2 u_{j-1},\;\; \Delta^2 u_j), \Delta u_{j+\frac{1}{2}} - \tfrac{1}{2}MM(\Delta^2 u_j, \Delta^2 u_{j+1})\right\},$$

with $\Delta^2 u_j = u_{j+1} - u_j + u_{j-1}$, and $MM(x,y) = \frac{1}{2}(\mathrm{sgn}(x) + \mathrm{sgn}(y)) \cdot \min(|x|, |y|)$. Connecting the piecewise linear approximations $L_j(x,t^n)$ into (1.5) reads,

$$\begin{aligned} u^{n+1}_{j+1/2} = \frac{1}{2}(u^n_j + u^n_{j+1}) + \frac{1}{8}((u_x)^n_j - (u_x)^n_{j+1}) + \frac{1}{\Delta x}\int_{t^n}^{t^{n+1}} f(u(x_j,t)) - f(u(x_{j+1},t))\,dt \\ + \frac{1}{\epsilon\Delta x}\int_{t^n}^{t^{n+1}}\int_{x_j}^{x_{j+1}} g(u(x,t))\;dx\,dt. \end{aligned} \tag{1.7}$$

It is possible to construct schemes based on semi-discrete or fully discrete approaches with good properties for conservation laws with relaxation source terms. This important issue is discussed in, e.g., [112], and more recently in [70] with an emphasis on the construction of numerical schemes that retain asymptotic preserving and well-balanced properties with respect to the continuous relaxation system.

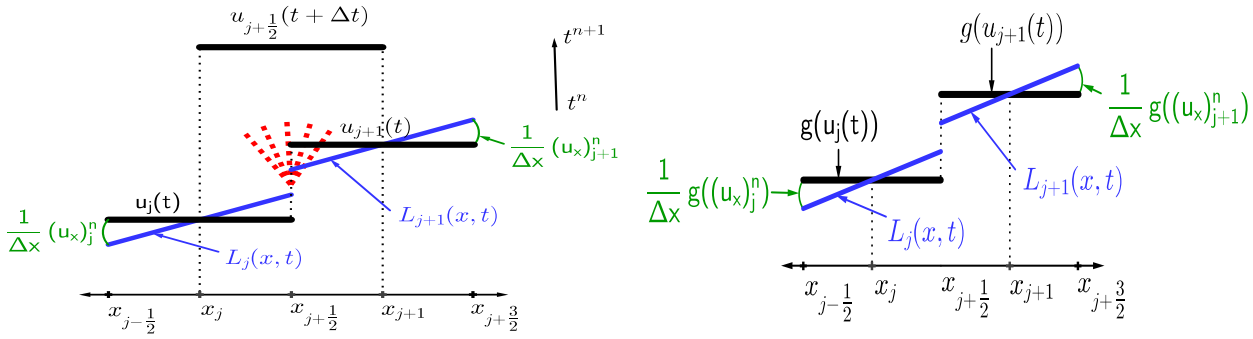

Figure 1.1: Linear reconstruction of the variable u (**Left**) and term source $g(u)$ (**Right**) in the staggered grid.

Essentially, this is true if the designed scheme accounts the delicate (local) nonlinear balance between the numerical approximations of the hyperbolic flux and the source term for balance law problems, but linked to the purely hyperbolic character of conservation laws. For instance, it has been shown [89] that semi-discrete central-upwind schemes may fail to converge to the unique entropy solution of non-convex purely hyperbolic conservation laws, and thus, it may fail recovering the Kruzhkov solution. On the other hand, central differencing is fully based on staggered-like control volumes, this seems to benefit of a natural structure in order to capture approximate entropy shock solutions [112], particularly for the flux function with explicitly spatial variation (see [2, 47, 85]). We use a fully discrete formulation based on a predictor-corrector approach for approximating the flux gradients and source terms (again, under a CFL-type constrain) to get,

$$\int_{t^n}^{t^{n+1}} f(u(x_j,t))\,dt \approx \Delta t\, f(u_j^{n+1/2}), \quad \text{along with} \quad u_j^{n+1/2} = u_j^n + \frac{\Delta t}{2}\left[g(u_j^n) - \frac{(f_x)_j^n}{\Delta x}\right]. \tag{1.8}$$

Again, we use the UNO choice for the numerical approximation of $f_x(u(x,t))$ at point (x_j,t^n) denoted by $(f_x)_j^n/\Delta x$ in (1.8); i.e., $(f_x)_j^n/\Delta x \equiv f_x(x,t)|_{x=x_j}+O(\Delta x)$. For approximating the source term $g(u(x,t))$, we use the interpolants (1.6) to get, (see Fig. 1.1, this approximation is quite distinct to what is done in [112]),

$$\begin{aligned}\frac{1}{\Delta x}\int_{t^n}^{t^{n+1}}\int_{x_j}^{x_j+1} L_j(g(u))\,dx\,dt = \frac{1}{\Delta x}\int_{t^n}^{t^{n+1}}\int_{x_{j+\frac{1}{2}}}^{x_{j+1}}[g(u_j(t)) + (x-x_j)\frac{\partial}{\partial x}g(u_j(t))]\,dx\,dt \\ +\frac{1}{\Delta x}\int_{t^n}^{t^{n+1}}\int_{x_{j+\frac{1}{2}}}^{x_{j+1}}[g(u_j(t)) + (x-x_{j+1})\frac{\partial}{\partial x}g(u_j(t))]\,dx\,dt.\end{aligned} \tag{1.9}$$

Following [2, 47, 112], the approximation of the source term, in (1.9), allow us to make use of the midpoint values x_j in a specific discrete time and position over the computational grid. Indeed, since these mid-values are bounded away from the jump discontinuities along the edges at $x_{j+1/2}$, we may use a Taylor expansion and the balance law (1.4) to evaluate the quantity $u(x,t)$ in time as a predictor step. Additionally, we will see in what follows that this will facilitate further the construction of our scheme. At first glance, it seems that it is not advisable to perform the reconstruction of the source term $g(u)$ due to its stiff nature, since this could lead to numerical instabilities limiting the piecewise linear value of u over the cells. This is not the case if we perform a clever approximate procedure, which, in turn, is motivated by

the proper balance between the fluxes and source approximations at the discrete level. Thus, by using (1.9) the integral of the source term on the right hand side of (1.7) can be written as,

$$\frac{1}{\Delta x}\left\{\int_{t^n}^{t^{n+1}}\int_{x_j}^{x_{j+\frac{1}{2}}}[g(u(x_j,t))+(x-x_j)\frac{1}{\Delta x}g_x(u(x_j,t))]\;dx\,dt \right. \\ \left. +\int_{t^n}^{t^{n+1}}\int_{x_{j+\frac{1}{2}}}^{x_{j+1}}[g(u(x_{j+1},t))+(x-x_{j+1})\frac{1}{\Delta x}g_x(u(x_{j+1},t))]\right\}dx\,dt, \tag{1.10}$$

where we also use the UNO choice for $g_x(u(x,t))$ at point (x_j,t^n).

Notice that, the balance law (1.4) under a proper CFL condition, we can write from (1.10) the following approximations,

$$\begin{aligned}\frac{1}{\Delta x}\int_{x_j}^{x_{j+\frac{1}{2}}}&[g(u(x_j,t))+(x-x_j)\frac{1}{\Delta x}g_x(u(x_j,t))]\;dx \\ &=\frac{g(u(x_j,t))}{\Delta x}\int_{x_j}^{x_{j+\frac{1}{2}}}dx+\frac{g_x(u(x_j,t))}{\Delta x}\int_{x_j}^{x_{j+\frac{1}{2}}}(x-x_j)\;dx, \\ &=\frac{1}{2}g(u(x_j,t))+\frac{1}{8}g_x(u(x_j,t)),\end{aligned}$$

and

$$\begin{aligned}\frac{1}{\Delta x}\int_{x_{j+\frac{1}{2}}}^{x_{j+1}}&[g(u(x_{j+1},t))+(x-x_{j+1})\frac{1}{\Delta x}g_x(u(x_{j+1},t))]\;dx \\ &=\frac{g(u(x_{j+1},t))}{\Delta x}\int_{x_{j+\frac{1}{2}}}^{x_{j+1}}dx+\frac{g_x(u(x_{j+1},t))}{(\Delta x)^2}\int_{x_{j+\frac{1}{2}}}^{x_{j+1}}(x-x_{j+1})\;dx, \\ &=\frac{1}{2}g(u(x_{j+1},t))-\frac{1}{8}g_x(u(x_{j+1},t)).\end{aligned}$$

Thus, we might write (1.10) as,

$$\int_{t^n}^{t^{n+1}}\left\{\frac{1}{2}[g(u(x_j,t))+g(u(x_{j+1},t))]+\frac{1}{8}[(g_x)_j^n-(g_x)_{j+1}^n]\right\}\;dt. \tag{1.11}$$

Motivated by the stability of IMEX-methods (Implicit-explicit, see, e.g., [54, 112]) we use a trapezoidal rule on the two first terms in (1.11) to get,

$$\int_{t^n}^{t^{n+1}}g(u(x_j,t))\,dt\approx\frac{\Delta t}{2}\Big(g(u(x_j,t^{n+1}))+g(u(x_j,t^n))\Big) \tag{1.12a}$$

and

$$\int_{t^n}^{t^{n+1}}g(u(x_{j+1},t))\,dt\approx\frac{\Delta t}{2}\Big(g(u(x_{j+1},t^{n+1})+g(u(x_{j+1},t^n)\Big), \tag{1.12b}$$

and then equation (1.11) is now rewritten as,

$$\frac{\Delta t}{4}\Big(g(u_j^{n+1})+g(u_{j+1}^{n+1})+g(u_j^n)+g(u_{j+1}^n)\Big)+\frac{1}{8}\int_{t^n}^{t^{n+1}}[(g_x)_j^n-(g_x)_{j+1}^n]\;dt, \tag{1.13}$$

and in the central differencing framework, we use a trapezoidal-like rule to perform the approximation in (1.13) $\frac{1}{2}(g(u_{j+1}^{n+1})+g(u_j^{n+1}))=g(u_{j+1/2}^{n+1})$, yielding the predictor-corrector central

differencing scheme:

$$\begin{aligned} u_{j+\frac{1}{2}}^{n+1} =& \frac{1}{2}\left(u_j^n + u_{j+1}^n\right) + \frac{1}{8}\left[(u_x)_j^n - (u_x)_{j+1}^n\right] - \frac{\Delta t}{\Delta x}\left[f(u_{j+1}^{n+1/2}) - f(u_j^{n+1/2})\right] \\ &+ \frac{\Delta t}{2}\left[g(u_{j+1/2}^{n+1}) + \frac{1}{2\epsilon}\left(g(u_j^n) + g(u_{j+1}^n)\right)\right] + \frac{1}{8\epsilon}\int_{t^n}^{t^{n+1}} \left[(g_x)_j^n - (g_x)_{j+1}^n\right]\, dt, \end{aligned} \tag{1.14}$$

where $u_j^{n+1/2} \equiv u(x_j, t + \Delta t/2)$ is determined by (1.8). Notice that (1.14) can be viewed as a one-level time-step predictor-corrector scheme. It can be designed to be explicit, semi-implicit or fully implicit since the leapfrog method requires an *initial data* at two consecutive time levels at *stages* $t^{n+1/2}$ and t^{n+1}. At first glance, our scheme seems to be costly in terms of computations since information is needed at time-level t^{n+1} for evaluation of $g(u_{j+1/2}^{n+1})$ in (1.14). Although the trapezoid rule is not L-stable [100], the use of the trapezoid rule here allows us to perform two very convenient approximations depicted in equation (1.12) and in equation (1.13), which in turn allows us to define an approximation for $g(u(x,t))$ at time t^{n+1} in the grid cell $x_{j+1/2}$.

The essential key behind such procedure is precisely a balanced approximation/discretization of the source term by means of a predictor step equation. This means that there is another important issue, the stability in the time integration, that is, the delicate local nonlinear balance between the numerical approximations of the hyperbolic flux and the source term for balance law problems, but linked to the purely hyperbolic character of conservation law counterpart. This issue is also very well explained in [31, 33, 39, 49, 61]; see also [70]. Indeed, algorithm (1.14) is quite simple to describe and implement.

We note that only two new evaluations, $g_x(u(x_j,t))$ and one prediction to $u_{j+1/2}^{n+1}$, per time step are required in comparison with similar schemes for stiff balance laws (see, e.g., [38, 54, 61, 83, 112]). For a time level t^n the grid functions u_j^n are satisfied:

1. Quantities $g(u_j^n)$ and $(u_x)_j^n$ are easily evaluated.

2. Next, $u_j^{n+1/2}$ is determined by (1.8) then now $f(u(x_{j+1}, t + \Delta t/2)$ and $g_x(u(x_j,t)$ can be evaluated.

3. Finally, we need a prediction to $u_{j+1/2}^{n+1}$.

Hereinafter we will discuss another two numerical schemes based on *splitting* and *unsplitting* strategies, but in the same framework of the central differencing scheme. Indeed, such schemes might also be used to predict $u_{j+1/2}^{n+1}$ for (1.14). In summary, with the novelty reconstruction of the source term we have now another way to balance the discretizations between fluxes and source term linked to the original differential balance system (1.3).

1.1.2.1 An unsplitting predictor scheme to $u_{j+1/2}^{n+1}$

As discussed in Section 1.1.2, under the CFL condition, say

$$\max\left\{|f'(u)|\frac{\Delta t}{\Delta x}\right\} < \frac{1}{2},$$

we can write $\int_{t^n}^{t^{n+1}} g(u(x_j,t))\, dt \approx \Delta t\, g(u_j^{n+1/2})$ and from (1.4)-(1.5) reads,

$$\begin{aligned} u_{j+1/2}^{n+1} = \frac{1}{\Delta x}\int_{x_j}^{x_{j+1}} u(x,t^n)\, dx + \frac{1}{\Delta x}\int_{t^n}^{t^{n+1}} [f(u(x_j,t)) - f(u(x_{j+1},t))]\, dt \\ + \frac{\Delta t}{\epsilon \Delta x}\int_{x_j}^{x_{j+1}} g(u^{n+1/2}(x))\, dx. \end{aligned} \tag{1.15}$$

There are many options available (see [47, 112]) for the approximation of quantity $u^{n+1/2}(x)$ to evaluate the source term apearing in (1.15). Motivated by the stability of IMEX-methods [54, 112]), we use the robust trapezoidal rule,

$$u_{j+1/2}^{n+1} = \frac{1}{2}\left(u_j^n + u_{j+1}^n\right) + \frac{1}{8}\left[(u_x)_j^n - (u_x)_{j+1}^n\right] - \frac{\Delta t}{\Delta x}\left[f(u_{j+1}^{n+1/2}) - f(u_j^{n+1/2}))\right] + \frac{\Delta t}{2\,\epsilon}\left[g(u_j^{n+1/2}) + g(u_{j+1}^{n+1/2})\right]. \tag{1.16}$$

where $u_j^{n+1/2}$ is determined (again) by (1.8). We stress at this point that even though we need a *prediction* to $u_{j+1/2}^{n+1}$, these does not need additional computation at this time since all quantities that appears in (1.16) are already available to use (if properly stored of course). Thus, equations (1.8), (1.14) and (1.16) define our new scheme, which, in turn, have the benefit of all the desirable properties of being locally conservative (by construction) and Riemann problems and field-by-field decompositions are avoided. The numerical viscosity is reduced by means of high-resolution interpolants [47, 54, 112].

1.1.2.2 A splitting predictor scheme to $u_{j+1/2}^{n+1}$

We will first, give a very brief description of the splitting approach for balance law with stiff relaxation, in the IMEX-methods framework discussed in [54, 112]. For simplicity of presentation, we rewrite the equation (1.4) as,

$$\mathcal{H}_t + f_x(\mathcal{H}) = q(\mathcal{H}), \tag{1.17}$$

where $q(\mathcal{H}) = \dfrac{1}{\epsilon} g(\mathcal{H})$ with $u(x,t) \equiv \mathcal{H}(x,t)$. By means of an operator splitting procedure [54, 70, 112] we are interested in solving sequentially, the hyperbolic problem and the ODE subproblems, respectively, given by,

$$(\mathcal{H}_H)_t + f_x(\mathcal{H}_H) = 0 \quad \text{and} \quad (\mathcal{H}_R)_t = q(\mathcal{H}_R), \tag{1.18}$$

under the assumption of no spatial variations $(f(\mathcal{H}))_x = 0$. Suppose suitable initial conditions to (1.18.a) and (1.18.b) are given. Let $\mathcal{S}_H$, $\mathcal{S}_R$ denote the exact solution of the hyperbolic operator (1.18.a) and the relaxation operator (1.18.b), respectively. Now, assume that the solution $\mathcal{H}(x,t)$ of the differential problem (1.17) is available at a time t. Next, let us introduce a time step Δt (under a CFL constrain) and evolve the solution of (1.17) from time t to time $t + \Delta t$ in two sequential sub steps. First, solve the purely hyperbolic conservation law (1.18.a) in the interval $(t, t + \Delta t]$,

$$\mathcal{H}^*(x) = \mathcal{S}_H(\Delta t)\mathcal{H}(x,t), \tag{1.19}$$

and then let us applied the relaxation solution operator over $\mathcal{H}^*(x)$ to produce an approximate solution at time $t + \Delta t$,

$$\mathcal{H}(x, t+\Delta t) = \mathcal{S}_R(\Delta t)\mathcal{H}^*(x,t) = \mathcal{S}_R(\Delta t)\mathcal{S}_H(\Delta t)\mathcal{H}(x,t). \tag{1.20}$$

Alternative operator splitting solutions might be achieved considering distinct time-splitting configurations (under a proper CFL-like condition), although the associated error might lead to an exponential amplification of the time-splitting error [70]; (see also [54, 112]) and references distinct procedures related to the splitting procedure (1.19)-(1.20) for balance laws. Thus,

equations (1.8), (1.14) and (1.19)-(1.20) define an alternative and a new scheme for the solution of the original differential balance law problem (1.4).

Although we have proposed an alternative algorithm based on a splitting approach, it is necessary to point out that we do not make use of such approach in our numerical computations. Instead, we only use the unsplitting algorithm for solving the hyperbolic conservation laws with stiff relaxation that account the nonlinear balance between numerical approximations of the hyperbolic flux function and the source term dynamics. This choice relies upon the fact that the operator splitting approach might fail to solve the balance laws [70]; see also [32, 113].

Of course, there are well known situations where the operator splitting strategy works and then should be use to achieve accurate numerical computation with the desired efficiency in the computational time (see, e.g., [33, 54, 95, 112]). We believe that in such situations our operator splitting approach might give good results, but we need to work later on this subject. Here we are dealing with a nonlinear system of balance in which its properties are not well known and thus we belive be advisable to avoid the operator splitting approach. This is our motivation to only use the unsplitting approach for solving the hyperbolic conservation laws with relaxation source terms throughout the thesis.

We can now turn our attention to verify the viability of the unsplitting finite volume scheme for solving a set of nontrivial test problems of balance laws.

1.2 Numerical experiments

In this section we illustrate some numerical experiments performed with the numerical method described in the Section 1.1.2 for the scalar and the system balance law with stiff term. We use some physical phenomena to show the robustness and simplicity of our method, for example, Euler equation with friction and gravity with different pressure types and shallow water. These results are compared with examples found in the literature.

1.2.1 Euler equations with gravity and friction

The Euler's equations system in gas fluid dynamics has been focus of an intense discussion to explain some physical phenomena that generate problems of interest for many branches of mathematics ranging from theory to numerical analysis with its applications. In [33], we can find the study of the 2×2 Euler's system that describes an isentropic gas flow at a time $t \geq 0$ and at point $x \in \mathbb{R}$ through the gas density $\rho(x,t) \geq 0$ and its velocity $u(x,t) \in \mathbb{R}$ by the hyperbolic equation

$$\frac{\partial}{\partial t}\begin{bmatrix} \rho \\ \rho u \end{bmatrix} + \frac{\partial}{\partial x}\begin{bmatrix} \rho u \\ \rho u^2 + p(\rho) \end{bmatrix} = \begin{bmatrix} 0 \\ -\alpha \rho u \end{bmatrix}, \tag{1.21}$$

where α is the friction coefficient. In this model only is considered the polytropic gases case with pressure, which is given by the state equation $p(\rho) = k\rho^{\gamma}$ with $1 < \gamma \leq 3$ and $k > 0$. They consider an heterogeneous domain composed mainly of two areas, in the first area the friction coefficient vanishes, whereas, in the second area the friction coefficient $\alpha(x)$ is very large ($\alpha >> 1$). We notice that the high friction coefficient acts like a *natural* barrier; in this manner, we expected the attenuation of the gas density in the high friction region. This system, at appropriate time scale, is reduced to a parabolic equation called *porous media* [107]. In [33]

the author studied the system (1.21) by two different numerical strategies, upwind source at interfaces and finite volume schemes. Unfortunately they did not specify neither the physical and numerical parameters nor initial and boundary conditions in their test problems. Thus, we consider that all the numerical calculations inside the windows of observation are in the computational domain $[a, b]$, with the following initial value

$$\begin{cases} (\rho, u)^L = (1.65, 0) \text{ if } x \leq 0, \\ (\rho, u)^R = (0.01, 0) \text{ if } x > 0, \end{cases}$$

where the stiffness parameter $\alpha = \alpha(x)$ takes value 0 if $x \leq 0$ (purely hyperbolic Euler's equations without any friction) and it takes value 1500 if $x > 0$ (Euler's equations with large friction). We choose the parameter $\gamma = 2.8$, and we report our numerical results in the Fig. 1.2(b), at the simulation time $t = 2$ in the computational domain $[-3, 1]$. In order to account the interaction of a wave structure induced by friction term, due to the existences of an interface that separates the hyperbolic regime with the friction regime of Euler's equation. Here we use $p(u) = k\rho^\gamma$ with $k = \frac{(\gamma-1)^2}{4\gamma}$ and $\gamma = 2.88$, but several admissible values $\gamma \in [1, 3]$ were used in this study. It has been observed the same asymptotic wave structure for all considered parameters after some time of simulation. It seems that parameter γ plays a scaling factor role in this model.

In [61] the authors studied the system (1.21) with addition of the energy balance equation:

$$\frac{\partial}{\partial t}\begin{bmatrix} \rho \\ \rho u \\ \rho E \end{bmatrix} + \frac{\partial}{\partial x}\begin{bmatrix} \rho u \\ \rho u^2 + p \\ (\rho E + p)u \end{bmatrix} = -\alpha \begin{bmatrix} 0 \\ \rho u \\ \rho u^2 \end{bmatrix}, \tag{1.22}$$

where E is the total energy. The authors studied two numerical strategies, volume schemes (WENO-ENO) and a local space–time discontinuous Galerkin (DG) finite element scheme. They apply these numerical strategies to the isentropic Euler's system with stiff friction and full Euler's system with stiff friction, i.e., $p = k\rho^\gamma$ and $p = (\gamma - 1)\left(\rho E - \frac{1}{2}\rho u^2\right)$ respectively. The numerical study was performed using the following parameters, $k = 1$, $\gamma = 1.4$ in the computation domain $[0, 1]$ with Dirichlet boundary conditions $\mathbf{u}(0, t) = \mathbf{u}(0, 0)$ and $\mathbf{u}(1, t) = \mathbf{u}(1, 0)$, where $\mathbf{u} = (\rho, \rho u, \rho E)^T$. For the friction coefficient we have $\alpha(x) = 0$, if $x < 0.25$ and $\alpha(x) = 1500$, if $x \geq 0.25$. The initial condition is

$$\begin{cases} \mathbf{u}^L = (1.65, 0, 0.539849068)^T \text{ if } x \leq 0.25, \\ \mathbf{u}^R = (0.01, 0, 0.003962233)^T \text{ if } x > 0.25. \end{cases} \tag{1.23}$$

Notice that the parameters are similar to those used in the previously studied Euler's system for the case 2×2, [33].

The numerical results are presented in Fig. 1.2, the references solutions are the solid black lines. The computed solutions are obtained using the methods discussed in Section 1.1 at time $t = 2$, which are the unsplitting schemes 1.1.2: Fully Implicit FI version in dash-dotted line and predictor-corrector PC version in dashed lines. The references solutions were obtained on 10000 cells using the PC version 1.1.2.

On the Fig. 1.2(a) it is shown the isentropic Euler system (1.22), On the Fig. 1.2(c) it is shown the full Euler system (1.22) with stiff friction. In all numerical experiments performed by the numerical methods designed for stiff Euler systems, we do not observe any negative values

neither for the total energy ρu nor for the density ρ. We would like to stress the fact that asymptotic behaviour (steady- state solutions) are not well solved for the considered test case for the full Euler equations on coarser meshes like 100 or 500 grids as such in [33, 61], although an extension of our scheme for multidimensional problems is straightforward since no characteristic decomposition and Riemann solvers are required. Indeed, our numerical scheme is quite simple to implement making it a feasible mathematical tool for stiff systems under investigation where no extensive analytic analysis has been conducted as such for Euler's equations and related problems.

Following [38, 39] we consider the gas dynamics equations with gravity and friction terms in Eulerian coordinates given by the system

$$\frac{\partial}{\partial t}\begin{bmatrix}\rho\\ \rho u\\ \rho E\end{bmatrix}+\frac{\partial}{\partial x}\begin{bmatrix}\rho u\\ \rho u^2+p\\ (\rho E+p)u\end{bmatrix}=\begin{bmatrix}0\\ \rho(g-\alpha\varphi(u))\\ \rho(gu-\alpha\psi(u))\end{bmatrix}, \tag{1.24}$$

where $\varphi(u)$ and $\psi(u)$ model friction terms and the constant $\alpha > 0$ can became very large; $g = 9.81m/s^2$ is the gravity constant. The functions $\varphi(u)$ and $\psi(u)$ satisfy $\varphi(0) = \psi(0) = 0$, $\varphi' > 0$ and $\psi'(0) = 0$. The friction terms usually use the expression

$$\begin{aligned}&\varphi(u) = |u|^{\chi}u,\\ &\psi(u) = a|u|^{\chi+2}, \quad \text{with } 0 \le a \le 1,\end{aligned}$$

we have used the linear friction, i.e. $\chi = 0$ and $a = 1$. The energy E satisfies $E = \varepsilon + u^2/2$, ε is the internal energy. The pressure $p = p(\rho, \varepsilon)$ is the classical ideal gas polytropic law $p = (\gamma - 1)\rho\varepsilon$, with $\gamma = 1.4$. The initial condition corresponds to a centered arch function $(\rho, u, p) = (1, 0, 10000)$ if $-0.2 \le x \le 0.2$ and $(\rho, u, p) = (2, 0, 2639.2)$ otherwise. Here we used periodic boundary conditions. The final time is $t = 0.001$.

The objective here is to perform a numerical study. We want to show that our numerical approach is able to capture the complex solution behaviour of the Euler system with a large friction, although our computational method primarily was not designed for such unsteady test limit regime, as was detailed discussed in [38, 39]. The graphics presented in Fig. 1.3 are related to a sensitivity study of the velocity (left frame) and pressure (right frame) with respect to a large friction on an unsteady test case. We can see from these results that, although the sign of the velocity (left frame) and thus also the changes upon the energy source term, the numerical solutions seems to capture the expected behaviour on the pressure variations, and thus our scheme were able to preserve (qualitatively) the well-balanced and asymptotic preserving behaviour between gravity and friction to the full model problem of Euler system with respect to a large friction. Our results are in a good agreement with those discussed in [38, 39]. The scheme discussed in Section 1.1 is serial and it was implemented in pure C programming language. All computations were performed on a basic laptop and the one-dimensional experiments were quite fast (see Table 1.1 and Table 1.2). This yields a very simple mathematical tool for reliability studies for balance laws with stiff relaxation source terms, along with the pertinent analysis.

We finish this section with the study of a compressible gas dynamic equation with gravity and friction for a linear friction model discussed in [49]; the numerical approximations are shown in Fig. 1.4. We consider a compressible flow with $\varrho = 1/2$ and initial condition $(\rho, u, p) = (1, 0, 1)$ if $1/2 \le x \le 2/3$ and $(\rho, u, p) = (1, 0, 2)$ otherwise. The one-dimensional computational domain is $[0, 1]$ that periodic boundary condition the final simulation time is $t = 2$ as reported

# Cells	Δt	Δx	# time steps	elapsed time (sec)	CFL condition
250	0.000002	0.004	5100	0.845238	0.25500
500	0.000002	0.002	5500	1.741483	0.27500
1000	0.000002	0.001	5600	3.506431	0.28000
10000	0.0000005	0.0001	20000	126.647973	0.25000

Table 1.1: Parameters related to numerical experiments reported in Fig. 1.3, Chalons et al. (2010), ref. [38], based on a Godunov-Type Scheme.

# Cells	Δt	Δx	# time steps	elapsed time (sec)	CFL condition
250	0.001538	0.004	1300	0.845238	0.24993
500	0.000833	0.002	2400	1.741483	0.24990
1000	0.0005	0.001	4000	3.506431	0.25000
10000	0.000038	0.0001	52000	346.0514	0.24700

Table 1.2: Parameters related to numerical experiments reported in Fig. 1.4, Coquel & Godlewski (2011), ref. [49], based on an asymptotic preserving scheme.

in [49]. The energy E satisfies $E = e+u^2/2$, e is the internal energy and pressure law $p = p(\rho, e)$ is the ideal gas polytropic law $p = (\gamma-1)(\rho e)$ with $\gamma = 1.4$, gravity constant $g = 9.81 m/s^2$ and large friction value $\alpha = 10^3 s^{-1}$. The physical significance of density (Fig. 1.4(b)), velocity (Fig. 1.4(c)) and pressure (Fig. 1.4(a)), we can observe that our scheme has the ability to preserve positivity of density and pressure. As discussed in [49], the expected solution consists of two symmetric waves (this is quite clear for velocity and pressure profiles). The region between the two nonlinear waves is close to a low pressure region with respect to the initial data. Moreover, the symmetric sharp moving fronts related to the density variation is qualitatively correct. On physical grounds, such results ensures the positivity of the internal energy is preserved.

1.2.2 Shallow water flow down in an inclined open channel model

In [95], the authors presented a nonlinear balance laws to model the flow of water downing in a channel with rectangular cross section and inclined at a constant angle θ to the horizontal through the 2×2 system

$$\begin{bmatrix} h \\ hv \end{bmatrix}_t + \begin{bmatrix} hv \\ v^2 h + \frac{1}{2}h^2 \end{bmatrix}_x = \begin{bmatrix} 0 \\ h - C\frac{1+h}{\tan(\theta)}v^2 \end{bmatrix}, \tag{1.25}$$

where h is the height of the free surface and v is the averaged horizontal velocity. As in [95], the friction coefficient C is taken to be 0.1, while the inclination angle $\theta = \pi/6$. Indeed, model (1.25) correspond to uniform flow (v_0 and h_0 constants) with the frictional and gravitational forces in perfect balance. To test our numerical scheme, a *perturbation of a uniform flow* is considered as initial condition in order to account the balance between the gravitational and frictional forces as expected from the model problem (1.25). As in [95], the initial velocity is taken to be $v_0 = 1.699$, while the initial height of the free surface consists of a *triangular perturbation* of the uniform flow level, $h_0(x) = x + 1.5$, $-0.5 \leq x < 0$, $h_0(x) = -x + 1.5$, $0 \leq x \leq 0.5$, and 1 elsewhere. The numerical approximations by means of the scheme 1.14 for the above initial value problem is shown in Fig. 1.5. As in [95], if there is no friction ($C = 0$)

then two symmetrical waves will arise from the announced initial data (left column frames). On the other hand, the introduction of friction not only down the velocity of these waves, but also changes the shape (right column frames). For instance, if $C = 0.1$ is considered, one can still observe two waves, but the symmetry is now lost as expected. Here it is shown mesh refinement study computed solutions for h (height of the free surface on the top frames) and for v (averaged horizontal velocity on the right column frames) with scheme (1.8)-(1.16) for the initial value problem described just above at simulation time $t = 1$, for three mesh grids, but one using 2000 cells, namely the reference "exact" solution and another three: grid 100 (top), grid 200 (middle) and grid 400 (bottom).

1.2.3 A Cauchy problem for the inviscid Burgers equation with source term for multiple equilibria

In [95], Langseth et al. propose to study an operator splitting procedure applied to the Cauchy problem of a hyperbolic conservation laws with source term,

$$u_x + f_x(u) = g(u), \text{ with } -\infty < x < \infty,$$

where f and g are smooth functions. The equation has a piecewise initial data. The smooth source function $g(u) = u(1-u)$ has multiple equilibria in the domain of interest, hence it is not a decreasing function. The authors considered the Burgers flux function $f(u) = u^2/2$ along with initial condition

$$u(x,0) = 0.1 + 0.1\sin(2\pi x), \quad 0 \leq x \leq 1 \text{ and } u(x,0) = 0.1,$$

elsewhere. In Fig. 1.6 it is shown the numerical approximations by means of the scheme 1.14. In the case of no availability of an analytic solution (see [95]), we used the numerical approximation to denote the reference solution using a fine mesh (2000 cells), it is called reference solution (solid line in Fig. 1.6). As in [95], the initial data give rise into a shock. But due to the balance between flux function and source term, the left and right state of the shock will increase and asymptotically reach the steady-state equilibrium $u = 1$. Comparing the computed solution with scheme 1.14 and that one reported in [95], it is found that our solution is quite accurate and captures all qualitative details, even in a coarse grid (left picture in Fig. 1.6). Again, our scheme seems to be well-balanced in the sense that the method captured the correct steady states entropy-solution as reported in [95].

1.2.4 Steady-state equilibrium solutions linked with shallow water equations

In [74, 73], Greenberg et al. consider a conservation law of the form

$$\frac{\partial u}{\partial t} + \frac{\partial f(u)}{\partial x} = a_x, \tag{1.26}$$

where $a(\cdot)$ is a bounded piecewise smooth source term and f an even convex function satisfying $f(0) = 0$ and $f(u) > 0$. The authors propose a series of numerical experiments in order to observe the transient behaviour towards steady-state equilibrium solutions. They developed a Godunov-type difference schemes and proved that these schemes are L^∞ stable and have

stable steady solutions similar in structure to those in problem (1.26). The interested reader is referred to [74] (see also [73]) for a detailed description of analytical solutions for all design prototype Cauchy problems.

Here we present the simulations for two cases introduced in Greenberg et al. [74] with flux function $f(u) = u^2/2$ and two different kind of source terms for a balance law of type (1.26). The first test problem (see right column pictures in Fig. 1.7) is given by $G(u) = a_x(x)$ with $a(x) = cos^2(x\,\pi/2))$, if $-1 \leq x \leq 1$, and $a(x) = 0$, in other case. The second test problem is somewhat similar, but the solution exhibits a distinct wave profile (see left column pictures in Fig. 1.7), and it is given by $G(u) = a_x(x)$ with $a(x) = -cos^2(x\,\pi/2))$, if $-1 \leq x \leq 1$, and $a(x) = 0$, in other case. All numerical solutions reported in Fig. 1.7 are computed with our scheme (1.14), along with a uniform mesh grid under CFL stability criterion. A numerical refinement study for such tests problem are also reported in Fig. 1.7 for the discrete counterparts L_1 and L_2 norms with observed $O(1)$.

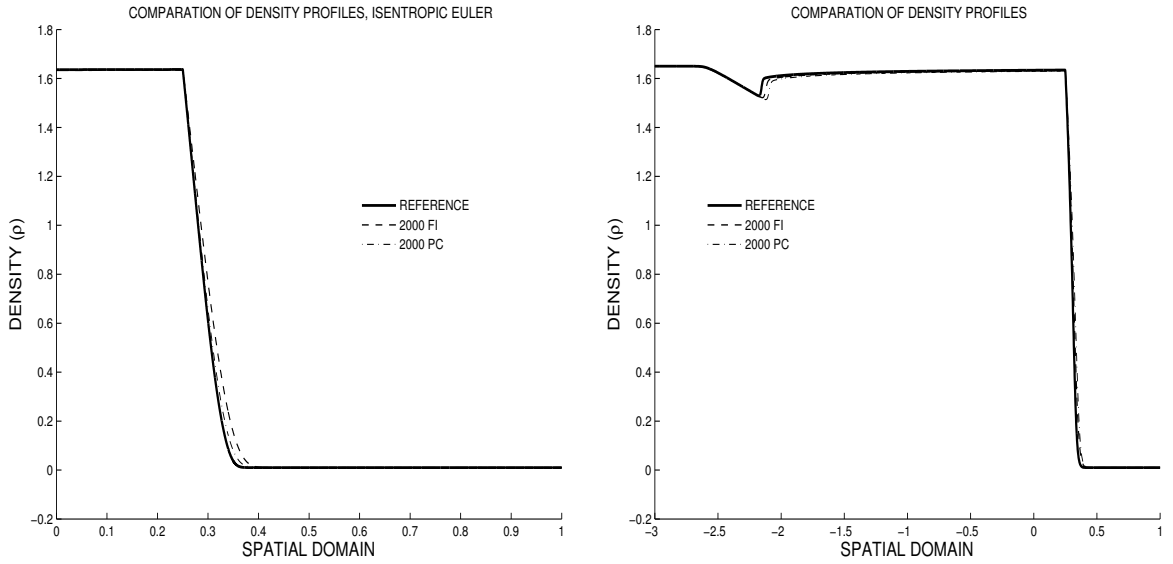

(a)

(b)

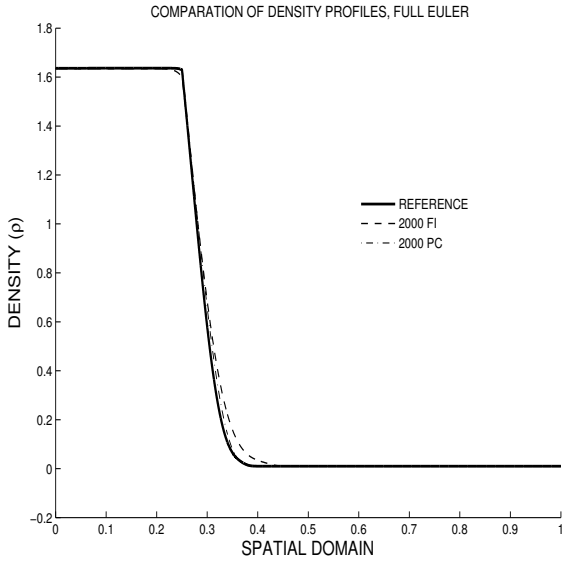

(c)

Figure 1.2: Reference solutions (solid black lines) and computed solutions using the methods discussed in Section 1.1 at time $t = 2$: unsplitting schemes 1.1.2 (Fully Implicit FI version in dash-dotted line and predictor-corrector PC version in dashed lines); the reference solution was obtained on 10000 cells using the PC version 1.1.2. In 1.2(a) it is shown the isentropic Euler system (1.24) with $p(u) = k\rho^{\gamma}$, where $k = 1.0$, $\gamma = 1.4$ and $\varrho = 1.0$. In Fig. 1.2(b) it is shown a snapshot frame at the simulation time $t = 2$ over the computational domain $[-3, 1]$ in order to account for the interaction of a wave structure induced by the friction term at the interface that separates the purely hyperbolic Euler equations from the Euler equations with friction regime. In Fig 1.2(c) it is shown the full Euler system (1.24) with stiff friction, where $p(u) = (\gamma - 1)\left(\rho E - \frac{1}{2}\rho u^2\right)$ along with $k = 1.0$ and $\gamma = 1.4$.

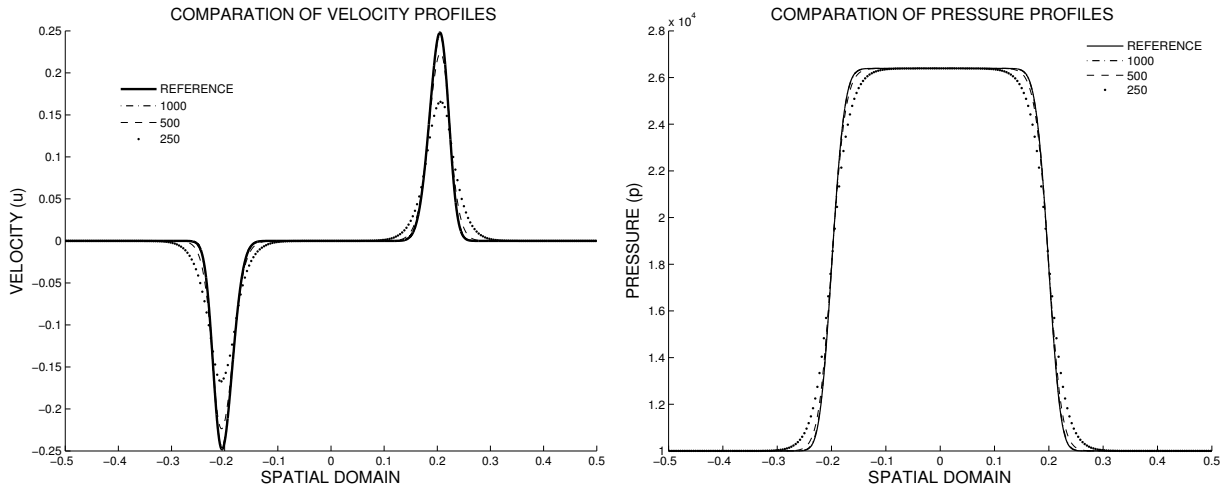

Figure 1.3: In [38] the authors have developed a precise numerical methodology based on a Godunov-type scheme on the model problem of Euler system with gravity and friction; such scheme exhibits the good properties to be well-balanced and asymptotic preserving (see also Table 1.1). Although with less resolution, our scheme is able to capture the correct qualitative behaviour of the velocity sign (left) as well as the energy (right) source term changes. Furthermore, the computations are very stable under mesh refinement without oscillations.

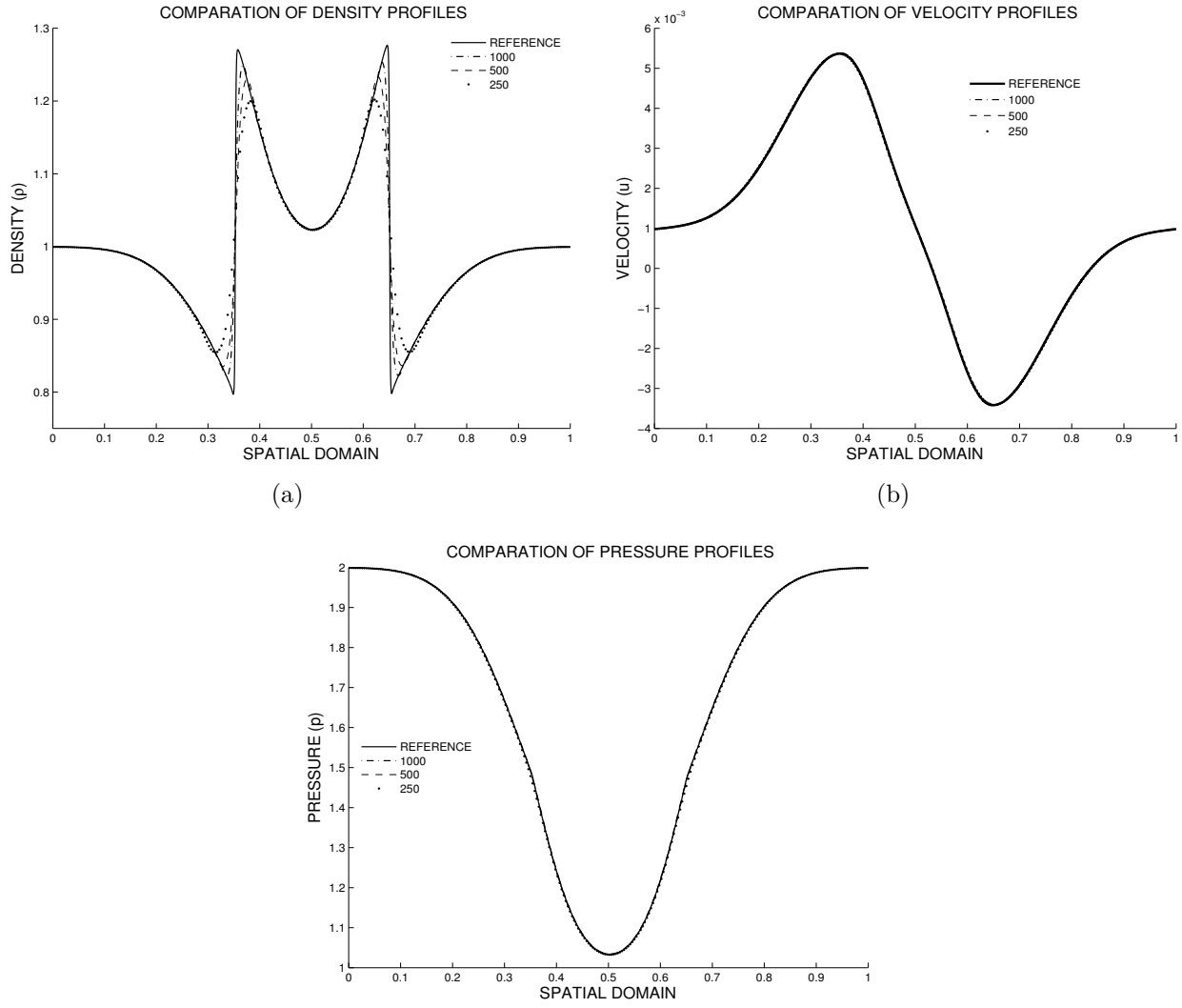

Figure 1.4: Profile comparison of density (a), velocity (b) and pressure (c) through of mesh refinement experiments; see also Table 1.2. Here our scheme is also able to capture the correct qualitative behaviour of the solutions in a coarse-grid as in [49] (which in turn is based on an asymptotic preserving scheme) yielding good verification performance upon hard test problems for gas dynamics and in connection with the Darcy-like system [107] in porous media.

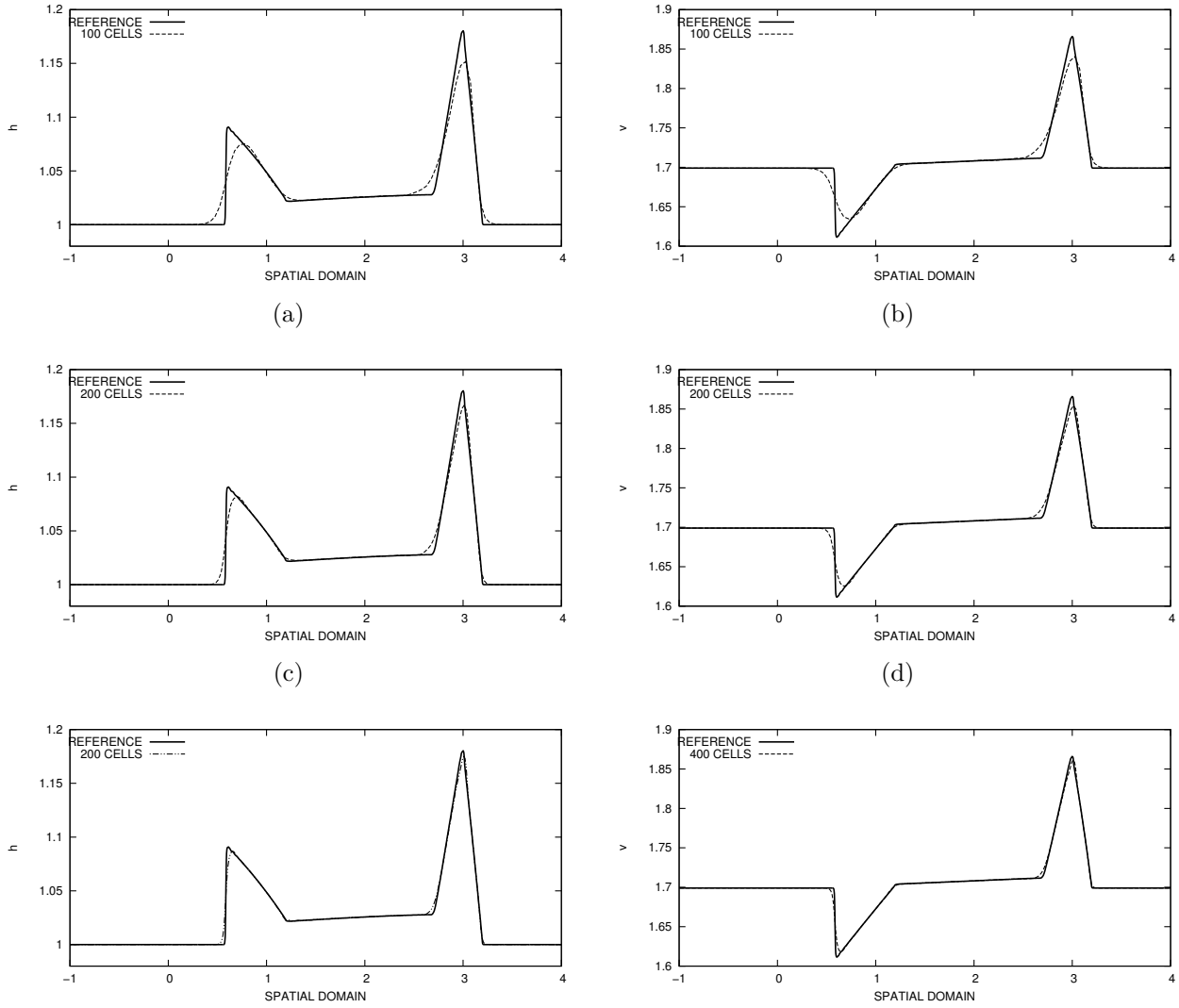

Figure 1.5: The numerical solutions are in a very good agreement to that reported in [95], corresponding to the balance between the frictional and gravitational forces as the time evolves.

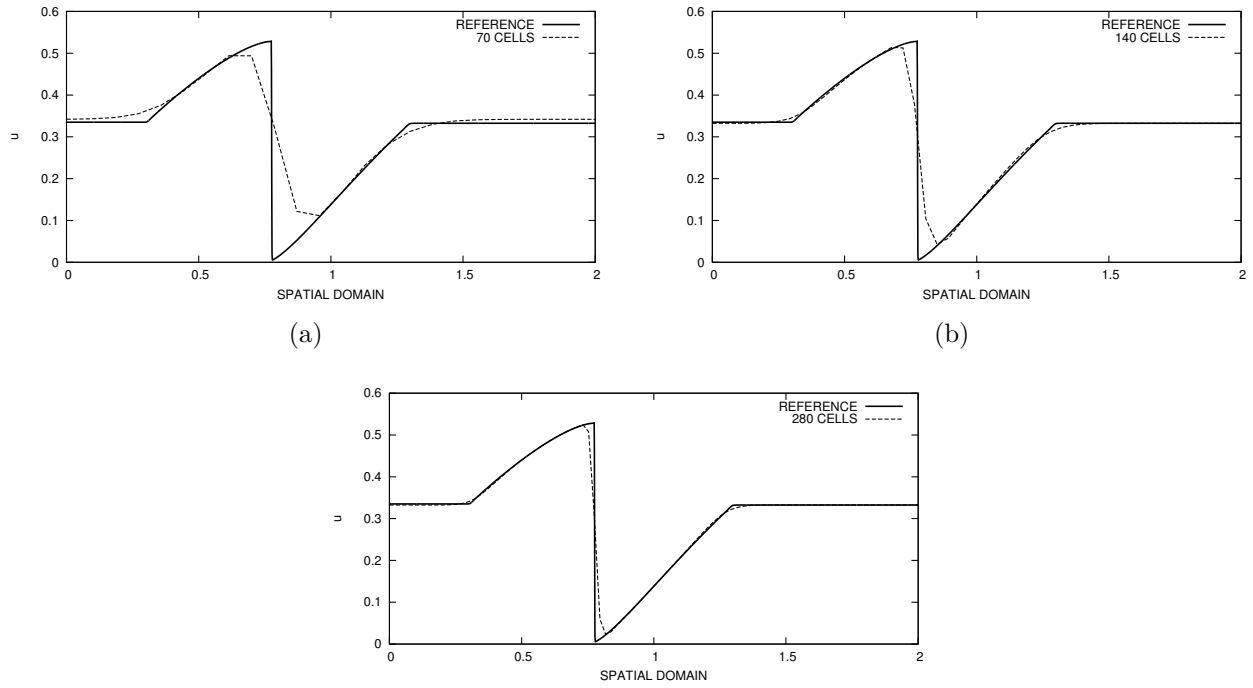

Figure 1.6: Numerical solutions with our scheme (1.14) to the model problem reported originally in Langseth et al. [95]. The reference solution in a fine mesh (2000 grids) is shown in solid line for comparison purpose with numerical approximations with 70 cells (a), 140 cells (b) and 280 cells (c). Such solutions are in a good agreement with that reported in [95], page 856; the elapsed computation times are as follows: 0.002496 segs (left), 0.004601 segs (middle) and 0.020163 segs (right).

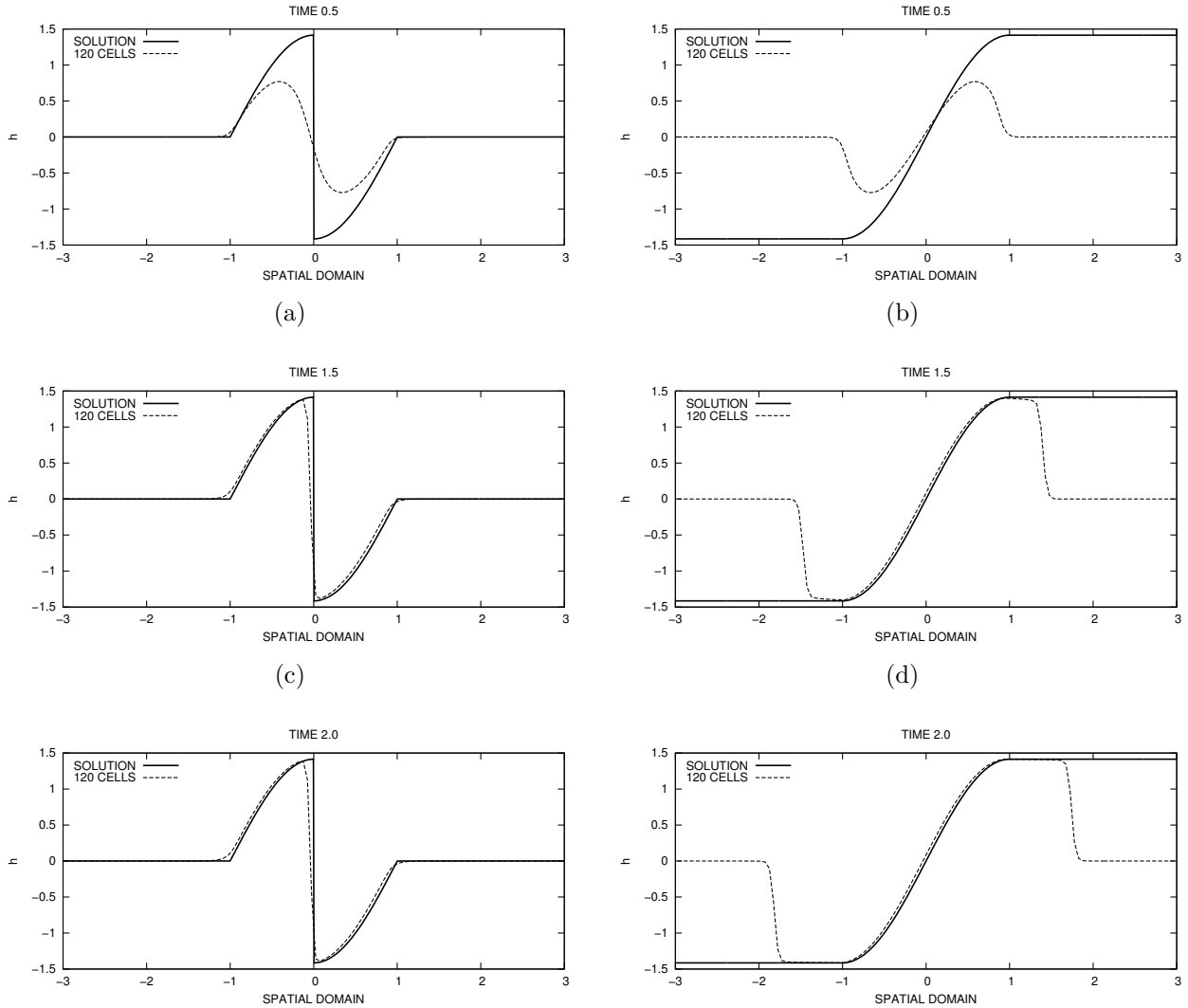

Figure 1.7: Numerical solutions for the equation (1.26) with time, $t = 0.5$ s, $t = 1.5$ s and $t = 2.0$ s., on right column we present the simulations with a function $a(x) = \cos^2(x\pi/2)$ and on left column we use $a(x) = -\cos^2(x\pi/2)$. We note that equilibrium solution for first column is obtained fastly (see Fig (c),(d)), in contrast for second case the solution evolves as time passes. Thus, based on the computed solution we can say that our method show some numerical evidence to preserve such "Well Balanced" nice property [74, 73] (see also [70]).

Chapter 2

An analysis of the existence of a non-monotonic travelling wave for Euler equations with relaxation

The mathematical structure of Euler equations systems with gravity and friction (1.24) is addressed in [31, 33, 38]. Here we focus on such model to motivate the use of a reduced isothermal Euler system, with some nonlinear properties as will be discussed next. Indeed, in many physical problems (see, e.g., [23, 31, 43, 48, 66, 69, 75, 76, 94, 128]) there is an equilibrium relationship between the variables that is essentially maintained at all times. If the solution is perturbed away from this equilibrium, then it rapidly relaxes back towards the equilibrium as introduced in [103]; see also [42]. As a concrete model we consider a simpler Euler system with a relaxation term driving the temperature towards a constant value. In this model we find a non-monotonic travelling wave, which seems to be unusual in Euler equations.

For concreteness, here we studied the existence of non-monotone travelling wave solutions and its properties. In particular we consider the Euler equation with a relaxation in a Riemann problem, for an isothermal flow for gas in one-dimensional tube surrounded by a bath at constant temperature. In order to confront our results using three different approach, we first approximate the analytical solution. Second, we use the outer expansion and finally we use our finite volume central differencing scheme to capture the same travelling wave.

2.1 Thermal relaxation Euler equation as a model problem

We study the following Euler equations with a relaxation temperature towards a constant value [99, 128]:

$$\frac{\partial}{\partial t}\begin{bmatrix}\rho\\ \rho u\\ E\end{bmatrix}+\frac{\partial}{\partial x}\begin{bmatrix}\rho u\\ \rho u^2+p\\ (\beta E+p)u\end{bmatrix}=\frac{1}{\epsilon}\begin{bmatrix}0\\ 0\\ (\overline{E}(\rho,\rho u)-E)\end{bmatrix}. \tag{2.1}$$

Quantity $\overline{E}(\rho,\rho u)$ is viewed as the required energy in the gas that results if we bring the temperature T to a reference temperature $\overline{T}$ without any disturbance in the gas system's temperature and thus with no change in momentum or density. Let is consider the equation

of state for an ideal polytropic gas reads (see [99, 128]) $p = R\rho\overline{T} = a^2\rho$, where $a = \sqrt{R\overline{T}}$ is the isometrically sound speed. Using this in the equation of state for an ideal polytropic gas, it gives

$$\overline{E}(\rho, \rho u) = \frac{a^2\rho}{\gamma - 1} + \frac{1}{2}\rho u^2.$$

The quantity ϵ is called *relaxation time*, which is associated to the time were there energy E is far from the equilibrium $\overline{E}(\rho, \rho u)$. In practice, although the time is very small, it is different from zero. Note that if we take the limit $\epsilon \to 0$, we obtain the isothermal equation

$$\frac{\partial}{\partial t}\begin{bmatrix} \rho \\ \rho u \end{bmatrix} + \frac{\partial}{\partial x}\begin{bmatrix} \rho u \\ \rho u^2 + a^2\rho \end{bmatrix} = 0, \tag{2.2}$$

that is the system (2.1) in equilibrium. Note that the subcharacteristic condition [103] is satisfied for the system (2.1) if $a \leq c$, where $c = \sqrt{\gamma p/\rho}$. In order to simplify our notations, we define the variable $m = \rho u$. To study the main features of this system, we considered a Riemann problem

$$(\rho_l, m_l, E_l), \text{ if } x \leq 0 \quad \text{and} \quad (\rho_r, m_r, E_r), \text{ if } x > 0. \tag{2.3}$$

for the system (2.1). In fact for the numerical examples we use $(m_l, \rho_l, E_l) = (2, 1, 1)$ and $(m_r, \rho_r, E_r) = (1, 0.13961, 1)$ in this chapter. We notice that the system (2.1) is more general, than that isothermal Euler model discussed in [99], which is recovered if we set $\beta = 1$. In the case $\beta = 1$ we proved there is no travelling wave structure. Furthermore, instead of [99] (since we want to address the issue of the method giving good qualitative approximate solutions close to steady states at rest), we will not only split the variables $(\rho, \rho\, u, E)$ into variables $(\rho, \rho\, u)$ with an equilibrium state E. Actually, we also explore the feature that the two first equations of the system (2.1) for the variables (ρ, m) does not depend on E, then we split the system (2.1) for $(\rho, \rho\, u)$ and we use the solution obtained for these two equations to solve the complete system by using the characteristic technique, see [62]. We will perform an approximation in the form of an asymptotic series by treating as a separate *perturbation problem* to (2.1) with respect to a near steady state.

2.1.1 A local approximate analytic solution for the isothermal Euler system

Since the two first equations of (2.1) depend only on (ρ, m), we split the system in the form of a 2×2 hyperbolic conservation system for the variables (ρ, m) as follows

$$\frac{\partial}{\partial t}\begin{bmatrix} \rho \\ m \end{bmatrix} + \frac{\partial}{\partial x}\begin{bmatrix} m \\ m^2/\rho + a^2\rho \end{bmatrix} = \begin{bmatrix} 0 \\ 0 \end{bmatrix}, \quad a \equiv \text{constant}, \quad t > 0, \quad -\infty < x < \infty, \tag{2.4}$$

from (2.3). The initial Riemann $(\rho(x,0), m(x,0))$ data for this case is,

$$(\rho(x,0), m(x,0)) = \begin{cases} (\rho_l, m_l) & \text{if } x < 0, \\ (\rho_r, m_r) & \text{if } x > 0. \end{cases} \tag{2.5}$$

We present the analysis for the case $\rho_l > \rho_r$ and $m_l > m_r$; similar calculations can be done for other Riemann problems. It is an exercise to see that (2.4) is strictly hyperbolic (i.e., the

eigenvalues of Jacobian flux function are real and distinct, thus, it has a complete set of right eigenvectors) using the Lax theory (see [52]), and we obtain the Riemann solution to (2.4)-(2.5) (see the solution in Figure 2.1),

$$\rho(x,t) = \begin{cases} \rho_l, & \text{if } x < t\,\lambda_l, \\ \rho_l e^{-\dfrac{(x/t-\eta_l)}{a}}, & \text{if } t\,\lambda_l \le x < t\,\lambda_m, \\ \rho_m, & \text{if } t\,\lambda_m \le x < t\,s, \\ \rho_r, & \text{if } t\,s \le x, \end{cases} \tag{2.6a}$$

$$m(x,t) = \begin{cases} m_l, & \text{if } x < t\,\lambda_l, \\ \rho_l\left(\dfrac{x}{t}+a\right) e^{-\dfrac{(x/t-\eta_l)}{a}}, & \text{if } t\,\lambda_l \le x < t\,\lambda_m, \\ m_m, & \text{if } t\,\lambda_m \le x < t\,s, \\ m_r, & \text{if } t\,s \le x, \end{cases} \tag{2.6b}$$

where (ρ_m, m_m) is an intermediate state, $s \equiv m_m/\rho_m + \sqrt{\rho_r/\rho_m}$, $\eta_l = \lambda_l \equiv \frac{m_l}{\rho_l} - a$, and $\lambda_m \equiv \frac{m_m}{\rho_m} - a$. Thus, the analytical solution for the reduced Euler system (2.4)-(2.5) is given by (2.6).

Now we will able to find the solution for the energy $E = E(x,t)$, which is governed by the third equation of the system (2.1). First, we set the initial condition $E(x,0) = E_0 \equiv 1$. Notice that we can set any initial value for E_0, since the solution will reach the equilibrium very fast and does not dependent on the initial data.

To solve the equation for $E(x,t)$, we take into account the solutions of system (2.4)-(2.5). Since we are interested in apply the method of characteristic lines, see [62], we will need smooth solutions for ρ and m. However, from (2.6), we can see that the solution exhibits discontinuities (shocks), rarefactions and constant states. We can smooth solutions using the convolution with a mollifier. Thus, we can use the heat kernel, which is a very known mollifier to regularize functions in the variable x, which we denoted by, $K_\tau(x,y) = \dfrac{1}{\sqrt{\pi\tau}} exp\left(-\dfrac{(x-y)^2}{\tau}\right)$.

Then, the regularized solutions for $\rho(x,t)$ and $m(x,t)$ with a fixed time $t = t^*$ are written as (again, see the solutions in Figure 2.1),

$$\rho_\tau(x,t^*) = \frac{1}{\sqrt{\pi\tau}} \int_{-\infty}^{\infty} exp\left(-\frac{(x-y)^2}{\tau}\right) \rho(y,t^*)\,dy, \tag{2.7}$$

and

$$m_\tau(x,t^*) = \frac{1}{\sqrt{\pi\tau}} \int_{-\infty}^{\infty} exp\left(-\frac{(x-y)^2}{\tau}\right) m(y,t^*)\,dy. \tag{2.8}$$

First of all, we notice from (2.7) that we can prove that functions $\rho_\tau(x,t^*)$ and $m_\tau(x,t^*)$ are $\mathcal{C}^\infty(\Omega)$ with $\Omega \subset \mathbb{R}$ is open and bounded functions over $\overline{\Omega}$. In the second place, from the previous fact and by means of Theorem 6, pag. 630 of [62], we can prove that for $\tau \longrightarrow 0$ we have convergence of $\rho_\tau(x,t^*) \longrightarrow \rho(x,t^*)$ and $m_\tau(x,t^*) \longrightarrow m(x,t^*)$, in $L^p(\Omega)$.

We use $\rho_\tau(x,t)$ and $m_\tau(x,t)$ into the third equation of (2.1) to find (after a bit of calculation) the initial value problem for $E = E(x,t)$

$$E_t + E_x\,\beta\,\frac{m_\tau}{\rho_\tau} = -E\left(\left[\beta\frac{m_\tau}{\rho_\tau}\right]_x + \frac{1}{\epsilon}\right) + \frac{1}{\epsilon}\left(\frac{a^2\rho_\tau}{\gamma-1} + \frac{1}{2}\frac{m_\tau^2}{\rho_\tau}\right) - a^2\,[m_\tau]_x\,. \tag{2.9}$$

Since ρ_τ and m_τ are functions of x and t, the equation (2.9) is a scalar linear partial differential equation with non-constant coefficients, which we can be solved using the characteristic method, see [62]. After some manipulation, we find what we call an *approximate analytical system for (2.9)*

$$\frac{dx}{dt} = \beta\frac{m_\tau}{\rho_\tau}, \quad \frac{dE}{dt} = -E\left(\beta\left[\frac{m_\tau}{\rho_\tau}\right]_x + \frac{1}{\epsilon}\right) + \frac{1}{\epsilon}\left(\frac{a^2\rho_\tau}{\gamma-1} + \frac{1}{2}\frac{m_\tau^2}{\rho_\tau}\right) - a^2\left[m_\tau\right]_x, \tag{2.10}$$
$$x(0) = x_i \quad \text{and} \quad E(x_i, 0) = E_0(x_i),$$

where $x_i \in \mathbb{R}$ is the mapping of interval of the solutions. Indeed, see the numerical experiments in Figure 2.2 for distinct values of β for the solution of characteristic curves given by (2.10). For convenience we denote

$$f(x,t) = \beta\frac{m_\tau}{\rho_\tau}, \qquad g(x,t) = -\left(\beta\left[\frac{m_\tau}{\rho_\tau}\right]_x + \frac{1}{\epsilon}\right),$$

and

$$h(x,t) = \frac{1}{\epsilon}\left(\frac{a^2\rho_\tau}{\gamma-1} + \frac{1}{2}\frac{m_\tau^2}{\rho_\tau}\right) - a^2\left[m_\tau\right]_x \tag{2.11}$$

(which are $\mathcal{C}^\infty$ for $x \in \mathbb{R}$, cause each function is $\mathcal{C}^\infty$ and ρ_τ never vanishes). Solving the EDO (2.10), we obtain an implicit expression for the solution of $E(x(t), t)$ on the characteristic waves $x = x(t)$, named *approximate analytical solution*:

$$E(x(t),t) = \frac{1}{\mu(t)}\int_0^t \left(\mu(s)h(x(s),s)ds + E_0(x_i)\mu(0)\right), \tag{2.12}$$

where $\mu(t) = exp\left\{\int g(x(t),t)\,dt\right\}$.

We can state the following Proposition (**Proof See Appendix A**):

Proposition 2.1.1. *The system* (2.1) *over open set, for fixed τ the energy E_τ is bounded around the shock curve, and E_τ tends to the equilibrium solution E when $\epsilon \longrightarrow 0$. Moreover, if ϵ is fixed and $\tau \longrightarrow 0$ then $(m_\tau)_x$ tends to $(m_r - m_m)\delta_{st}$ (δ_{st} stand for Dirac delta) when m_m and m_r are the intermediary and right states for m, respectively.*

Our objective is now to illustrate numerically the trajectories of non monotonicity of the energy by means of the characteristic curves in the space-time plane (for all pictures in Figure 2.2, and for several distinct values of β discussed here, which can be viewed as related to friction and gravity terms in connection to the porous media equation [107]), which in turn we show that for fixed τ the energy E is bounded around the shock curve, and E tends to the equilibrium solution when $\epsilon \longrightarrow 0$. The profile wave provide visual verification of the nature of the non-monotonic travelling wave solutions for gas dynamics Euler equations with stiff relaxation source terms. Let us mathematically describe the behaviour of the Energy E as we change β; this can be viewed as different regimes controlled by the interplay of energy, velocity, pressure and density induced by friction and gravity for more general models. On 2.2(a) shows that the characteristics curves are parallel straight lines for $\beta = 0$. The Figure 2.2(b) we take $\beta = 1$. Notice that there is a similar region as such of a rarefaction wave on the (t, x)-plane just after coming out of the curve at $x = 0$. The shock curve with Rankine-Hugoniot speed s from the reduced system (2.4) for variable (ρ, m) will cross over the characteristic curves there and

at the same with interaction upon the solution of E: the solution does not display a viscous profile in this case, proved in Section 2.3. In Figure 2.2(c) shows that for $\beta = 8$ can be seen now that all the characteristic curves seems to collide (in fact, this will not occur thanks to the existence and uniqueness of the characteristic curves). Here, the solution clearly exhibits a viscous profile. Additionally, in this case, the shock curves cross over the characteristic curves of the solution in such way that the solution impinge upon one another at appropriate speeds on both sides of the shock s. This is not a bona fide shock, but a remarkable feature of the Euler system (2.4). The Figure 2.2(d) setting $\beta = 12$ we have found a similar qualitative behaviour of the previous case.However, the characteristics curves seems to impinge faster leading to a bona fide shock wave: here the solution also exhibits a viscous profile, see Section 2.3. Similar conclusions for the quantities energy, velocity, pressure and density are related to the analysis reported in Section 2.2 and in Section 2.3.

2.2 Outer expansion analysis for the solution

We can also study another approximation technique for the Riemann problem for system (2.1), the *asymptotic expansion*. This technique is well known and widely used to obtain several degrees of approximation of solution far from the manifold equilibrium $\mathcal{E}$, which is given by:

$$\mathcal{E} = \left\{ (\rho, m, E), \text{ such that } E = \frac{a^2\rho}{\gamma - 1} + \frac{1}{2}\rho u^2 \right\}. \tag{2.13}$$

This technique is valuable in order to validate the qualitative behaviour of our numerical method and to find the order of each amplification factor. Here is our we first attempt to address an "outer expansion" for the Euler equations (2.1). Thus, let us consider

$$U_j = (\rho_j(x,t), (m)_j(x,t), E_j(x,t))^\top.$$

We will assume the solution of the system (1.3) reads,

$$U = U_0 + \epsilon U_1 + \epsilon^2 U_2 + \cdots, \qquad \text{where } U_0, U_1, U_2, \cdots, \tag{2.14}$$

are the approximations of the solution for each order. Notice that if $\epsilon \longrightarrow 0$, the solution tends to U_0, that is the equilibrium solution. But we are interested in the behaviour of the solution for non-zero ϵ.

Remark 2.2.1. *We stress out that our analysis is formal, without a proper convergence analysis, where is described some conditions to convergence and stability of this expansion, besides the technique described in Section* 2.2.1.

We also expand the initial conditions (2.5) as $\rho(x,0) = \rho_0(x,0) + \epsilon\rho_1(x,0) + \epsilon^2\rho_2(x,0) + \cdots$ and $m(x,0) = m_0(x,0) + \epsilon m_1(x,0) + \epsilon^2 m_2(x,0) + \cdots$. Since the initial data for $\rho(x,0)$ and $m(x,0)$ are on the equilibrium manifold $\mathcal{E}$, we fix: $\rho_1(x,0) = \rho_2(x,0) = \cdots = 0$ and $m_1(x,0) = m_2(x,0) = \cdots = 0$. In calculations below it is not necessary to know the initial values for the variable $E(x,0)$, because each order of the energy is obtained as function of ρ, m and previous orders of E. Connecting the approximation (2.14) into (2.1) and matching coefficients of adequate order power ϵ reads:

1. Order $\mathcal{O}(\epsilon^0)$, the energy $E_0 = \dfrac{a^2\rho_0}{\gamma-1} + \dfrac{1}{2}\dfrac{m_0^2}{\rho_0}$, where ρ_0 and m_0 are solutions of $(\rho_0)_t + (m_0)_x = 0$ and with $\rho_0(x,0)$ and $m_0(x,0)$ are the initial Riemann condition.

2. Order $\mathcal{O}(\epsilon^1)$, the energy E_1 is given by:

$$E_1 = -E_{0t} - \left(\frac{E_0 m_0}{\rho_0} + a^2 m_0\right)_x + \frac{a^2\rho_1}{\gamma-1} + \frac{1}{2}\left(2\frac{m_0 m_1}{\rho_0} - \frac{m_0^2}{\rho_0^2}\rho_1\right). \tag{2.15}$$

   where ρ_1 and m_1 are solutions of $(\rho_1)_t + (m_1)_x = 0$ and $m_{1t} + \left(\frac{2m_0m_1}{\rho_0} - \frac{m_0\rho_1}{rho_0^2} + a^2\rho_1\right)_x = 0$. Notice that $\rho_1(x,0) = m_1(x,0) = 0$, so from the existence and uniqueness of solution we have $m_1(x,t) = \rho_1(x,t) = 0$. From (2.15), we get:

$$E_1 = -E_{0t} - \left(\frac{E_0\beta m_0}{\rho_0} + a^2 m_0\right)_x. \tag{2.16}$$

3. Order $\mathcal{O}(\epsilon^n)$, the energy E_n for $n = 2, 3, 4, \cdots$ is as follows: by using the same arguments, one can prove that $\rho_i(x,t) = m_i(x,t) = 0$ for $i = 1, 2, 3, \cdots$. After the calculations the n-th order energy $E_n(x,t)$ is given by solving:

$$E_n = -(E_{n-1})_t - \left(E_{n-1}\beta\frac{m_0}{\rho_0}\right)_x. \tag{2.17}$$

2.2.1 Asymptotic analysis around constant states, shock and rarefactions

The asymptotic expansion is a well known technique, but there are some obstacles to apply it for hyperbolic equations. The first problem appears because the zero order approximation solutions on the equilibrium manifold $\mathcal{E}$ exhibits discontinuities and non-smooth regions. The first attempt to overcome this problem is to regularize the solutions by using mollifiers. However, we have another difficulty, the equations are non-linear, exhibiting time derivatives, which are very hard to take, even numerically. To overcome both problems, we propose a new way to perform the asymptotic expansion for system of equations of the same class of (2.1). Our technique is based on the main ingredients building the Riemann solution: shocks, rarefactions and constant states, see [52].

To obtain this technique, we substitute the asymptotic expansion (2.14) into (2.1)-(2.3) and we perform some simplifications, which allow us split the expansion in three regions: constant states, shock and rarefaction regions. However, the shock region is actually only a single point travelling with speed s. It is impossible to obtain derivatives on this region. So, we propose a region of regularization around the point st (for any time t) of lenght 2δ, i.e., $st-\delta \leq x \leq st+\delta$.

Then, we split the (x,t) space as:

1. The 2δ shock region given by $\mathcal{R}_{s,\delta} = \{(x,t) \text{ such that } st-\delta \leq x \leq st+\delta\}$.

2. The rarefaction region $\mathcal{R}_r = \{(x,t) \text{ such that } \lambda_l t \leq x \leq \lambda_m t\}$.

3. The constant region $\mathcal{R}_c = \{(x,t) \text{ such that } (x,t) \notin \mathcal{R}_{s,\delta} \cup \mathcal{R}_r\}$,

here λ_l is the eigenvalue evaluated in the left state (ρ_l, m_l) and λ_m is the eigenvalue evaluated in the intermediate state (ρ_m, m_m). Notice that for $t > (s-\lambda_m)\delta$, from uniqueness of Riemann solution, we obtain that $\mathcal{R}_{s,\delta}$, $\mathcal{R}_r$ and $\mathcal{R}_c$ are disjoint regions. Since δ is very small, our approximation is performed by assuming that $t > (s-\lambda_m)\delta$ and the regions are disjoint.

2.2.1.1 On the constant regions, i.e., $(x,t) \in \mathcal{R}_c$

The system of partial differential equations becomes an ordinary equation for the energy,

$$\frac{dE}{dt} = \frac{1}{\epsilon}\left(-E + \frac{a^2\rho_\tau}{\gamma-1} + \frac{1}{2}\frac{m_\tau^2}{\rho_\tau}\right).$$

The general solution is

$$E(x,t) = \frac{a^2\rho_\tau}{\gamma-1} + \frac{1}{2}\frac{m_\tau^2}{\rho_\tau} + \left(E(x,0) - \frac{a^2\rho_\tau}{\gamma-1} - \frac{1}{2}\frac{m_\tau^2}{\rho_\tau}\right) exp(-t/\epsilon), \tag{2.18}$$

where $E(x,0)$ is the initial condition. Notice that E reaches the equilibrium very fast, then we assume that the constant states are in equilibrium in order to calculate each order of approximation at shock and rarefaction regions, i.e., $E_1 = E_2 = \cdots = 0$.

2.2.1.2 On the shock region, i.e., $(x,t) \in \mathcal{R}_c$

We notice that the shock travels without changing the profile, then the solution depends on the variable $\eta = x - st$. We perform a regularization, first for the solutions ρ_0 and m_0, and next for E_0, in such way that the shock becomes a smooth function connecting (ρ_m, m_m) and (ρ_r, m_r); here we used (2.7). We notice that in the shock region the solution does not change in the variable $\eta = x - st$, for $(x,t) \in \mathcal{R}_{s,\delta}$, so we can apply the chain rule such that we can write the operators $\partial/\partial t = -sd/d\eta$ and $\partial/\partial x = d/d\eta$. Applying this strategies in Eqs. (2.16) and (2.17), we obtain each order of approximation in $\mathcal{R}_{s,\delta}$, which we denote as $E_{n,s}$ for $n = 0, 1, 2, \cdots$. The variables $m_{0,s}$ and $\rho_{0,s}$ represent m_0 and ρ_0 for $(x,t) \in \mathcal{R}_{s,\delta}$. The first order $E_{1,s}$ is written:

$$\begin{aligned} E_{1,s} &= s\frac{d}{d\eta}E_{0,s} - \frac{d}{d\eta}\left(\frac{\beta m_{0,s}}{\rho_{0,s}}E_{0,s}\right) - a^2\frac{d}{d\eta}m_{0,s} \\ &= \left(s\frac{d}{d\eta} - \frac{d}{d\eta}\left(\frac{\beta m_{0,s}}{\rho_{0,s}}\right)\right)E_{0,s} - a^2\frac{d}{d\eta}m_{0,s}. \end{aligned} \tag{2.19}$$

By (2.17) $E_{n,s}$ becomes:

$$\begin{aligned} E_{n,s} &= s\frac{d}{d\eta}E_{n-1,s} - \frac{d}{d\eta}\left(\frac{\beta m_{0,s}}{\rho_{0,s}}E_{n-1,s}\right) \\ &= \left(s\frac{d}{d\eta} - \frac{d}{d\eta}\left(\frac{\beta m_{0,s}}{\rho_{0,s}}\right)\right)E_{n-1,s}. \end{aligned} \tag{2.20}$$

Applying, recursively, $E_{n,s}$, for $n = 2, 3, \cdots$, we obtain:

$$E_{n,s} = \left(s\frac{d}{d\eta} - \frac{d}{d\eta}\left(\frac{\beta m_{0,s}}{\rho_{0,s}}\right)\right)\cdots\left(s\frac{d}{d\eta} - \frac{d}{d\eta}\left(\frac{\beta m_{0,s}}{\rho_{0,s}}\right)\right)E_{1,s} = \left(s\frac{d}{d\eta} - \frac{d}{d\eta}\left(\frac{\beta m_{0,s}}{\rho_{0,s}}\right)\right)^{n-1}E_{1,s}.$$

The index $n-1$ on operator $\left(s\frac{d}{d\eta} - \frac{d}{d\eta}\left(\frac{\beta m_{0,s}}{\rho_{0,s}}\right)\right)$ indicates that we apply this operator $n-1$ times on E_1. Substituting E_1 given by (2.19), we finally obtain:

$$E_{n,s} = \left(s\frac{d}{d\eta} - \frac{d}{d\eta}\left(\frac{\beta m_{0,s}}{\rho_{0,s}}\right)\right)^{n}E_{0,s} - a^2\left(s\frac{d}{d\eta} - \frac{d}{d\eta}\left(\frac{\beta m_{0,s}}{\rho_{0,s}}\right)\right)^{n-1}\frac{d}{d\eta}m_{0,s}. \tag{2.21}$$

2.2.1.3 On the rarefaction region, i.e., $(x,t) \in \mathcal{R}_c$

Following [92], we notice that each order of approximation E_n depends only on the variable $\xi = x/t$. Moreover, the expansion decays with the time t, as:

$$E(x,t) = E_0(\xi) + \frac{1}{t}\left(\epsilon E_1(\xi) + \epsilon^2 E_2(\xi) + \epsilon^3 E_3(\xi) + \cdots\right). \tag{2.22}$$

We denote each order of approximation E_n and functions m_0 and ρ_0 for $(x,t) \in \mathcal{R}_c$ as $E_{n,r}$, $m_{0,r}$ and $\rho_{0,r}$. To get each order of approximation we use $E(x,t)$, given by Eq. (2.22). We substitute each order of approximation $E_{n,r}/t$ for $n = 1, 2, \cdots$ in Eq. (2.16) for $n = 1$ and in Eq. (2.17) for $n = 2, 3, \cdots$. Since we assume that $E_{n,r}$ depends only on $\xi = x/t$, we apply the chain rule $\partial/\partial t = -(\xi/t)d/d\xi$ and $\partial/\partial x = (1/t)d/d\xi$, we obtain:

$$\frac{E_{1,r}}{t} = \frac{\xi}{t}\frac{d}{d\xi}E_{0,r} - \frac{1}{t}\frac{d}{d\xi}\left(\frac{\beta m_{0,r}}{\rho_{0,r}}E_{0,r}\right) - a^2\frac{1}{t}\frac{d}{d\xi}m_{0,s} = \left(\xi\frac{d}{d\xi} - \frac{d}{d\xi}\left(\frac{\beta m_{0,r}}{\rho_{0,r}}\right)\right)E_{0,r} - a^2\frac{d}{d\eta}m_{0,r}. \tag{2.23}$$

By using Eq. (2.17), and the chain rule, $E_{n,r}$ becomes:

$$\begin{aligned}\frac{E_{n,r}}{t} &= \frac{\xi}{t}\frac{d}{d\xi}E_{n-1,r} - \frac{1}{t}\frac{d}{d\xi}\left(\frac{\beta m_{0,r}}{\rho_{0,r}}E_{n-1,r}\right)\\ &= \left(\xi\frac{d}{d\xi} - \frac{d}{d\xi}\left(\frac{\beta m_{0,r}}{\rho_{0,r}}\right)\right)E_{n-1,r}\end{aligned}$$

On applying, recursively, $E_{n,r}$ and using $E_{1,r}$, given by Eq. (2.23), we obtain,

$$E_{n,r} = \left(\xi\frac{d}{d\xi} - \frac{d}{d\xi}\left(\frac{\beta m_{0,r}}{\rho_{0,r}}\right)\right)^n E_{0,r} - a^2\left(\xi\frac{d}{d\xi} - \frac{d}{d\xi}\left(\frac{\beta m_{0,r}}{\rho_{0,r}}\right)\right)^{n-1}\frac{d}{d\xi}m_{0,r}. \tag{2.24}$$

2.2.1.4 Composing the solutions

Applying this technique, we obtain each order of approximation E_n, for $n = 1, 2, \cdots$, given as,

$$E_n(x,t) = 0, \text{ if } x \in \mathcal{R}_c, \qquad E_n(x,t) = E_{n,s}, \text{ if } x \in \mathcal{R}_{s,\delta}, \qquad E_n(x,t) = E_{n,r}, \text{ if } x \in \mathcal{R}_r. \tag{2.25}$$

This solution is, in general, not continuous. However, we can regularize this solution by using the same heat kernel to obtain a continuous function for each order of approximation, which we also denote as $E_n(x,t)$ and is given by

$$E_n(x,t) = \frac{1}{\sqrt{\pi\gamma}}\int exp\left(-\frac{(x-y)^2}{\gamma}\right)E_n(y,t)dy, \tag{2.26}$$

for some very small positive constant γ.

In the numerical experiments reported in Figure 2.3, we obtain the equilibrium solution and the first and second corrections. In this expansion we use two different regularizations for the shock, along with a detailed discussion as follows. On the left picture in Figure 2.3 we represent the profile wave: the equilibrium (E_0), the first approximation ($E_0 + \epsilon E_1$), and the second approximation ($E_0 + \epsilon E_1 + \epsilon^2 E_2$). Here the regularization used for the shock region is

given by Eq. (2.7), with $\tau = 0.01$ and $\epsilon = 0.1$. Notice that the first order solution has the correct direction of the solution, however the second order exhibits an oscillatory behaviour. The oscillation occurs because this regularization has derivatives that changes very fast its behaviour in order to become smooth, moreover, when $\tau < \epsilon$ and for each derivative the solution is scaled as $1/\tau$, and then the solution is unstable. In Figure 2.3, right picture, the regularization used for the shock region is shown as two straight line. One line connects ρ_l and ρ_r with slope $(\rho_r - \rho_l)/(2\tau)$, the other one connects m_l and m_r with slope $(m_r - m_l)/(2\tau)$. Here $\tau = 0.05$ and $\epsilon = 0.1$. Notice, that the solution is more suitable to the correct solution. An important question that arises in this analysis is: "What is the good size of τ?".

2.3 Conditions for the existence of travelling wave solutions

The solution given by (2.7) is a solution that essentially account for the qualitative behaviour of system (2.1)-(2.3). The latter is shown to exhibit an unusual non-monotonic behaviour with high gradient variation in the variable m as a function of the interaction, parameters which can be understood as a natural consequence of the nonlinear interacting balance between the source terms and the flux gradients of (2.10) linked to the friction mechanism, which might be interpreted in terms of the porous media equations as also described in the literature [107]. We verify the stability of the non-monotonic wave by analysing the solutions of the regularized problem. Thus, a very natural question is: what is the mathematical nature of this wave? By means of a large number of numerical simulations it was found strong evidence that the wave profile of such a wave does not change for long times (asymptotic behaviour). Thus, would this be a travelling wave solution? Indeed, such analysis will also be important for a qualitative validation of the new finite volume method developed.

The travelling wave is one of several techniques used to "select" the entropy shocks that are physically feasible. The existence study of a travelling wave is one of the main tools for analysing problems involving hyperbolic conservation laws in order to know if a shock, in fact, comes from a physical admissible system.

Thus it is natural to use this technique to analyse under what conditions the mathematical wave containing a peak in the variable E correspond to a *bona fide* travelling wave. This technique introduces a artificial diffusion scaling η to system (2.1), which is written as:

$$\begin{aligned} \frac{\partial}{\partial t}\rho + \frac{\partial}{\partial x}m &= \eta\frac{\partial^2}{\partial x^2}\rho, \\ \frac{\partial}{\partial t}m + \frac{\partial}{\partial x}\left(\frac{m^2}{\rho} + a^2\rho\right) &= \eta\frac{\partial^2}{\partial x^2}m, \\ \frac{\partial}{\partial t}E + \frac{\partial}{\partial x}\left[\beta E\frac{m}{\rho} + a^2 m\right] &= \frac{1}{\epsilon}\left(\frac{a^2\rho}{\gamma - 1} + \frac{1}{2}\frac{m^2}{\rho} - E\right). \end{aligned} \tag{2.27}$$

The key question is: under what conditions, the shock connecting (ρ_m, m_m) and (ρ_r, m_r) behaves like a travelling wave solution? In other words, a state variable solution $U^\eta = (\rho, m, E)$ of (2.27) can be written in a travelling coordinate system $\dfrac{x - st}{\eta}$, where $U^\eta = U\left(\dfrac{x - st}{\eta}\right)$ such that $s = \dfrac{m_r - m_n}{\rho_r - \rho_m}$ is the speed of shock wave. Notice that for the new variable η, the existence

of the viscous profile is associated to the existence of a wave connecting the state (ρ_m, m_m, E_m) when $\eta \longrightarrow -\infty$ with the state (ρ_r, m_r, E_r) when $\eta \longrightarrow +\infty$. Substituting $U^\eta = (\rho, m, E)$ into (2.27) leads to the ODE system,

$$\begin{aligned}
\frac{-s}{\eta}\frac{dp}{d\xi} + \frac{1}{\eta}\frac{dm}{d\xi} &= \frac{\eta}{\eta^2}\frac{d^2\rho}{d\xi^2},\\
\frac{-s}{\eta}\frac{dp}{d\xi} + \frac{1}{\eta}\frac{dm}{d\xi}\left(\frac{m^2}{\rho} + a^2\rho\right) &= \frac{\eta}{\eta^2}\frac{d^2m}{d\xi^2},\\
-s\frac{dE}{d\xi} + \frac{d}{d\xi}\left[\beta E\frac{m}{\rho} + a^2 m\right] &= \frac{\eta}{\epsilon}\left(\frac{a^2\rho}{\gamma-1} + \frac{1}{2}\frac{m^2}{\rho} - E\right).
\end{aligned}$$

By performing integration in the first two equations of the system above over interval $(-\infty, \xi)$ respect to variable ξ, and from the fact that solutions $\frac{d}{d\xi}\rho$ and $\frac{d}{d\xi}m$ are equilibria vanishing at infinity $-\infty$, it yields an ODE system at equilibrium,

$$\frac{d}{d\xi}\rho = -s\rho + m + s\rho^- - m^-, \tag{2.28}$$

$$\frac{d}{d\xi}m = -sm + \frac{m^2}{\rho} + a^2\rho + sm^- - \left(\frac{m^2}{\rho}\right)^- - a^2\rho^-, \tag{2.29}$$

$$\frac{d}{d\xi}E = \frac{1}{\left(-s + \beta\frac{m}{\rho}\right)}\left[-E\left(\frac{\eta}{\epsilon} + \beta\frac{d}{d\xi}\left(\frac{m}{\rho}\right)\right) - a^2\frac{d}{d\xi}(m) + \frac{\eta}{\epsilon}\left(\frac{a^2\rho}{\gamma-1} + \frac{1}{2}\frac{m^2}{\rho}\right)\right]. \tag{2.30}$$

Write (2.28)-(2.30) as $\frac{dV}{dt} = F(V)$ by setting $V = (\rho, m, E)^T$ and $F(V) = (F_1(V), F_2(V), F_2(V))^T$ in order to study the behaviour of the resulting nonlinear dynamical Euler system (2.28)-(2.30) near the equilibrium points, (p_m, m_m, E_m) and (p_r, m_r, E_r) with $E_m = \frac{a^2\rho_m}{\gamma-1} + \frac{1}{2}\frac{m_m^2}{\rho_m}$ and $E_r = \frac{a^2\rho_r}{\gamma-1} + \frac{1}{2}\frac{m_r^2}{\rho_r}$. The linearization of system (2.28)-(2.30) around the equilibrium points yields three distinct real eigenvalues, $\lambda_1 = -s + \frac{m^-}{\rho^-} - a$, $\lambda_2 = -s + \frac{m^-}{\rho^-} + a$ and $\lambda_3 = \frac{\frac{\eta}{\epsilon} + \beta\frac{d}{d\xi}\left(\frac{m}{\rho}\right)}{s - \beta\frac{m}{\rho}}$. Notice that the first two eigenvalues do not depend on E. This allows us to decouple the analysis with respect to the equilibrium solutions. First, we will study the existence of connecting orbits in the plane (ρ, m). Next, we will address the analysis for the variable energy E. It was found that the equilibrium (ρ_m, m_m) is a saddle point. This means that the dimension of the repeller space is 1. For the equilibrium (ρ_r, m_r) we have found it is an attractor with dimension 2. In this case the equilibrium points will be a 3-dimension connecting space. This is the classical shock satisfying Lax shock inequalities. The existence of this type of connection is well known in the literature and can be found in [52]; see also Figure 2.4. However, we are interested in analysing the existence of an orbit connecting the states E_r and E_m. Notice that by means of equation (2.30), the qualitative behaviour of the solution of the ODE follows the leading value of the coefficient multiplying E, i.e., $-\dfrac{\eta/\epsilon + \beta\frac{d}{d\xi}(m/\rho)}{(-s + \beta(m/\rho))}$. Moreover, m/ρ is constant in $x = -\infty$, i.e., for (ρ, m) equals to (ρ_m, m_m) and decreasing through ξ to $+\infty$, i.e., for (ρ, m) close to (ρ_r, m_r) e thus $\frac{d}{d\xi}(m/\rho) = 0$ at $\pm\infty$; see Figure 2.4. Indeed, $\frac{d}{d\xi}(m/\rho) < 0$ for $-\infty < x < \infty$. The same holds for $a^2\frac{d}{d\xi}(m)$, i.e., $a^2\frac{d}{d\xi}(m)$ is zero at the equilibrium points and negative in the interior of the connecting interval. Then, from Eqs. (2.30), we obtain $dE/d\xi = 0$ at $\pm\infty$.

Next, two specific analysis must be performed to understand the global behaviour of the solution. First, we assume that $s < \beta(m/\rho)$, then $-s + \beta(m/\rho) > 0$. From Eq. (2.30) we see that quantity E is stable and its behaviour depends on the ratio of two scale parameters η/ϵ; this means that we can subdivide the analysis in two parts:

case (1.1) The relationship between η/ϵ is small. Initially, $dE/d\xi$ is positive since the derivatives of m and m/ρ and its derivatives are negative. Note that these variables are solutions of the system (2.28). Thus E will grow to values satisfying $dE/d\xi = 0$, which is a maximum. In fact, this maximum is bounded and it is obtained when the energy function E takes a value determined by the following relationship between the variables ρ and m given by (see also numerical experiments in Figure 2.7):

$$E = \left(-a^2 \frac{d}{d\xi}(m) + \frac{\eta}{\epsilon}\left(\frac{a^2\rho}{\gamma - 1} + \frac{1}{2}\frac{m^2}{\rho}\right)\right)\left(\frac{\eta}{\epsilon} + \beta\frac{d}{d\xi}\left(\frac{m}{\rho}\right)\right)^{-1}. \tag{2.31}$$

It is easy to see that quantity energy E will be bounded if $\epsilon << \eta$, i.e., the relaxation occurs in a smaller scale than the diffusion scale, and thus the peak virtually does not appear, see left picture in Figure 2.5. On the other hand if $\eta >> \epsilon$, diffusion occurs in a smaller scale than the relaxation and the peak in the solution is more pronounced, see left picture in Figure 2.5.

After the maximum we have $dE/d\xi < 0$ and the function E decreases. The situation is described in details next. In left picture in Figure 2.5, we observe that the behaviour of the travelling wave depends on the relation η/ϵ. Notice that if this relation is larger, the peak almost does not appear, not appear. In contrast, for smaller value of η/ϵ the peak is pronounced. In the right picture in Figure 2.5, we observe an instability in the wave profile E for $\eta/\epsilon >> 1$. For small times of simulation, we can observe that solution diverges. For large times the solution seems to converge. This fact occurs because of the limitation of the numerical method. Actually, the energy equation becomes very stiff. This numerical behaviour leads to the erroneous interpretation of existence of the viscous profile, depending on the relation between η and ϵ. However, we prove that the existence of this profile depends only on the sign of $-s + \beta\frac{m}{\rho}$ and it is independent on the relation between relaxation time and diffusion; see also Figure 2.7. A detailed analysis can be performed on this case. Note from Equation (2.30) E satisfies (2.31) being an unstable equilibrium for the variable E. However, since $(-s + \beta(m/\rho)) > 0$, the ODE system is stable. This means that E tends again to bounded values when $\xi \longrightarrow \infty$ while $\frac{d}{d\xi}(m/\rho)$, $a^2\frac{d}{d\xi}(m)$ and $dE/d\xi$ go to zero, so, the solution tends to equilibrium. In this situation there is a stable orbit that connects the states of equilibrium E_l and E_r.

case (1.2) In this case, the relation η/ϵ is sufficiently large and $dE/d\xi < 0$ for initial states, then there is no peak in the solution for the orbit connecting the states E_l and E_r. The numerical solutions are shown in Figures 2.2(c)-2.2(d). It is shown that, for certain values of β, the characteristics curves are very close to the point of shock formation but this is not the case due to the (local) theorem of existence and uniqueness for ODEs. In this case the curves cross the shock with speed s and the information has a discontinuity in this wave, causing the solution to be, in fact, a travelling wave for system (2.28)-(2.30). Moreover, this orbit is stable for perturbation in the initial state while solving (2.30), i.e., for any initial value E the solution tends to two equilibrium E_l and E_r.

In the second case, we consider $s > \beta(m/\rho)$, then $-s + \beta(m/\rho) < 0$. From the equation (2.30) we can see that the variable E is strongly unstable and the behaviour depends strongly on the ratio η/ϵ and the relation between the two involved scales can be divided in two cases. For the cases shown below no trajectories exists for equilibrium points.

case (2.1) η/ϵ is sufficiently small. Notice that β is very small, the solution initially $dE/d\xi > 0$, because m and ρ decreases and $dm/d\xi$ is sufficiently negative. For this case, since the equation (2.30) is unstable, E is unbounded and it increases very fast to $+\infty$. If we increase β then $dE/d\xi$ quickly approaches to zero, and thus it is very hard to get a satisfactory numerical approximation. Because of this limitation we do not give any example since it is far from the scope of this work. For large β, we obtain $dE/d\xi < 0$ for initial values of E and the solution decreases to $-\infty$.

case (2.2) η/ϵ is sufficiently large. In this case we have a very interesting behaviour. This wave is unstable and does not converge. However, by using numerical approximations for large times, the equation apparently converges. This happens because of the stiffness of the system

$$\frac{d}{d\xi}E = \frac{\eta}{\epsilon}\frac{1}{\left(-s + \beta\frac{m}{\rho}\right)}\left[-E + \frac{a^2\rho}{\gamma - 1} + \frac{1}{2}\frac{m^2}{\rho}\right],$$

see Figure (2.5.*b*); in whatever way, for very small times we can see that the solution does not reach any equilibrium state and diverges. Notice that the numerical stability is hard to be obtained.

Indeed, if we see more carefully the numerical solutions shown in Figure 2.2(b) it can be seen that for small values of β we have characteristic curves that seem as if they were a rarefaction wave starting at $x = 0$ (i.e., this is not a rarefaction). Nevertheless, the wave from E is similar to a travelling wave, since the relaxation acts strongly and makes the values in this region tends rapidly to equilibrium. However, it can be seen from the results shown in Figures 2.2(b) that the shock cross the curves of the energy equation E and interacts with the solution for a long period of time. Thus, it is not possible to be the structure of a travelling wave in this case. To further study the nature of the peak associate to the non-monotone travelling wave, a more detailed analysis is made below.

The introduction of the β parameter into the reduced Euler system (2.4) allow us the ability to get the rules for which such remarkable peak behaves as a bona fide travelling wave or not. On physical grounds, the β parameter is associated with the speed at which the wave energy travels. This theoretical analysis was verified by the behaviour of the characteristic curves in the (x, t)-plane through a set of numerical experiments. For large values of the parameter β (see Figures 2.2(c) and 2.2(d)) the characteristic curves tend to impinge as such a typical behaviour of shock formation (which in fact is not the case because the reduced system is linear). Indeed, in this case, the behaviour is that of a non-monotonic travelling wave. We proved this fact by means of the analysis of the associated dynamic system for Euler system (2.4). On the other hand, for small β values, these characteristic curves open in the (x, t)-plane as an usual rarefaction fan. For such cases we prove the non-existence of the travelling wave. However, virtually, such a wave seems to behave like a travelling wave due to the small relaxation source term, which in turn makes the solution tends quickly to the equilibrium. These observations give rise to the following proposition:

Proposition 2.3.1. *The Euler system (2.1) with initial data (2.3) such that* $\rho_l > \rho_r$ *and* $m_l > m_r$ *exhibits a wave connecting* E_m *and* E_l*. Such wave is a bona fide travelling wave with speed* $s = (m_n - m_l)/(\rho_m - \rho_r)$ *for* $\beta > s(\rho/m)$*. This wave is a stable non-monotonic travelling wave with a maximum satisfying* (2.31)*. Besides, the amplitude of the peak only depends on the ratio between the scales of diffusion* η *and of relaxation* ϵ*.*

2.4 Numerical experiments linked to the order expansion approach for a Euler system model

We now turn our attention to a comparison between the numerical solution computed with our scheme discussed in Section 1.1 and the approximated analytical solution based on the discussion presented in Section 2.2 and in Section 2.3, along with an explanation with respect to the nature of the existence of the peak in the region of discontinuity of ρ and m and its relation for distinct values of β.

On the top left picture of Figure 2.7 we have a comparison between the numerical solution and the approximated analytical solution. On the top right picture of Figure 2.7 we have a comparison between the second order expansion solution and the approximated analytical solution (in the Figure 2.8 present the empirically observed order of convergence of our method for $\beta = 1$ and $\beta = 10$). Notice that for small values of β (in this example, $\beta = 1$) the numerical and the approximated analytical solution exhibit a very similar behaviour, moreover the expansion also captures the existence of a peak and the rarefaction region is very well suitable. Notice in both pictures the existence of the peak in the region of discontinuity of ρ and m. This peak does not exhibit a viscous profile for this value of β. This peak seem to exhibit a "trail".

On the top left picture of Figure 2.7 we have a comparison between the numerical solution and the approximated analytical solution. In the top right picture of Figure 2.7 we have a comparison between the second order expansion solution and the approximated analytical solution. Notice that for larger value of β (in this example, $\beta = 10$) the numerical method seems to capture better the correct behaviour of the solution and the existence of a peak with viscous profile. Since many characteristic are very close, see Figure 2.2, the approximated analytical solution is not able to capture the existence of the peak, even with a excessive number of grid cells in the x-axes to obtain the solution along the characteristics. The asymptotic expansion also exhibits the existence of this peak, which is higher than the one obtained in the numerical method because of the regularization used in this case. Also, the peak is even more concentrated than the peak in the top pictures because we prove that for $\beta = 10$, the peak has a viscous profile. It is remarkable the quality of this numerical method in both cases. Our numerical experiments point out that all the stability assumptions are fulfilled and we observe, indeed, a first-order high resolution convergence behaviour that holds uniformly in the spatial mesh width. If we increase the value of β the equation becomes more "nonlinear" and "stiff" and then we observe a reduction of the order of convergence nearly to 1, which is somewhat typical of such type of numerical integration; see the numerical convergence study in Figure 2.8.

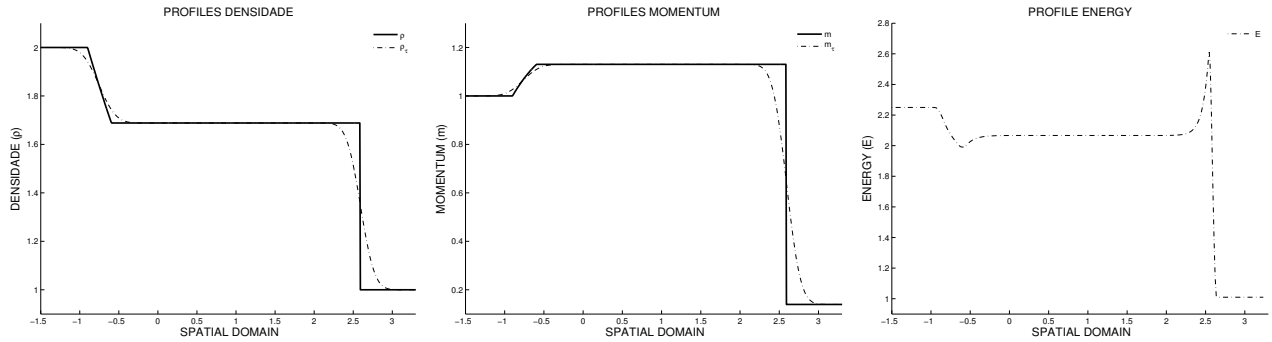

Figure 2.1: Analytical (2.6) (resp. approximated (2.7)) solution for the isothermal Euler Riemann problem given by (2.4)-(2.5) are shown in black (reps. dashed line) lines in the pictures: solutions for ρ (resp. m) are shown on the left (resp. middle) at computed time $t = 1.8$. On the right picture is shown the approximate analytical solution given by (2.10) along with $\beta = 1$.

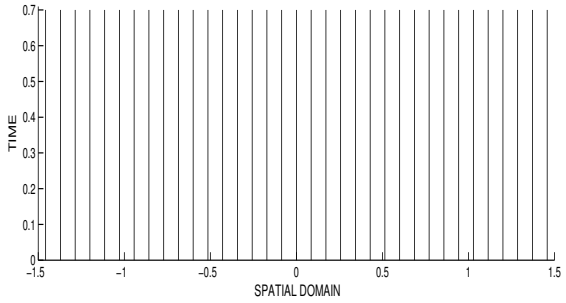

(a)

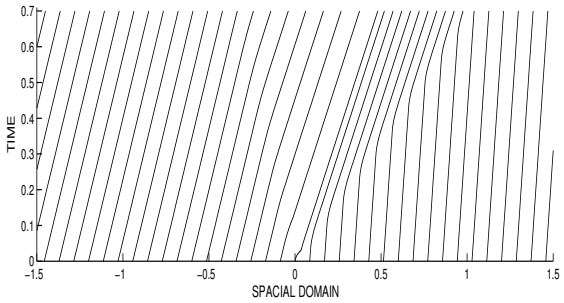

(b)

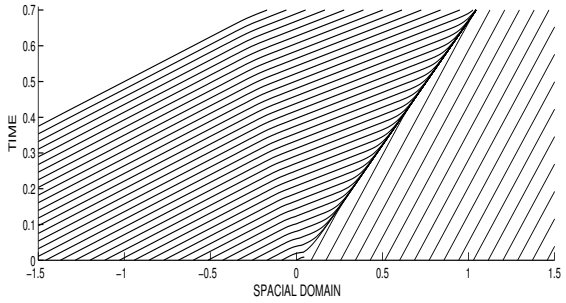

(c)

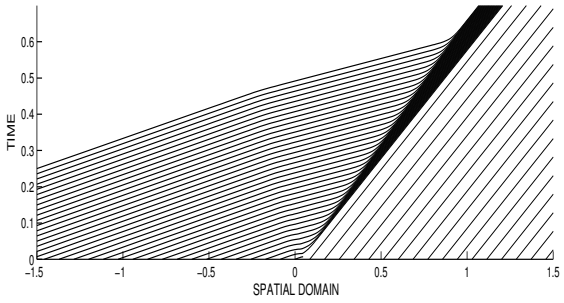

(d)

Figure 2.2: Qualitative behaviour of the non monotonic travelling wave nature for energy E solutions of gas dynamics Euler equations with stiff relaxation source terms induced by β, which, in turn, can be viewed as different regimes controlled by the interplay of friction and gravity.

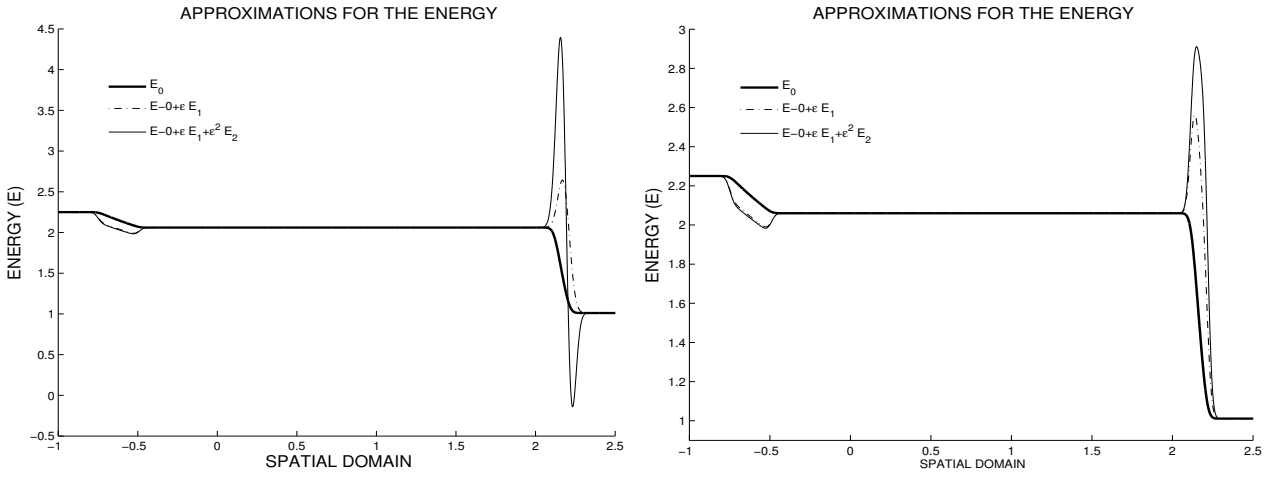

Figure 2.3: Numerical experiments to obtain the equilibrium solution along with the first and second corrections to the energy quantity E. The main question here is: "What is the good size of τ?".

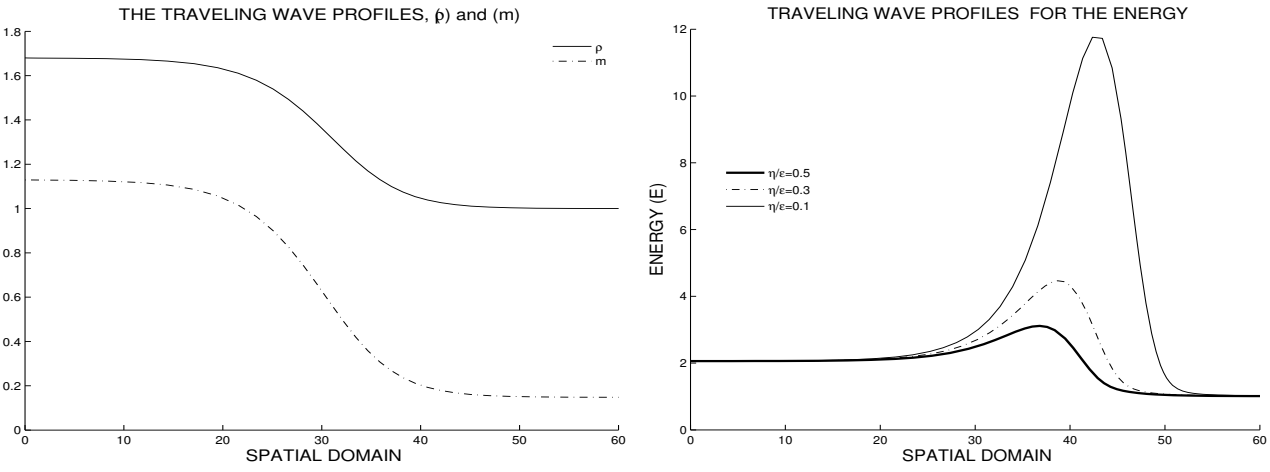

Figure 2.4: **Left:** Viscous profiles are shown for variables (ρ, m) and the connecting equilibrium states that are being connected are $(\rho_m = 1.68, m_m = 1.12)$ and $(\rho_r = 1.032, m_r = 0.186)$. **Right:** It is shown distinct orbits connecting the equilibria E_m and E_r for distinct values of the ratio η/ϵ.

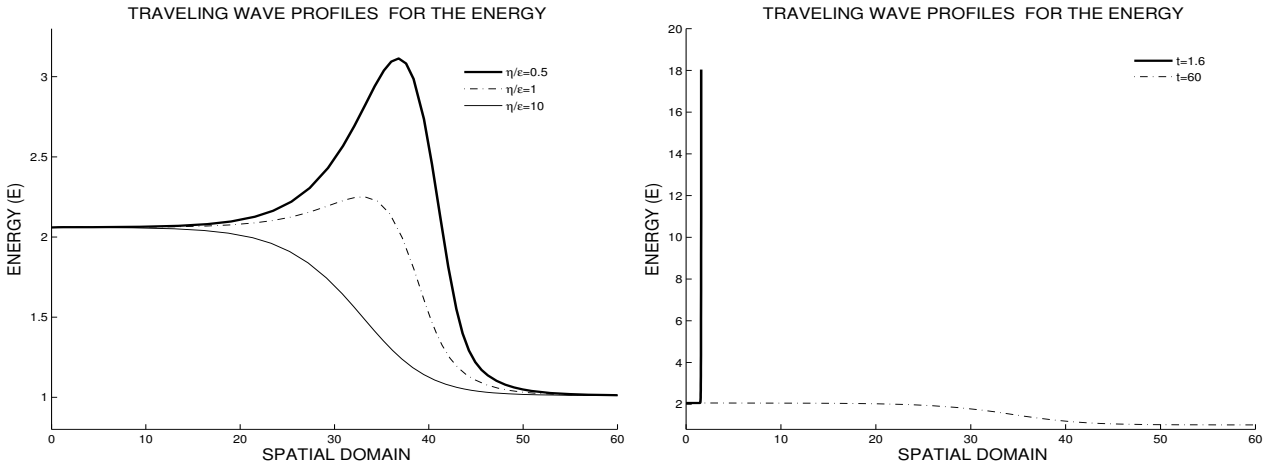

Figure 2.5: The behaviour of travelling wave depending on the relation between the parameters η and ϵ.

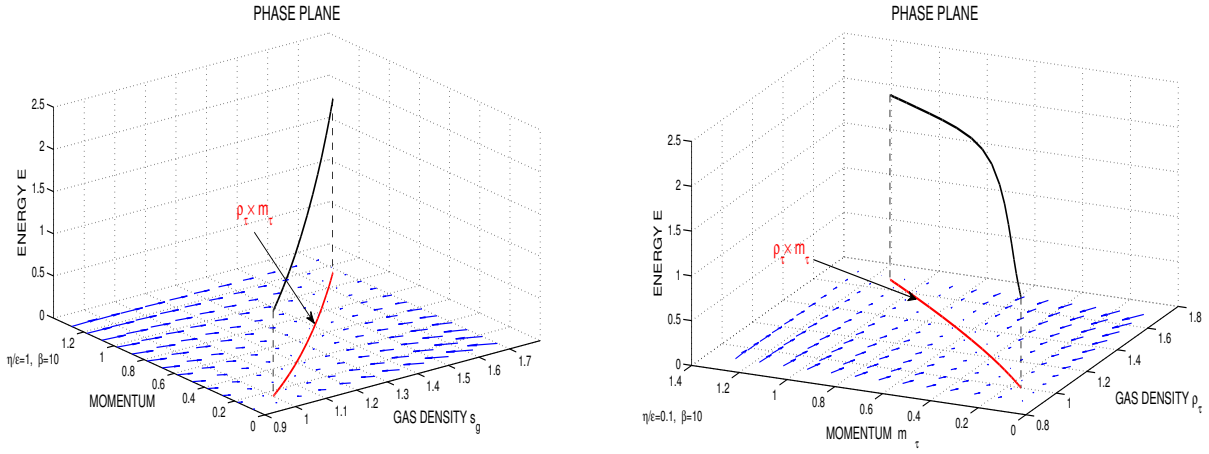

Figure 2.6: The behaviour of travelling wave depending on the relation between the parameters η and ϵ, with parameter $\beta = 10$. On left $\eta/\epsilon = 1$, on right $\eta/\epsilon = 0.1$.

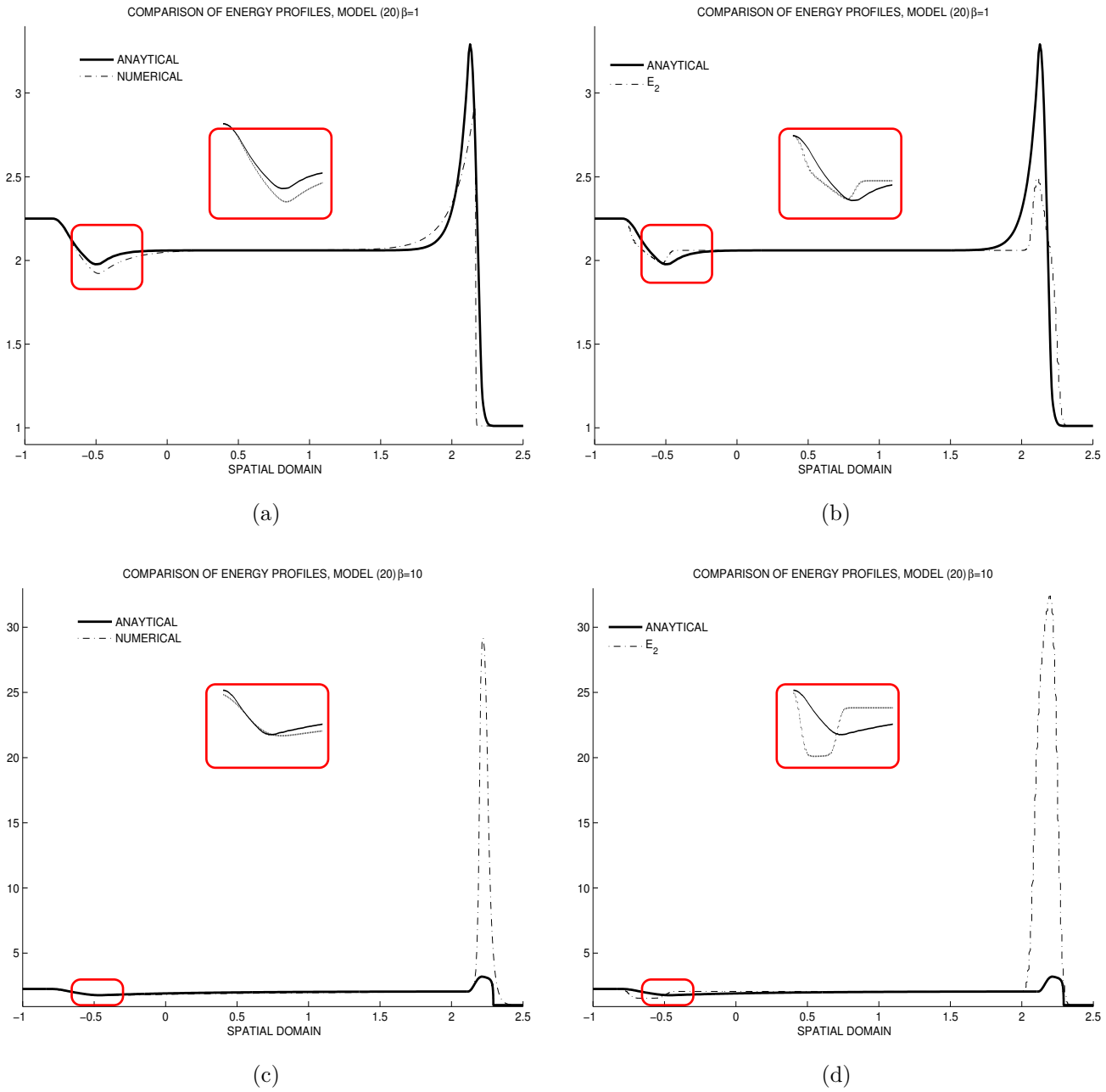

Figure 2.7: Comparison between the numerical solution (with our method; see Section 1.1) and the approximated analytical solution discussed in details in Sections 2, 2.2 and 2.3.

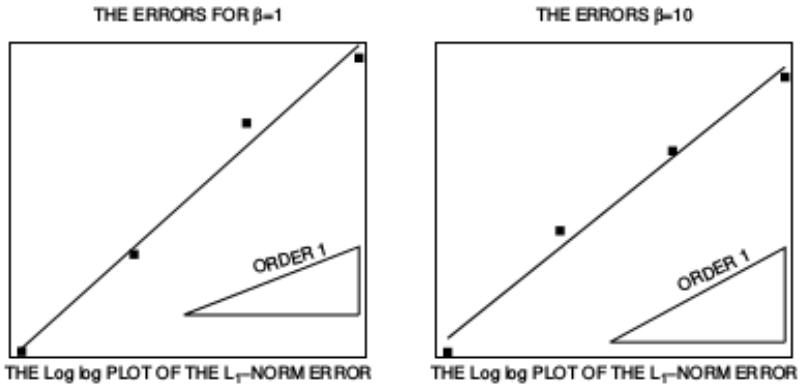

Figure 2.8: The empirically observed order of convergence (slightly greater than 1) is obtained by successively adding levels of refinement, which in turn is related to the numerical experiment reported in Fig. 2.7; $\beta = 1$ on the left and $\beta = 10$ on the right.

Chapter 3

A physical, mathematical and computational modelling for a nitrogen and steam injection in porous media

In this chapter, we give a brief description of the nitrogen and steam injection model problem in a one-dimensional porous medium with presence of water (see [35, 93, 94]). This kind of model is studied in the context of petroleum engineering. Indeed, it is an example of multiphase fluids flows with mass transfer between different phases (i.e., with phase transition). The methodology to obtain the governing systems of equations is based in using the mass balance for different chemical species in different phases, and also, an equation that represents the total energy balance; see, e.g., [36, 91, 35, 93, 94, 105]. The energy balance considered in this thesis can be obtained from conservation laws (see [90, 94]). In addition, we present a mathematical study of this model, find the all eigenparts of system and present the graphics of coincidence loci and inflection loci for its eigenvalues and find the Hugoniot locus.

3.1 Injection of nitrogen and steam in porous media

The nitrogen and steam injection problem in an one-dimensional porous media can be modelled by a 4×4 system of hyperbolic balance laws:

$$\frac{\partial}{\partial t}G(\mathcal{V}) + \frac{\partial}{\partial x}\Big(uF(\mathcal{V})\Big) = \epsilon^{-1}Q(\mathcal{V}), \quad \text{along with a rexalation time factor} \quad \epsilon > 0, \tag{3.1}$$

where G, F and Q are smooth vector-valued functions, u denote the Darcy speed (or Darcy velocity), uF_i is the flux for the accumulation vector G_i. The pair $(\mathcal{V}, u)$ is called the state variable and the variable u does not appear in the accumulation vector. The theory for this class of equations was estabilished in [93, 94]. In system (3.1), we admit that the fluids are under an incompressible regime, i.e., they can expand or contract when subjected to changes in temperature, thermal variations or phase change, and thus the Darcy speed u is not constant. This model was first introduced in [35] and revisited in [93, 94]. In all of these works the study of Riemann problems are developed admitting the hypothesis of thermodynamic equilibrium. Some important results were found in these works. In [90, 93] the authors described, under thermodynamical equilibrium, two types of variables, namely, $\mathcal{V}$, called *primary variables* or *basic variables*, and secondary variable. The variable u is secondary variable, because it is

obtained from the primary variables. Moreover, they consider different *physical situation* like each physical phase, where the chemical species may exist under a thermodynamic equilibrium, which are

i. *spl*, single-phase liquid situation, in which only water lies in the core,

ii. *spg*, single-phase gaseous situation, in which only gaseous steam and nitrogen in the core,

iii. *tp*, the two-phase situation, where liquid water, steam and nitrogen coexist under a thermodynamic equilibrium.

In addition, in the works [93, 94] were found a condensation shock and a (surprising) evaporation rarefaction wave associated to each phase. They also found the important bifurcation structures (secondary bifurcations, inflection loci, coincidences and so on) and they extend the theory for this class of equations (3.1), developing a systematic approach for solving problems described by this equation.

Another interesting mathematical structure is the shock between different phase configurations (see [90, 94]), where turn such type of wave connects the different phases. We point out that this structure exhibits nonuniqueness, even if we consider entropy conditions such as Lax and Liu. In the present work discussed in this thesis, we give a contribution to overcome this nonuniqueness for some problems exhibiting phase transitions in the Riemann problem. We propose a new methodology, where we model thermal problems (phase transition) by using a system of balance laws with relaxation terms. We solve the Riemann problem for the large system. First, disregarding the balance terms, we study all waves in the system and we take the limit of the relaxation term going to zero. Next, we study the convergence of this problem. It is worth taking into consideration that in this work we only calculate the waves (shock and rarefactions) appearing in the 4×4 system.

3.2 Physical models and equations of state for steam and nitrogen injetion problems in porous media

We consider the steam and nitrogen injection into an one-dimensional horizontal porous rock cylinder. We disregard gravity effects and heat conductivity. The porous rock has a constant porosity φ and absolute permeability k (Appendix C). We assume that the fluids are incompressible and we also assume that the gas density does not change due to small variations in the pressure, i.e., the density is only a function of the temperature. These assumptions are valid provided that the pressure variations along the porous rock are small compared to the prevailing pressure that do not affect the physical properties of the gas phase.

The model uses multiphase extension of the Darcy's law for

$$u_w = -\frac{k k_{rw}}{\mu_w}\frac{\partial p_w}{\partial x}, \qquad u_g = -\frac{k k_{rg}}{\mu_g}\frac{\partial p_g}{\partial x}. \tag{3.2}$$

Here water and gas relative permeability functions k_{rw} and k_{rg} are considered to be functions of their own respective saturations, and μ_w and μ_g denote the viscosities of the liquid and gaseous phases and are functions of the temperature T. The functions p_w and p_g are the pressures in the liquid and gaseous phases.

The capillary pressure P_c and the capillary diffusion coefficient Ω are, by definition,

$$P_c = P_c(s_w) = p_g - p_w \qquad \Omega = -f_w \frac{k k_{rg}}{\mu_g} \frac{dP_c}{ds_w} \geq 0. \tag{3.3}$$

The *fractional flows* for water and steam are saturation-dependent functions defined by,

$$f_w = \frac{k_{rw}/\mu_w}{k_{rw}/\mu_w + k_{rg}/\mu_g}, \tag{3.4a}$$

$$f_g = \frac{k_{rg}/\mu_g}{k_{rw}/\mu_w + k_{rg}/\mu_g}. \tag{3.4b}$$

Using the definition of P_c (3.3) and the Darcy's law (3.4) in (3.2), we obtain:

$$u_w = u f_w - \Omega \frac{\partial s_w}{\partial x}, \qquad u_g = u f_g - \Omega \frac{\partial s_g}{\partial x}, \tag{3.5}$$

where $u = u_w + u_g$ is called the *total Darcy speed*. Here s_w and s_g are the water and gaseous saturations, i.e., the fractions of the pore filled with water and gas, respectively. We suppose that the rock profile is fully saturated, i.e., $s_w + s_g = 1$. We also assume that the Darcy speeds in the gaseous phase are equal, which we set as u_g.

The mass balance for liquid water, gaseous water and nitrogen are:

$$\frac{\partial}{\partial t}(\varphi \rho_W s_w) + \frac{\partial}{\partial x}(\rho_W u_w) = q_{g\to a,w}, \tag{3.6}$$

$$\frac{\partial}{\partial t}(\varphi \rho_{gw} s_g) + \frac{\partial}{\partial x}(\rho_{gw} u_g) = -q_{g\to a,w}, \tag{3.7}$$

$$\frac{\partial}{\partial t}(\varphi \rho_{gn} s_g) + \frac{\partial}{\partial x}(\rho_{gn} u_g) = 0, \tag{3.8}$$

where $q_{g\to a,w}$ is the mass source term (this term is later explained), ρ_W is the water density, which is assumed to be constant, ρ_{gw} (ρ_{gn}) denote concentration of steam (nitrogen) in the gaseous phase that depends only on the temperature. In this model we neglect the molecular diffusive effects. Thus, we use the total Darcy's speed and the equation (3.5) so equations (3.6)-(3.8) became,

$$\begin{aligned}
\frac{\partial}{\partial t}(\varphi \rho_W s_w) + \frac{\partial}{\partial x}(u \rho_W f_w) &= \frac{\partial}{\partial x}\Big(\rho_w \Omega \frac{\partial s_w}{\partial x}\Big) + q_{g\to a,w}, \\
\frac{\partial}{\partial t}(\varphi \rho_{gw} s_g) + \frac{\partial}{\partial x}(u \rho_{gw} f_g) &= \frac{\partial}{\partial x}\Big(\rho_{gw} \Omega \frac{\partial s_g}{\partial x}\Big) - q_{g\to a,w}, \\
\frac{\partial}{\partial t}(\varphi \rho_{gn} s_g) + \frac{\partial}{\partial x}(u \rho_{gn} f_g) &= \frac{\partial}{\partial x}\Big(\rho_{gn} \Omega \frac{\partial s_g}{\partial x}\Big).
\end{aligned} \tag{3.9}$$

We assume that nitrogen and steam in the gaseous phase behave as ideal gases and that there are no volume effects due to mixing of both gases. Thereby the volume of components are additive,

$$\rho_{gw}/\rho_{gW}(T) + \rho_{gn}/\rho_{gN}(T) = 1. \tag{3.10}$$

Here ρ_{gW} and ρ_{gN} are the densities of steam and nitrogen, respectively, which we assume that are obtained from the equation for ideal gases.

From the previous equation, we can define the steam and nitrogen composition as,

$$\psi_{gw} = \rho_{gw}/\rho_{gW}(T), \tag{3.11a}$$
$$\psi_{gn} = \rho_{gn}/\rho_{gN}(T), \tag{3.11b}$$
$$\text{so} \quad \psi_{gn} + \psi_{gw} = 1. \tag{3.11c}$$

These compositions are unknowns in the system of equations However, using the restriction (3.11*c*), we can use only ψ_{gw} as the unknown. In this way, the system (3.9) have 4 unknowns $\{s_g, T, \psi_{gw}, u\}$ and we need to introduce another equation to represent the energy conservation, using enthalpies:

$$\frac{\partial}{\partial t}\Big((1-\varphi)H_r + \varphi s_w \rho_W h_w + \varphi s_g(\rho_{gw}h_{gw} + \rho_{gn}h_{gn})\Big) + \frac{\partial}{\partial x}\Big(u_w\rho_W h_w + u_g(\rho_{gw}h_{gw} + \rho_{gn}h_{gn})\Big) = 0, \tag{3.12}$$

where H_r is the rock enthalpy; h_w, h_{gn} and h_{gw} are the rock enthalpy per mass unit. These functions depends on temperature. They utilizes the thermal capacity of each component to describe the conservation of the thermal energy between the rock and the different components and phases. For the enthalpy of h_{gw} we take into account its sensible part, where the variation of thermal energy is proportional to temperature variation, and the latent part, which corresponds to the heat necessary to obtain steam from water for a fixed boiling temperature.

We substitute the equation (3.4b) in (3.12) after some algebraic operations and obtain:

$$\frac{\partial}{\partial t}\Big(\varphi(\hat{H}_r + s_w H_w + s_g H_g)\Big) + \frac{\partial}{\partial x}\Big(u(f_w H_w + f_g H_g)\Big) = \frac{\partial}{\partial x}\Big((H_g + H_w)\Omega\frac{\partial s_g}{\partial x}\Big), \tag{3.13}$$

where we define,

$$\hat{H}_r = \frac{(1-\varphi)}{\varphi}H_r, \quad H_w = \rho_W h_w, \quad H_g = \psi_{gW}\rho_{gW}h_{gw} + \psi_{gN}\rho_{gW}h_{gn};$$

all functions can be found in Appendix C.

We are interested in scales dictated by field reservoirs. The effect of spatial second derivative terms (capillary pressure, heat conductivity, etc) is to widen the heat condensation front as well as other shocks, while the convergence of the characteristics tries to sharpen them. The balance of these effects yields the width of these fronts. In the field this width is typically a few tenth of centimetres; on the other hand, the distance between injection and production wells is of the order of 1000 meters. Thus this width is negligible, so we can set it to zero and simplify our analysis with no error of practical importance. From now on we disregard the diffusive terms in (3.9) and (3.13), resulting in the following system of balance equations,

$$\frac{\partial}{\partial t}(\varphi\rho_W s_w) + \frac{\partial}{\partial x}(u\rho_W f_w) = q_{g\to a,w}, \tag{3.14}$$
$$\frac{\partial}{\partial t}(\varphi\psi_{gw}\rho_{gW}s_g) + \frac{\partial}{\partial x}(u\psi_{gw}\rho_{gW}f_g) = -q_{g\to a,w}, \tag{3.15}$$
$$\frac{\partial}{\partial t}(\varphi\rho_{gN}\psi_{gn}s_g) + \frac{\partial}{\partial x}(u\rho_{gN}\psi_{gn}f_g) = 0, \tag{3.16}$$
$$\frac{\partial}{\partial t}\Big(\varphi(\hat{H}_r + s_w H_w + s_g H_g)\Big) + \frac{\partial}{\partial x}\Big(u(f_w H_w + f_g H_g)\Big) = 0. \tag{3.17}$$

It is also useful to substitute (3.14) by the sum of (3.15) with (3.14):

$$\frac{\partial}{\partial t}(\varphi(\rho_W s_w + \psi_{gw}\rho_{gW}s_g)) + \frac{\partial}{\partial x}(u(\rho_W f_w + \psi_{gw}\rho_{gW}f_g)) = 0. \tag{3.18}$$

3.2.1 Thermodynamical equilibrium and physical situations

In [35, 90, 92, 93], the authors assumed a thermodynamic equilibrium to obtain all solutions. Thus, under the thermodynamic equilibrium there is a law that states the number of degrees of freedom of thermodynamical variables in the system, this *Gibbs phase rule*, is given by,

$$f = p - c + 2, \tag{3.19}$$

where f is the number of degrees of freedom, p is the number of phases and c is the number of chemical components. Here we assume the fixed pressure flow, thus (3.19) reduces to,

$$f = p - c + 1. \tag{3.20}$$

In [35, 90, 92, 93], the authors showed that for the model steam and nitrogen, Eqs. (3.15)-(3.18), we can identify three different physical situations (or physical phases) under thermodynamical equilibrium, which are: single phase liquid situation (*spl*), single-phase gaseous situation (*spg*) and two phases situation (*tp*).

The main mathematical feature of this thermodynamic equilibrium is that the balance term $q_{g\to a,w}$ vanishes. Thus, it is possible to describe each physical situation under thermodynamic equilibrium and the corresponding system of equations, which in turn allows us to define in a natural way the term $q_{g\to a,w}$.

3.2.1.1 Single-phase gaseous situation (*spg*)

In this physical situation we have one phase (gaseous phase), $c = 1$, and two components (H_2O and N_2), $c = 2$. From the Gibbs' rule , Eq. (3.20), we have,

$$f = 2 - 1 + 1 = 2,$$

i.e., we have two degrees of freedom which are the temperature and the steam composition ψ_{gw}. Notice here $s_w = 0$ and $s_g = 1$, thus $f_w = 0$ and $f_g = 1$. The system (3.15)-(3.18) becomes

$$\frac{\partial}{\partial t}(\varphi\rho_{gW}\psi_{gw}) + \frac{\partial}{\partial x}(u\rho_{gW}\psi_{gw}) = 0, \tag{3.21}$$

$$\frac{\partial}{\partial t}(\varphi\rho_{gN}\psi_{gn}) + \frac{\partial}{\partial x}(u\rho_{gN}\psi_{gn}) = 0, \tag{3.22}$$

$$\frac{\partial}{\partial t}(\varphi(\hat{H}_r + \rho_{gW}\psi_{gw}h_{gw} + \rho_{gN}\psi_{gn}h_{gn})) + \frac{\partial}{\partial x}(u(\rho_{gW}\psi_{gw}h_{gw} + \rho_{gN}\psi_{gn}h_{gn})) = 0, \tag{3.23}$$

for the unknowns (T, ψ_{gw}, u).

3.2.1.2 Single-phase liquid situation (*spl*)

In this phase situation there is one component (H_2O), $c = 1$, and only one phase (liquid), $p = 1$. From the Gibbs' rule, Eq. (3.20), we have,

$$f = 1 - 1 + 1 = 1,$$

i.e., there is only one degree of freedom. Since there is no gas in this physical situation, we utilize as a thermodynamic degree of freedom the temperature T.

Moreover, we are assuming that water density is constant. Then, one can prove that the Darcy speed is also constant. So the system (3.15)-(3.18) reduces to a single equation. Since $s_w = 1$ and $s_g = 0$ we have $f_w = 1$ and $f_g = 0$, we obtain,

$$\frac{\partial}{\partial t}(\varphi(\hat{H}_r + H_w)) + u_w \frac{\partial H_w}{\partial x} = 0. \tag{3.24}$$

As rock and liquid water have constant heat capacity, i.e., both enthalpies are linear functions of temperature, we rewrite the above equation as,

$$\frac{\partial}{\partial t}T + \lambda_T^W \frac{\partial T}{\partial x} = 0, \qquad \text{where } \lambda_T^W = \frac{u_W}{\varphi}\frac{C_W}{C_W + \hat{C}_r}, \tag{3.25}$$

where C_W is the water heat capacity and $\hat{C}_r = C_r/\varphi$ is the rock heat capacity, see Appendix C.

3.2.1.3 Two-phase situation (*tp*)

In this case there are two chemical species (N_2 and H_2O), $c = 2$, and two phases (liquid water and gas), $p = 2$. Again, from the Gibbs' rule, Eq. (3.20), we write:

$$f = 2 - 2 + 1 = 1.$$

Here we have only one degree of freedom. Then T and ψ_{gw} are not both independent and we can write one unknown as function of other. We choose T as degree of freedom and we assume that ψ_{gw} is function of variable T, i.e.,

$$\psi_{gw} = \frac{\rho_{gw}(T)}{\rho_{gW}(T)}, \tag{3.26}$$

in which $\rho_{gw}(T)$ is obtained in Appendix C.

We have three unknowns s_w: (or, equivalently, s_g), T and u.

Under thermodynamic equilibrium, in this physical situation, the system of equation is written as,

$$\begin{aligned} \frac{\partial}{\partial t}(\varphi(p_W s_w + \rho_{gw} s_g)) + \frac{\partial}{\partial x}(u(p_W f_w + \rho_{gw} f_g)) &= 0 \\ \frac{\partial}{\partial t}(\varphi \rho_{gn} s_g) + \frac{\partial}{\partial x}(u \rho_{gn} f_g) &= 0 \\ \frac{\partial}{\partial t}(\varphi(\hat{H}_r + H_w s_w + H_g s_g)) + \frac{\partial}{\partial x}(u(H_w f_w + H_g f_g)) &= 0. \end{aligned} \tag{3.27}$$

Notice that the composition is given by (3.26).

Here we need to highlight some relevant considerations. First of all, the full system (3.15)-(3.18) does not reduces to (3.27) by simple substitution of variables, as the previous in cases *spg* and *spl*. In Section 3.2.1.4, we exhibit the form for the relaxation term and we discuss the limit of relaxation term leading the system (3.15)-(3.18) to (3.27). We point out that we do not prove this condition. Actually, we do not believe that both formulations are equivalent for small ϵ. Moreover, we divide each class of system in two different methodologies: with thermodynamic equilibrium and without thermodynamic equilibrium. In the first one we solve

the problem by assuming the existence of the three situations before explained: *spg*, *spl* and *tp*. In the second we solve the complete system of balance equations (3.15)-(3.18).

Although we were not able to solve the complete Riemann problem associated to the pertinent balance system under consideration (by a matter of time, not for technical reasons), we believe that based on our preliminary numerical experiments as well as from our few analytical results, we can see good evidences that allows us to identify some differences and similarities in the solutions obtained from the formulations with thermodynamic equilibrium and without thermodynamic equilibrium. Additionally, we believe might be proposed a future work to give more assertive answers to several questions that arise from in this thesis. We would like to remark that the unsplitting numerical finite volume method played an important role as a fundamental tool to study this problem of balance law with phase transition, which in turn gave us more intuition on several questions of this problem, as previously announced throughout the text so far.

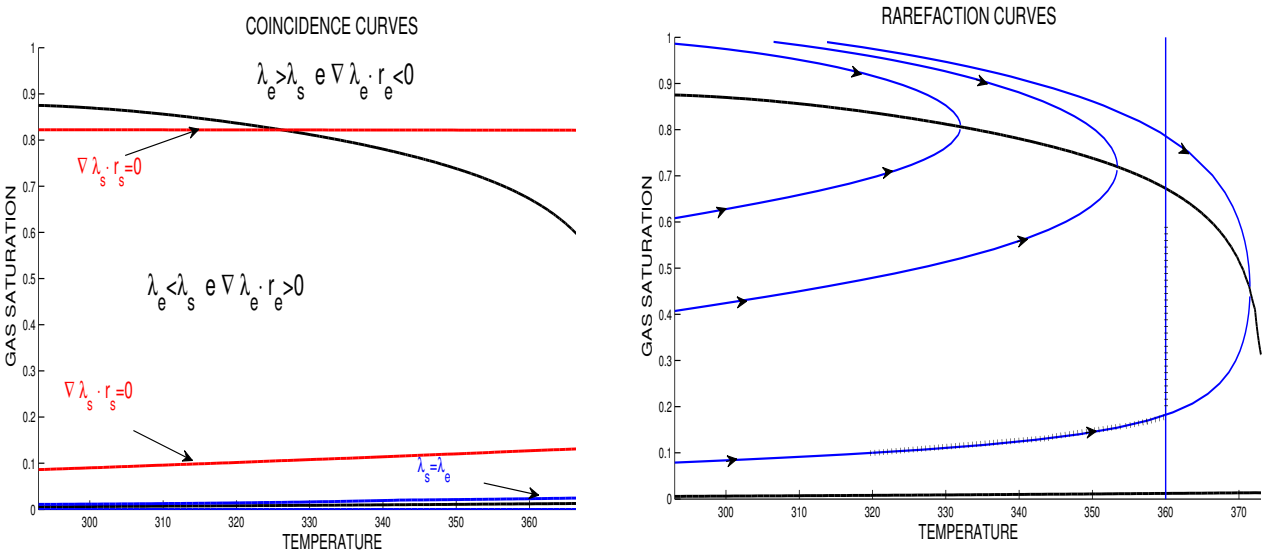

Figure 3.1: Left, Coincidence curves and inflection loci two-phase situation (*tp*) see,[90]. Right, rarefaction curves projected in the plane t, s_g. The dotted line show solution for Riemann problem yield to problem (4.23)-a.

3.2.1.4 The relaxation term $q_{g\to a,w}$ and the phase space

Here we describe in details some features related to the relaxation term $q_{g\to a,w}$ in order to facilitate our understanding of the phase space.

We remark that the relaxation term $q_{g\to a,w}$ have two main characteristics, namely:

1. The kernel of relaxation term $q_{g\to a,w}$ is composed by the physical situations described above described (*spg*, *spl* and *tp*).

2. The quantity $q_{g\to a,w}$ can be viewed as an "attractor" for the evolution part of the balance system, i.e., we obtain an ODE from the system of balance equations. This means that

each physical situation corresponds to an equilibrium for this ODE. Then, for any state in the phase space $\mathcal{V}$, for a long time behavior for this ODE, we have the corresponding solution tends to some phase space (equilibrium).

The above mentioned characteristics linked to the relaxation term $q_{g\to a,w}$ can be put in the following general context. Consider the system of balance equations (3.1). Thus, the condition

1. states that the union of all phase situations is in the kernel of $Q(\mathcal{V})$. If we define each physical situation (in a general setting) as $\mathcal{P}_i$, and also for a set of indices i, we have:

$$\cup_i \mathcal{P}_i = \{\mathcal{V}, \text{ such that } Q(\mathcal{V}) = 0\}. \tag{3.28}$$

On the other hand, the condition:

2. we study only the ODE associated to (3.1). In [90], the author have proved that for any system written as in the form (3.1) there is a linear transformation, which in turn allows us to decouple the underlying system in two counterparts. For one part, we have a hyperbolic conservative system and for the another part we have a pertinent balance system in a reduced form. Moreover, this linear transformation does not modify the kernel of the source term $Q(\mathcal{V})$.

For example, for the original system (3.14)-(3.17) we apply a linear transformation whose matrix is given by,

$$A = \begin{pmatrix} 1 & -1 & 0 & 0 \\ 0 & 1 & 0 & 0 \\ 0 & 0 & 1 & 0 \\ 0 & 0 & 0 & 1 \end{pmatrix},$$

in order to obtain (3.16)-(3.18). From this new system, we can apply now the condition (2) for the ODE,

$$\frac{d}{dt}(\varphi \psi_{gw} \rho_{gW} s_g) = -q_{g\to a,w}. \tag{3.29}$$

From both conditions, we can define (notice that this is not the unique way to define this term) the relaxation term $q_{g\to a,w} = (\hat{q}_{g\to a,w})/\epsilon$ where,

$$q_{g\to a,w} = q_1(\rho_{gw}(T)/\rho_{gW}(T) - \psi_{gw})(1-s_g)s_g H(T^b - T) - q_2(T - T^b)H(T - T^b)(1-s_g). \tag{3.30}$$

The rate of evaporation (or condensation) is determine by the positive constants q_1 and q_2, ϵ is the relaxation time, and T^b is the boiling temperature for the pure water for a fixed pressure. We point out that, using Raoult's law, the boiling temperature for pure water is larger than the temperature for steam with dissolved nitrogen, as we can see in Appendix C. The function H is the heaviside function given by,

$$H(x) = \begin{cases} 1 & \text{if } x > 0, \\ 0 & \text{if } x \leq 0. \end{cases} \tag{3.31}$$

Indeed, we can see that the kernel of $q_{g\to a,w}$ is a given function for (3.30) that satisfies,

$$\begin{cases} \psi_{gw} = \dfrac{\rho_{gw}(T)}{\rho_{gW}(T)}, & \text{for } 0 < s_g < 1 \text{ and } T \leq T^b, \\ s_g = 0, & \text{for } T \leq T^b, \\ s_g = 1, & \text{for any T.} \end{cases} \tag{3.32}$$

This kernel corresponds to the union of *spg*, *spl* and *tp* and it is described in Figure 3.2 in the phase space (s_w, T, ψ_{gw}).

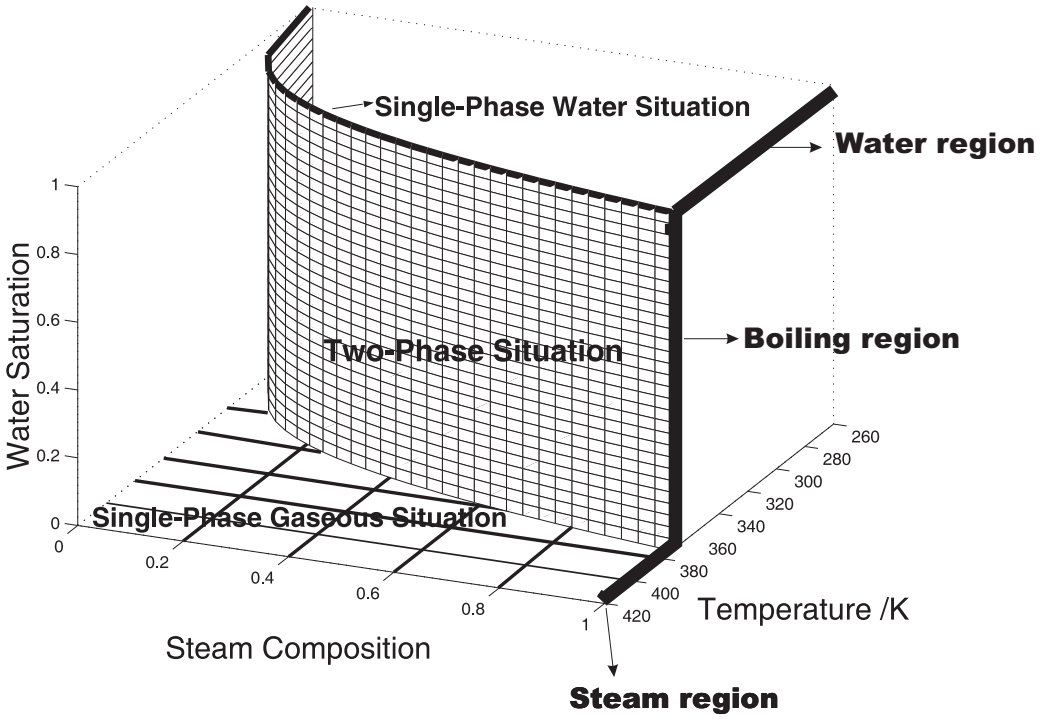

Figure 3.2: The kernel of $q_{g\to a,w}$ given all three physical situations *spg*, *spl* and *tp* in the phase space (s_w, T, ψ_{gw}). The black lines represent regions with pure water or pure steam without no nitrogen. This problem is described and solved [90].

Moreover, notice that the qualitative behavior of (3.29) is given by (at least formally):

1. If $0 < s_g < 1$ and $T \leq T^b$, then if $\psi_{gw} < \frac{\rho_{gw}(T)}{\rho_{gW}(T)}$. From Eq. (3.29), we can see that,

$$\frac{d}{dt}(\varphi\psi_{gw}\rho_{gW}s_g) > 0,$$

   then the product $\psi_{gw}\rho_{gW}s_g$ is increasing. Indeed, notice from the equation for conservation of energy that ρ_{gW} does not change so much. In the same way, notice also that s_g also does not change so much because the equation for mass conservation of saturation. Then, the affected quantity must be ψ_{gw} such that it increases to reach equilibrium $\frac{\rho_{gw}(T)}{\rho_{gW}(T)}$. The same argument is valid if $\psi_{gw} > \frac{\rho_{gw}(T)}{\rho_{gW}(T)}$, and ψ_{gw} decreases to reach the equilibrium.

2. If $T > T^b$ and $0 < s_g < 1$, then

$$\frac{d}{dt}(\varphi\psi_{gw}\rho_{gW}s_g) > 0,$$

   and $\psi_{gw}\rho_{gW}s_g$ increases to the equilibrium. Here the unique equilibrium is for $s_g = 1$.

To finish this subsection, let us perform a formal study of the underlying balance law with respect to its behaviour when the relaxation time ϵ tends to zero. Therefore, first we write the system (3.15)-(3.18) in the form:

$$\begin{aligned}
\epsilon(\frac{\partial}{\partial t}(\varphi\psi_{gw}\rho_{gW}s_g) + \frac{\partial}{\partial x}(u\psi_{gw}\rho_{gW}f_g)) &= -\hat{q}_{g\to a,w},\\
\frac{\partial}{\partial t}(\varphi(\rho_W s_w + \psi_{gw}\rho_{gW}s_g)) + \frac{\partial}{\partial x}(u(\rho_W f_w + \psi_{gw}\rho_{gW}f_g)) &= 0,\\
\frac{\partial}{\partial t}(\varphi\rho_{gN}\psi_{gn}s_g) + \frac{\partial}{\partial x}(u\rho_{gN}\psi_{gn}f_g) &= 0,\\
\frac{\partial}{\partial t}\Big(\varphi(\hat{H}_r + s_w H_w + s_g H_g)\Big) + \frac{\partial}{\partial x}\Big(u(f_w H_w + f_g H_g)\Big) &= 0.
\end{aligned}$$

Then, we take ϵ to zero to get,

$$\begin{aligned}
\hat{q}_{g\to a,w} &= 0,\\
\tfrac{\partial}{\partial t}(\varphi(\rho_W s_w + \psi_{gw}\rho_{gW}s_g)) + \tfrac{\partial}{\partial x}(u(\rho_W f_w + \psi_{gw}\rho_{gW}f_g)) &= 0,\\
\tfrac{\partial}{\partial t}(\varphi\rho_{gN}\psi_{gn}s_g) + \tfrac{\partial}{\partial x}(u\rho_{gN}\psi_{gn}f_g) &= 0,\\
\tfrac{\partial}{\partial t}\Big(\varphi(\hat{H}_r + s_w H_w + s_g H_g)\Big) + \tfrac{\partial}{\partial x}\Big(u(f_w H_w + f_g H_g)\Big) &= 0.
\end{aligned} \tag{3.33}$$

We remark that the "*limit equation*" (3.33) denotes exactly the conservation for each one of the individual phases as it would expect. However, it is crucial to point out that such analysis is only formal, with lack of stringent convergence arguments. In other words, the relaxation phenomena are usually present, although quite small, in the behaviour of most real material bodies or real fluid material and hence is often incorporated into the formulation (usually in the form of extra balance laws), more generally in the theories of extended thermodynamics (and also in the kinetic theory). Indeed, it has been an appealing topic to study conservation laws with relaxation and plenty of work has been done lately, study particularly in the behaviour of the vanishing relaxation limit, which is also done in this thesis. An obvious advantage from mathematical point of view is that the vanishing relaxation approximations also render dissipative mechanisms and hence give rise to certain stability criteria similar to the usual zero viscosity limit of the conservation laws. Actually, we have several evidences (from this doctoral thesis) to believe that the solutions obtained by the two distinct methodologies have differences and similarities. For instance, the Riemann solutions for a specific example show that the corresponding solution is quite different in the (x,t)-*space*. However the wave sequence when projected in the *phase space*, supported by the methodology when using *thermodynamic equilibrium* or *balance laws*, are *almost* the same everywhere. Of course, to better clarify our analysis we need more information about the Riemann solution, which we intend to solve in a near future as a natural continuation of this work.

In the next section we will show our preliminaries calculations with respect to the main structures that will serve as a building block to obtain the full Riemann solution to this model problem under investigation.

3.3 Hyperbolic system

Here we draw a general methodology to study the Riemann (or Riemann-Goursat) problem associated to same models described by systems of form (3.1). The Riemann problem consists on seeking functions $(\mathcal{V}, u)$ that solve the system (3.1) with initial conditions,

$$\begin{cases} (s_w, T, \psi_{gw}, u)_L \text{ if } x < 0, \\ (s_w, T, \psi_{gw}, \cdot)_R \text{ if } x > 0. \end{cases} \tag{3.34}$$

Notice that the Darcy speed u_L in the left state is specified. In [90, 93, 94, 122] the authors show that u_R is obtained from the primary variables. In the Riemann-Goursat problem the left condition L is set fix for $x = 0$, thus the initial datum (3.34) is given by,

$$\begin{cases} (s_w, T, \psi_{gw}, u)_L \text{ if } x = 0, \\ (s_w, T, \psi_{gw}, \cdot)_R \text{ if } x > 0. \end{cases} \tag{3.35}$$

Our strategy is to find all waves for the system,

$$\frac{\partial}{\partial t} G(\mathcal{V}) + \frac{\partial}{\partial x}\Big(uF(\mathcal{V})\Big) = 0, \tag{3.36}$$

and then solve the Riemann problem for this case. After we obtain the Riemann solution in the phase space $\mathcal{V}$, we project this solution on the *equilibrium manifold*.

This equilibrium variety is obtained when $\epsilon \to 0$ in (3.1), which defines a *stratified variety* $\mathcal{S}$ been the kernel of Q, as,

$$\mathcal{S} = \{\mathcal{V} \in \Omega \quad \text{such that } Q(\mathcal{V}) = 0\}. \tag{3.37}$$

In [35, 90, 93], the authors have solved the Riemann problem assuming the *thermodynamic equilibrium* hypothesis in order to solve the full Riemann problem in each pertinent physical situation, which is a system conservation law with fewer equations as

$$\frac{\partial}{\partial t} \mathcal{G}(V) + \frac{\partial}{\partial x}\Big(u\mathcal{F}(V)\Big) = 0. \tag{3.38}$$

In this manner, the set of variables V is a subset of the set of variables $\mathcal{V}$ and the flow functions $\mathcal{G}, \mathcal{F}$ are obtained from the function F and G with the property they have less components. In [90], it was given a general theory for the underlying system (3.36) with n variables. Thus, based of this same framework, we now turn our attention to discuss some results and definitions to be used to study our problem as follows.

The main feature of the system (3.36) is associated to its nature, i.e., it is needed to look at the eigenvalues associated to the spectrum of the undelying system (3.36). This means that in order to classify this system as hyperbolic we need to study the associated *generalized eigenvalue system*. We say that (3.36) is a hyperbolic system if,

$$A\vec{r} = \lambda B\vec{r}, \tag{3.39}$$

has real eigenvalues λ_i (not necessarily distinct), but these must have a basis of eigenvectors for the phase space $\mathcal{V}$. Here $A(\mathcal{V}, u)$ and $B(\mathcal{V})$ are the Jacobian matrices for the quantities uF and

G, respectively. Notice that the last column of the matrix B has null entries and then there are at most $n-1$ associated eigenvalues, where n is the number of equations in the system (3.36).

As in [90], by an eigenvector basis associated to the phase space $\mathcal{V}$, we mean only the first $n-1$ entries of the eigenvector field.

For the sake of simplicity in the remainder of this section with respect to notation, we use V, it refers that we are worked in a system is conservation law or balance law.

This comes to the fact that in [90] it was proved that the eigenvalues for the system (3.1) have the form,

$$\lambda_i = u\hat{\lambda}_i(V), \tag{3.40}$$

and the right eigenvector $\vec{r_i}$ and left eigenvector $\vec{l_i}$ have the form

$$\vec{r_i} = (r^1(V), r^2(V), ..., ur^n(V)) \qquad \text{and} \qquad \vec{l_i} = (l^1(V), l^2(V), ..., l^n(V)). \tag{3.41}$$

Moreover, if the eigenvalues are distinct, we say that the system (3.36) is *strictly hyperbolic*. In addition, we define a strictly hyperbolic system as *genuinely nonlinear* in the i-th characteristic field if

$$\nabla\lambda_i \cdot \vec{r_i} \neq 0; \tag{3.42}$$

if the equality is achieved, the eigenvalue is called linearly degenerate. Generically, in this class of problems, we have fields that satisfies (3.42) in some regions and vanishes for some states. When this occurs it defines a bifurcation structure called *inflection locus*.

The Riemann (or Riemann-Goursat) problem associated to equation (3.36) is invariant under uniform stretching of coordinates ($(x,t) \to (\alpha x, \alpha t)$). Therefore it admits a *self-similar solution*, i.e., the solution is constant along straight-line rays emanating from the origin. In the same way, the equation (3.36) is invariant under coordinates translation ($(x,t) \to (x+\overline{x}, t+\overline{t})$), in this manner the focal point of self-similar solutions may be moved from the origin to any point $(\overline{x}, \overline{y})$ in space-time plane. Note the solution of a balance law is not a self-similar function, therefore, this property is false in hyperbolic equation with source different to zero.

If the solution $(V,u)(x,t) = (V,u)(\xi)$ of equation (3.36) with $\xi = x/t$ for $t > 0$ is invariant then, by using the chain rule, for $t > 0$ the hyperbolic system reduces to ordinary differential equation in the variable ξ,

$$(A(V(\xi), u(\xi)) - \xi B(V(\xi)))\frac{d(V,u)}{d\xi} = 0. \tag{3.43}$$

Here, equation (3.43) can be written as a eigenvalue problem,

$$A\vec{r} = \xi B\vec{r}, \tag{3.44}$$

where ξ is the parameter in the integral and $\vec{r} = d(V,u)/d\xi$. From this equation, we have the set of integral curves solving,

$$\left(\frac{dV}{d\xi}(\xi), \frac{du}{d\xi}(\xi)\right) = \vec{r_i}, \quad \text{where} \quad \frac{du}{d\xi}(\xi) = r_i^n. \tag{3.45}$$

We are interested in the waves in which the curve speed ξ (or λ, because the most common way to parametrize these curves is by using the eigenvalue for each field) increases. In this way, we define a *centred rarefaction curve* as the solution of the following ordinary differential equation (3.45) satisfying,

$$\nabla\lambda_i(V,u) \cdot \vec{r_i}(V,u) > 0.$$

Notice that for genuinely nonlinear fields, we can fix on this wave a parametrization such that,

$$\nabla\lambda_i(V,u)\cdot\vec{r}_i(V,u)=1.$$

For linearly degenerate fields we do not have a rarefaction structure, as we will see below. This structure reduces to a kind of discontinuity, called *contact discontinuity*. In the (x,t) plane, we call the rarefaction curves as *rarefaction waves*.

As we know, hyperbolic systems exhibit discontinuous solutions. To obtain this structure, we consider a piecewise constant solution of the form,

$$(V,u)(x,t)=\begin{cases}(V,u)^- \text{ if } x<\sigma t,\\ (V,u)^+ \text{ if } x>\sigma t,\end{cases}$$

for a Riemann problem to (3.36). The speed of the discontinuity travels is labelled with σ, we call this as *shock speed*. The states satisfying this discontinuity should satisfy the Rankine-Hugoniot condition

$$u^+F(V^+)-u^-F(V^-)=\sigma(G(V^+)-G(V^-)). \tag{3.46}$$

Generically, we will reference to discontinuities satisfying the Rankine-Hugoniot condition as *shocks*.

Definition 3.3.1. *For a fixed state $W^-=(V^-,u^-)$, the* **Ranquine-Hugoniot locus** *(RH locus), denoted as $\mathcal{RHL}(V^-,u^-)$ is the parametrization of the discontinuous solutions of equation* (3.1)*, i.e., which consists on the points $W^+=(V^+,u^+)$ that satisfy the condition* (3.46)*, thus we define the function $\mathcal{H}=\mathcal{H}(W^-;W^+)$ as:*

$$\mathcal{H}:=\sigma(G^+(V^+)-G^-(V^-))-u^+F^+(V^+)+u^-F^-(V^-), \tag{3.47}$$

then we can define the RH locus for fixed $W^-=(V^-,u^-)$ as,

$$\mathcal{RHL}(V^-,u^-)=\{(V,u),|\exists\sigma\in\mathbb{R},\quad \text{with } uF(V)-u^-F(V^-)=\sigma(G(V)-G(V^-))\}. \tag{3.48}$$

Definition 3.3.2. *The Riemann (or Riemann-Goursat) solution consists of a sequence of shock, rarefactions and constant states connecting states given at the left side, i.e., for $x<0$ ($x=0$ for the Riemann-Goursat problem), with states at the right side, i.e. for $x>0$.*

However, it is well known that this solution, which is a weak solution (where the derivatives are defined in the distribuition sense), exhibits nonuniqueness, i.e., for initial Riemann data the solution exhibits more then one weak solution. To overcome this problem, several conditions have appeared, called *entropy conditions*, see [53].

For example, for genuinely nonlinear fields of strictly hyperbolic systems, Lax (see [96, 53]) defines a shock in the weak solution as a *entropy j-shock* (or a shock that is *physical shock*), for $2\neq j\neq n-2$, if the inequality,

$$\begin{aligned}\lambda_j(V^+,u^+)<\sigma<\lambda_j(V^-,u^-),\\ \lambda_{j-1}(V^-,u^-)<\sigma<\lambda_{j+1}(V^+,u^+),\end{aligned} \tag{3.49}$$

hold; here σ is the shock speed given by the Ranquine-Hugoniot condition. Notice that there are $n-j$ wave families reaching the shock from the left and j wave families reaching from the right.

However, for our purposes, since our field is not nonlinear (or even our system is not strictly hyperbolic), we use another admissibility criterion which is an adaptation of the Liu criterion, see [101, 102]. This criterion is the same appearing in [90]:

Definition 3.3.3. *We call* **shock curve** *the parts* (V, u) *of Ranquine-Hugoniot curve where the shock speed decreases when* V *moves away from* V^-*. As we also consider the waves in* (x, t)*, each point of the shock curve represent* **shock wave**. *The shock curve parametrizes the state* (V^+, u^+) *state admissible of shocks waves* (V^-, u^-).

In addition, we can also indentify another important structure, called as *bifurcation structures*, such as *secondary bifurcation manifold*, *coincidence loci*, *double contact curves*, *inflection curves*, *interior boundary contact* and so on. In [90, 93, 94], the authors have described and extended the theory for these structures for system of the form (3.38).

In the below sections, we will describe some structures to obtain the Riemann solution and some conclusions. The calculations are performed in Appendix B.

3.3.1 Characteristic speeds of system (3.14)-(3.17)

The system (3.14)-(3.17) can be written in general form as the system (3.1). We utilize the methodology previously described where we calculate the eingenpairs by solving a system of the form (3.39). The calculations are performed in Appendix B and we can summarize this in the following Proposition.

Proposition 3.3.1. *The system* (3.14)-(3.17) *has three different positive eigenvalues in the domain* $\Omega = [0, 1] \times [273, 373] \times [0, 1]$*, the eigenpairs are:*

$$\lambda_s = \frac{u}{\varphi}\frac{\partial f_g}{\partial s_g}, \qquad \vec{r_s} = (1, 0, 0, 0), \tag{3.50}$$

$$\lambda_c = \frac{u f_g}{\varphi s_g}, \qquad \vec{r_c} = (0, 0, 1, 0), \tag{3.51}$$

$$\lambda_e = \frac{u}{\varphi}\frac{f_g\Pi + H'_w\rho_{gW}\rho_{gN}}{s_g\Pi + (\hat{H}'_r + H'_w)\rho_{gW}\rho_{gN}}, \tag{3.52}$$

$$\vec{r_e} = \Big(\vartheta, -\rho_{gN}\zeta, 0, (uf_g - \lambda\varphi s_g)\rho'_{gN}\zeta\Big), \tag{3.53}$$

where the ϑ, ζ *and* φ *are*

$$\vartheta = (1 - f_g)(uf_g - \lambda\Pi s_g)\rho'_{gN} + u\frac{\partial f_g}{\partial T}\rho_{gN}, \qquad \zeta = u\frac{\partial f_g}{\partial s_g} - \lambda\varphi \tag{3.54}$$

and

$$\Pi = -H_g\rho_{gW}\rho'_{gN} + \gamma'\rho_{gW}\rho_{gN}. \tag{3.55}$$

The eigenpair associated to λ_c is a contact discontinuity, where only the composition ψ_{gw} changes since,

$$\nabla\lambda_c = \left(\frac{u}{s_g^2\varphi}\left(\frac{\partial f_g}{\partial s_g}s_g - f_g\right), \frac{u}{s_g\varphi}\frac{\partial f_g}{\partial T}, 0, \frac{1}{\varphi}\frac{\partial f_g}{\partial s_g}\right).$$

The eigenpair associated to λ_s is a Buckley-Leverett type, where only the saturation s_g changes and the inflection locus is obtained satisfying $\dfrac{\partial^2 f_g}{\partial s_g^2}$. For the eingenpair associated to λ_e all variables change.

3.3.1.1 Coincidence between eigenvalues

Another important structure is obtained from the coincidence between the characteristic speed, since the solution wave present a bifurcation in this structure, see [90]. The coincidence between λ_s and λ_e is labelled as $\mathbb{C}_{s,e}$. By using (3.52), the states in the coincidence $\mathbb{C}_{s,e}$ are,

$$\mathbb{C}_{s,e} = \left\{ (s_g, T, \psi_{gw}) \in \Omega \quad \text{satisfying} \quad \frac{\partial f_g}{\partial s_g} = \frac{f_g \Pi + H'_w \rho_{gW} \rho_{gN}}{s_g \Pi + (\hat{H}'_r + H'_w)\rho_{gW}\rho_{gN}} \right\}. \tag{3.56}$$

Similarly, we define the coincidence between λ_s and λ_c, denoted as $\mathbb{C}_{s,c}$, as the states satisfying in Ω satisfying,

$$\mathbb{C}_{s,c} = \left\{ (s_g, T, \psi_{gw}) \in \Omega \quad \text{satisfying} \quad \frac{\partial f_g}{\partial s_g} = \frac{f_g}{s_g} \right\}. \tag{3.57}$$

Notice that $\mathbb{C}_{s,c}$ is a ruled surface in Ω. Finally, we obtain the states satisfying the coincidence between λ_e and λ_c, denoted as $\mathbb{C}_{e,c}$ as,

$$\mathbb{C}_{e,c} = \left\{ (s_g, T, \psi_{gw}) \in \Omega \quad \text{satisfying} \quad \frac{f_g}{s_g} = \frac{f_g \Pi + H'_w \rho_{gW} \rho_{gN}}{s_g \Pi + (\hat{H}'_r + H'_w)\rho_{gW}\rho_{gN}} \right\}. \tag{3.58}$$

In the Figure 3.3.1.1 we present the coincidence between eigenvalues $\mathbb{C}_{s,e}, \mathbb{C}_{s,c}$ and $\mathbb{C}_{e,c}$ projected in plane $s_g \times T$ in range $\Omega = [0,1] \times [273, 383]$ and the values $\psi_{gw} = \{0, 0.5, 1\}$.

3.3.1.2 The inflection loci

This structure is very important because it determines the regions where the genuinely nonlinearity of each field fails. It is generically defined for an eigenpair $(\lambda, \vec{r})$ as,

$$\nabla \lambda \cdot \vec{r} = 0.$$

Using that for a 4×4 system, i.e., $V = (V_1 = s_g, V_2 = T, V_3 = \psi_{gw})$, the general form of $\lambda(V, u) = u\sigma(V)$ and $\vec{r} = (\gamma_1(V), \gamma_2(V), \gamma_3(V), u\gamma_4(V))$, following [90, 93], the inflection locus satisfies,

$$\nabla \lambda(V, u) \cdot \vec{r} = u \left(\frac{\partial \sigma}{V_1}\gamma_1 + \frac{\partial \sigma}{V_2}\gamma_1 + \frac{\partial \sigma}{V_2}\gamma_1 + \sigma(V)\gamma_4(V) \right) = 0. \tag{3.59}$$

In [90, 93], it is proved that for each field the inflection locus is an structure of codimension 1 in the projected state space (for the linearly degenerate case we do not consider the inflection locus), i.e., for the 4×4, for each field in the space $V = (V_1, V_2, V_3)$, if the inflection locus exists it is a bidimensional structure.

For the Buckley-Leverett eigenpair $(\lambda_s, \vec{r}_s)$, the inflection locus, denoted as $\mathcal{I}_s$, is obtained satisfying (3.59) and it is given by,

$$\mathcal{I}_s = \left\{ (s_g, T, \psi_{gw}) \in \Omega \quad \text{satisfying } \frac{\partial^2 f_g(s_g, T)}{\partial^2 s_g} = 0 \right\}. \tag{3.60}$$

Notice that $\mathcal{I}_s$ is a ruled surface with geratrix defined in the plane (s_g, T) for the states satisfying $\partial^2 f_g / \partial s_g^2 = 0$.

The eigenpair (λ_c, r_c) is a linearly degenerate field since $\nabla \lambda_s \cdot \vec{r}_s = 0$ for all (s_g, T, ψ_{gw}), as we see before. For the eigenpair $(\lambda_e, \vec{r}_e)$, we denote as $\mathcal{I}_e$. Calculations for this structure is straightfulll, but very tedious.

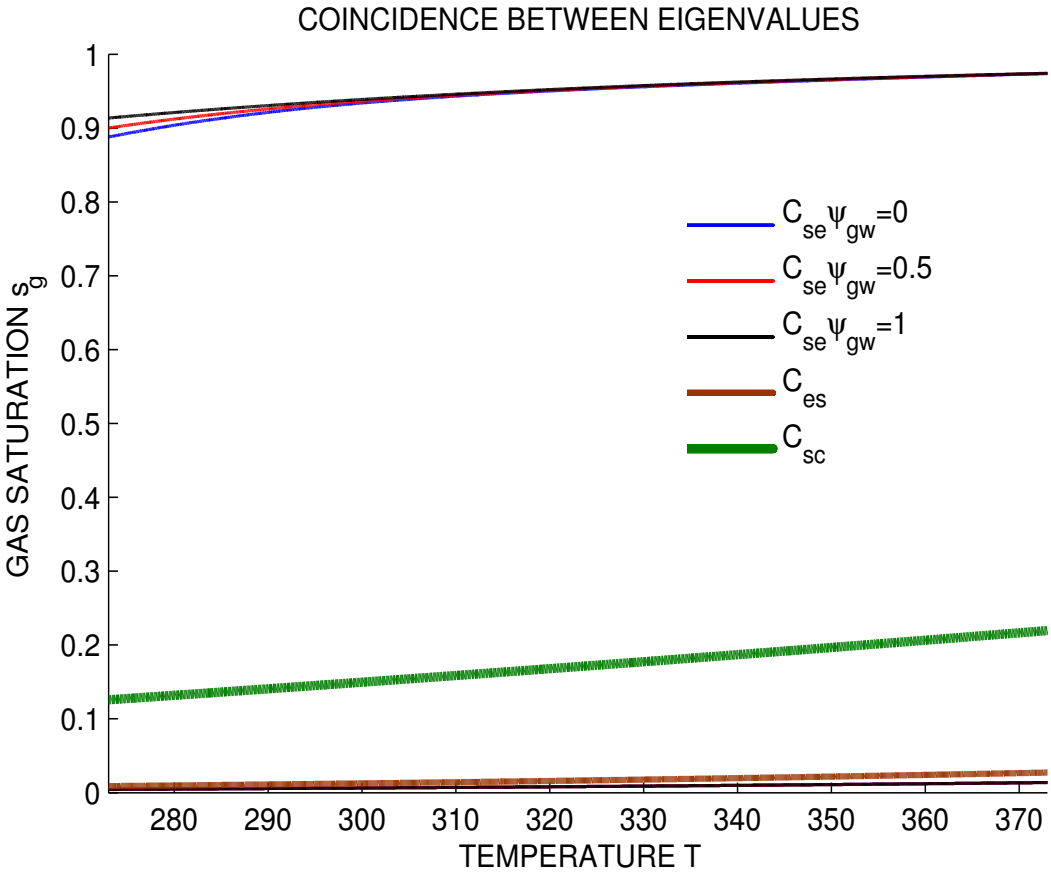

(a)

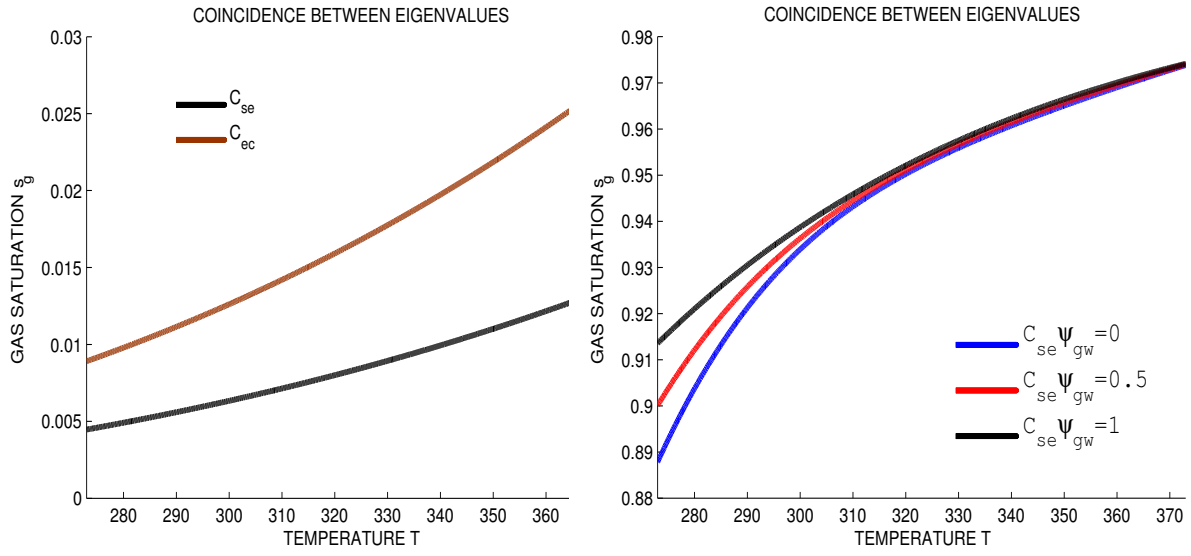

(b) (c)

Figure 3.3: Coincidence between eigenvalues projected in the plane $s_g \times T$ for the values $\psi_{gw} = \{0, 0.5, 1\}$. On the Fig 3.3(a) shows the coincidence cure in the domain $[273, 373] \times [0, 1]$, On the Fig 3.3(b) shows the coincidence cure in the domain $[273, 373] \times [0, 0.03]$ and 3.3(b) shows the coincidence cure in the domain $[273, 373] \times [0.88, 0.98]$.

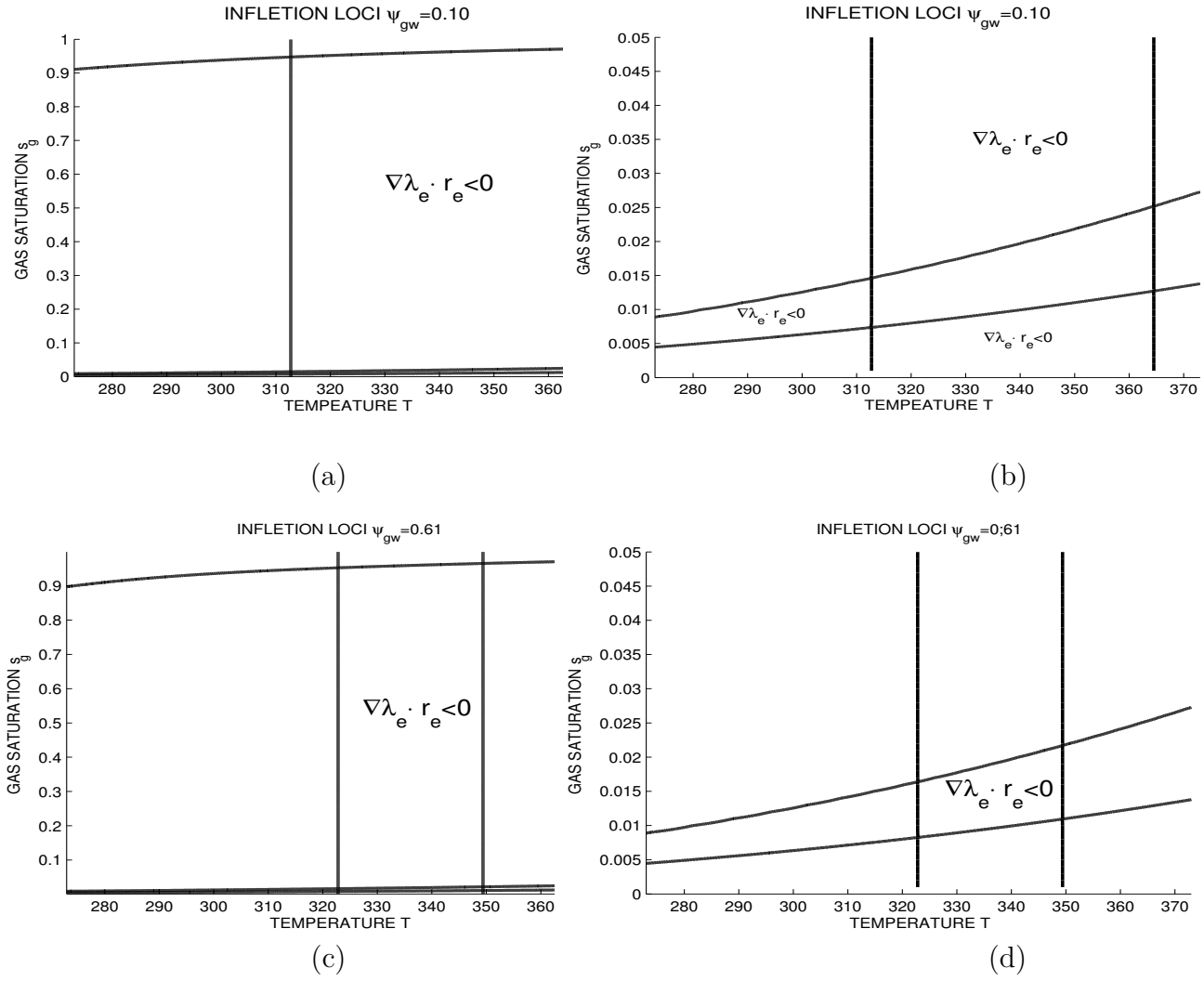

Figure 3.4: Inflection loci for the evaporation eigenvalue λ_e projected in the plane $s_g \times T$ for the values $\psi_{gw} = \{0.1, 0.6\}$. The regions show in the figure 3.4-a,c is in domain $[273, 373] \times [0, 0.99]$. In the Figure 3.4-b,d show the Inflection loci for the domain $[273, 373] \times [0, 0.1]$

Notice that the system (3.14)-(3.17) has only a unique contact discontinuities in the domain generate by the evaporation curve (see Figure 3.4). Thereby, a system strictly hyperbolic by continuity of the first derivatives, in the genuinely non-linear case the value is of λ_i is strictly monotonic (increasing or decreasing) along each integral curve of the vector field $\vec{r}_i$.

3.4 Hugoniot locus

The Hugoniot locus is obtained solving the Rankine-Hugoniot condition (3.46). In [90, 93], the author obtain a general way to find the Hugoniot locus and all possible singular regions.

Following this formalism, we can write (3.46) as a linear homogeneous system,

$$\begin{pmatrix} [G_1] & -F_1^+ & F_1^- \\ [G_2] & -F_2^+ & F_2^- \\ [G_3] & -F_3^+ & F_3^- \\ [G_4] & -F_4^+ & F_4^- \end{pmatrix} \begin{pmatrix} \sigma \\ u^+ \\ u^- \end{pmatrix} = 0, \qquad \text{or} \qquad \mathcal{M} \begin{pmatrix} \sigma \\ u^+ \\ u^- \end{pmatrix} = 0, \tag{3.61}$$

where $[G_i]$ for $i = 1, 2, 3, 4$ is given by:

$$[G_i] = G_i(V^+) - G_i(V^-),\ F_i^+ = F_i(V^+),\ \ F_i^- = F_i(V^-). \tag{3.62}$$

The 3×3 minors of the matrix $\mathcal{M}$ are denoted by $\mathcal{M}_{pqs}$:

$$\mathcal{M}_{pqs} = \begin{pmatrix} [G_p] & -F_p^+ & F_p^- \\ [G_q] & -F_q^+ & F_q^- \\ [G_s] & -F_s^+ & F_s^- \end{pmatrix} \qquad \text{for all distinct} \quad p,\ q \text{ and } s \text{ in } \mathcal{C} = \{1, 2, 3, 4\}. \tag{3.63}$$

The homogeneous linear system (3.61) has a non-trivial solution, if only if

$$\mathcal{H}_{pqs} = det\,(\mathcal{M}_{pqs}) = 0 \qquad \text{for all distinct} \quad p,\ q \text{ and } s \text{ in } \mathcal{C}. \tag{3.64}$$

The *RH* locus is given by implicit expressions for (V^-, u^-), as proved in [90, 93] the *RH* locus is projected on the space V and consists of the V^+ that satisfy $det(\mathcal{M}_{pqs}) = 0$ for all distinct p, q and s in $\mathcal{C}$. We denote the *RH* locus of a state V^- in the space V as $\mathcal{RHL}(V^-)$. Here, each $det(\mathcal{M}_{pqs}) = 0$ is a two-dimensional structure. Notice that there are $\mathbf{C}_4^3 = 4$ possible equations satisfying (3.64), however, it is possible to consider 3 different combinations (in the $n \times n$ case one can take $\mathbf{C}_n^3 - 1$ equations), see [90, 93]. Moreover the $\mathcal{RHL}(V^-)$ is a one-dimensional structure obtained as intersection between these different structures.

On the other hand, since the dependence on ψ_{gw} is linear in each equation, we can obtain a more explicit form to the Rankine-Hugoniot locus. Using system (3.15)-(3.18), the Rankine-Hugoniot condition (3.46) is written as,

$$\sigma\varphi\Big(\psi_{gw}^+\rho_{gW}^+ s_g^+ - \psi_{gw}^-\rho_{gW}^- s_g^-\Big) = u^+ f_g^+\psi_{gw}^+\rho_{gW}^+ - u^- f_g^-\psi_{gw}^-\rho_{gW}^-, \tag{3.65}$$

$$\begin{aligned}\sigma\varphi\Big(&\psi_{gw}^+\rho_{gW}^+ s_g^+ + \rho_W(1 - s_g^+) - \psi_{gw}^-\rho_{gW}^- s_g^- - \rho_W(1 - s_g^-)\Big) \\ &= u^+\left(f_g^+\psi_{gw}^+\rho_{gW}^+ + \rho_W(1 - f_g^+)\right) - u^-\left(f_g^-\psi_{gw}^-\rho_{gW}^- + \rho_W(1 - f_g^-)\right),\end{aligned} \tag{3.66}$$

$$\sigma\varphi\Big((1 - \psi_{gw}^+)\rho_{gN}^+ s_g^+ - (1 - \psi_{gw}^-)\rho_{gN}^- s_g^-\Big) = u^+ f_g^+(1 - \psi_{gw}^+)\rho_{gN}^+ - u^- f_g^-(1 - \psi_{gw}^-)\rho_{gN}^-, \tag{3.67}$$

$$\begin{aligned}\sigma\varphi\Big(&\hat{H}_r^+ - \hat{H}_r^- + H_W^+(1 - s_g^+) - H_W^-(1 - s_g^-) + H_g^+ s_g^+ - H_g^- s_g^-)\Big) \\ &= u^+(H_W^+ + f_g^+(H_g^+ - H_W^+)) - u^-(H_W^- + f_g^-(H_g^- - H_W^-)),.\end{aligned} \tag{3.68}$$

Subtracting (3.65) from (3.66), and if $s_g^+ \neq s_g^-$, we then obtain after some algebraic, v^s as,

$$\sigma = \frac{u^+(1 - f_g^+) - u^-(1 - f_g^-)}{\varphi(s_g^- - s_g^+)}. \tag{3.69}$$

Substituting σ, given by (3.69), into (3.65), after some algebraic we obtain u^+ as,

$$u^+ = u^- \frac{(\psi_{gw}^+\rho_{gW}^+ s_g^+(1 - f_g^-) - \psi_{gw}^-\rho_{gW}^-(s_g^- - f_g^- s_g^+)}{(\psi_{gw}^+\rho_{gW}^+(s_g^+ - f_g^+ s_g^-) - \psi_{gw}^-\rho_{gW}^- s_g^-(1 - f_g^+)}. \tag{3.70}$$

We also can isolate u^+, substituting σ, already indicated above, into (3.67), after some algebraic manipulation, we obtain u^+ as,

$$u^+ = u^- \frac{((1-\psi^+_{gw})\rho^+_{gN}s^+_g(1-f^-_g) - (1-\psi^-_{gw})\rho^-_{gN}(s^-_g - f^-_g s^+_g)}{((1-\psi^+_{gw})\rho^+_{gN}(s^+_g - f^+_g s^-_g) - (1-\psi^-_{gw})\rho^-_{gN}s^-_g(1-f^+_g)}. \tag{3.71}$$

We also can eliminate u^+ in σ by substituting u^+ given by (3.70) into (3.69) (a similar expression is obtained substituting u^+ given by (3.71) into (3.69)). After some algebraic manipulation we obtain,

$$\sigma = \frac{u^-}{\varphi}\frac{\psi^+_{gw}\rho^+_{gW}f^+_g(1-f^-_g) - \psi^-_{gw}\rho^-_{gW}f^-_g(1-f^+_g)}{\psi^+_{gw}\rho^+_{gW}(s^+_g - f^+_g s^-_g) - \psi^-_{gw}\rho^-_{gW}s^-_g(1-f^+_g)}. \tag{3.72}$$

Substituting u^+ and σ given by (3.70) and (3.72) in (3.68) we obtain a expression that does not depends on u^+, u^- and σ. Now, by equating (3.70) and (3.71), and after some algebraic manipulations, we obtain the following expression,

$$\left(\psi^+_{gw}(\rho^-_{gN}\rho^+_{gW}(1-\psi^-_{gw})\rho^+_{gN}\rho^-_{gW}\psi^-_{gw}) + \rho^+_{gN}\rho^-_{gw}\psi^-_{gw}\right)(s^+_g - s^-_g)(f^+_g s^-_g - f^-_g s^+_g) = 0. \tag{3.73}$$

Notice that (3.73) give us two equations for three unknowns that are s^+_g, T^+ and ψ^+_{gw}. We have three possibilities from (3.73), thus we consider the following calculation,

$$\psi^+_{gw}(\rho^-_{gN}\rho^+_{gW}(1-\psi^-_{gw}) + \rho^+_{gN}\rho^-_{gW}\psi^-_{gw}) + \rho^+_{gN}\rho^-_{gw}\psi^-_{gw} = 0, \tag{3.74}$$

which give us:

$$\psi^+_{gw} = \frac{\rho^+_{gN}\rho^-_{gw}\psi^-_{gw}}{\rho^-_{gN}\rho^+_{gW}(1-\psi^-_{gw}) + \rho^+_{gN}\rho^-_{gW}\psi^-_{gw}}, \tag{3.75}$$

since $\rho_{gW} = \frac{p_{at}M_W}{RT}$ and $\rho_{gN} = \frac{p_{at}M_N}{RT}$ then $\rho^+_{gW}\rho^-_{gN} = \rho^-_{gW}\rho^+_{gN}$, thus $\psi^+_{gw} = \psi^-_{gw}$ in this branch.

First, in order to obtain s^+_g and T^+, we substitute $\psi^+_{gw} = \psi^-_{gw}$ in (3.73) and we obtain the zero level curve, the Rankine-Hugoniot only on the plane (s_g, T).

Second, another possibility is,

$$f^+_g s^-_g - f^-_g s^+_g = 0. \tag{3.76}$$

Thus, by assuming that (3.76) is satisfied, we obtain (projection) the plane (s_g, T). To get ψ_{gw}, we substitute the values obtained from the implicit curve (3.76) obtained in the plane (s_g, T).

Third, as an alternative approach, we just assume that $s^+_g = s^-_g$. Then, by subtracting (3.66) from (3.65) and after some algebraic manipulations, it reads that,

$$u^+ = u^- \frac{(1-f^-_g)}{(1-f^+_g)}. \tag{3.77}$$

From (3.66) and (3.67), we isolate σs^+_g in both equations and we obtain, respectively,

$$\sigma s^+_g = \frac{u^+ f^+_g \psi^+_{gw}\rho^+_{gW} - u^- f^-_g \psi^-_{gw}\rho^-_{gW}}{\varphi(\psi^+_{gw}\rho^+_{gW} - \psi^-_{gw}\rho^-_{gW})},\ \sigma s^+_g = \frac{u^+ f^+_g(1-\psi^+_{gw})\rho^+_{gW} - u^- f^-_g(1-\psi^-_{gw})\rho^-_{gW}}{\varphi((1-\psi^+_{gw})\rho^+_{gW} - (1-\psi^-_{gw})\rho^-_{gW})}. \tag{3.78}$$

By using u^+ given by (3.77) and equating σs^+_g in (3.78), and after some algebraic we obtain,

$$(\rho^-_{gN}\rho^+_{gW}\psi_{gw} - \rho^+_{gN}\rho^-_{gW}\psi^-_{gw} + \rho^+_{gN}\rho^-_{gW}\psi_{gw}\psi^-_{gw} - \rho^-_{gN}\rho^+_{gw}\psi_{gw}\psi^-_{gw})(f^+_g - f^-_g) = 0. \tag{3.79}$$

Since we are using $\rho_{gW} = \frac{p_{at} M_W}{RT}$ and $\rho_{gN} = \frac{p_{at} M_N}{RT}$, then, after simplifications, we obtain,

$$(\psi_{gw}^{+} - \psi_{gw}^{-})(f_g^{+} - f_g^{-}) = 0, \quad \text{thus} \quad \psi_{gw}^{+} - \psi_{gw}^{-} \quad \text{or} \quad f_g^{+} - f_g^{-}. \tag{3.80}$$

If $f_g^{+} - f_g^{-} = 0$, since $s_g^{+} = s_g^{-}$, then $T^{+} = T^{-}$ and the shock speed σ and u^{+} satisfy,

$$\sigma = \frac{f_g^{-}}{s_g^{-}} \quad \text{and} \quad u^{+} = u^{-}. \tag{3.81}$$

The other possibility is $\psi_{gw}^{+} = \psi_{gw}^{-}$. In this case the shock speed is,

$$\sigma = u^{-} \frac{f_g^{+}\rho_{gW}^{+} - f_g^{-}\rho_{gW}^{-} - f_g f_g^{-}\rho_{gW}^{+} + f_g^{+} f_g^{-}\rho_{gW}^{-}}{s_g^{-}\varphi(\rho_{gW} - \rho_{gW}^{-})(f_g^{+} - 1)}. \tag{3.82}$$

Chapter 4

Numerical Simulation for the injection

In this chapter we present a novel numerical scheme for the differential partial equation (3.1), that is based on a generalization of the numerical algorithm introduced in Chapter 1 and the Rankine-Hugoniout condition. We focus on the problem of nitrogen and steam injection in porous media. To meet this aim, we do a study for a Riemann problem over a single physical situation, with the supposition that the initial value fully satisfies the subcharacteristic condition. Thereby, we compare the solution with the hypothesis of the equilibrium and without it.

Further, we do an analysis of our results and validate we numerical experiments. Thus, we obtain a non-monotonic travelling profile tracking all different waves associeted to the model problem (3.1); see [12, 93, 94]. Moreover, for a given Riemann initial data, we draw the qualitative behaviour of the solution. In addition, in absence of the hypothesis of thermodynamic equilibrium, the solution profiles are qualitatively similar to the profile under hypothesis of thermodynamic equilibrium, if the relaxation time is small or for large time.

4.1 An unsplitting approximate algorithm for relaxation balance laws

In this section we describe a generalization of the numerical method presented in the Section 1.1, in this manner, we consider

$$G(U)_t + F_x(U) = \frac{1}{\epsilon}Q(U),\ t>0, -\infty < x < \infty, U(x,0) = \eta(x),\ -\infty < x < \infty, \tag{4.1}$$

where G, F are smooth vector-valued functions. For simplicity, we will give a construction of the method for the scalar balance law, $g_t(u) + f_x(u) = 1/\epsilon q(u)$. Essentially, we will use a central differencing framework in a staggered mesh grid as in [112] (see also Section 1.1). The local average of $g(u) = g(u(x,t))$ over $[x_j, x_{j+1}]$ is given by, $g^n_{j+1/2} = \frac{1}{\Delta x}\int_{x_j}^{x_{j+1}} g(u(x,t^n))dx$. Under an appropriate CFL-constrain, integration of (4.1) over the local finite control volume $[x_j, x_{j+1}] \times [t^n, t^{n+1}]$ reads,

$$\begin{aligned} g^{n+1}_{j+1/2} = \frac{1}{\Delta x}\int_{x_j}^{x_{j+1}} g(u(x,t^n))\,dx + \frac{1}{\Delta x}\int_{t^n}^{t^{n+1}} [f(u(x_j,t)) - f(u(x_{j+1},t))]\,dt \\ + \frac{1}{\epsilon\Delta x}\int_{t^n}^{t^{n+1}}\int_{x_j}^{x_{j+1}} q(u(x,t))\ dx\,dt. \end{aligned} \tag{4.2}$$

At each time level $t^n = n\,\Delta t$, we reconstruct a piecewise first order linear interpolants of $g(u(x,t))$ over the staggered mesh grid $x_{j-1/2} < x < x_{j+1/2}$. We use a predictor-corrector approach to the approximation of the flux gradients to get,

$$\int_{t^n}^{t^{n+1}} f(u(x_j,t))\,dt \approx \Delta t\, f(u_j^{n+1/2}), \quad \text{along with} \tag{4.3}$$
$$g_j^{n+1/2} = u_j^n + \frac{\Delta t}{2}\left[q(u_j^n) - \frac{(f_x)_j^n}{\Delta x}\right].$$

We use the UNO choice for the numerical approximation of $f_x(u(x,t))$ at point (x_j, t^n). In the approximation of the source term $q(u(x,t))$, we use the interpolants linear in the score term, yielding the predictor-corrector central differencing scheme:

$$g_{j+\frac{1}{2}}^{n+1} = \frac{1}{2}\left(g_j^n + g_{j+1}^n\right) + \frac{1}{8}\left[(g_x)_j^n - (g_x)_{j+1}^n\right] - \frac{\Delta t}{\Delta x}\left[f(u_{j+1}^{n+1/2}) - f(u_j^{n+1/2}))\right]$$
$$+ \frac{\Delta t}{2\epsilon}\left[q(u_{j+1/2}^{n+1}) + \frac{1}{2}\left(q(u_j^n) + q(u_{j+1}^n)\right)\right] + \frac{1}{8\epsilon}\int_{t^n}^{t^{n+1}} \left[(q_x)_j^n - (q_x)_{j+1}^n\right]\,dt, \tag{4.4}$$

where $u_j^{n+1/2} \equiv u(x_j, t + \Delta t/2)$ is determined by (4.3). Notice that (4.4) can be viewed in general as an one-level time-stepping predictor-corrector scheme.

We turn our attention to the predictor step to $g(u_{j+1/2}^{n+1})$. As discussed in Section 4.1, under a the CFL condition, say $\max\left\{|\lambda(u)|\dfrac{\Delta t}{\Delta x}\right\} < \dfrac{1}{2}$, where λ is eigenvalue of (4.1), we can write $\int_{t^n}^{t^{n+1}} q(u(x_j,t))\,dt \approx \Delta t\, q(u_j^{n+1/2})$ and from (4.1) reads,

$$g_{j+1/2}^{n+1} = \frac{1}{\Delta x}\int_{x_j}^{x_{j+1}} g(u(x,t^n))\,dx + \frac{1}{\Delta x}\int_{t^n}^{t^{n+1}} \left[f(u(x_j,t)) - f(u(x_{j+1},t))\right]dt$$
$$+ \frac{\Delta t}{\epsilon \Delta x}\int_{x_j}^{x_{j+1}} q(u^{n+1/2}(x))\,dx. \tag{4.5}$$

There are many options available (see [112]) for the approximation of quantity $g_{j+1/2}^{n+1}$ to evaluate the source term appearing in (4.5). Motivated by the stability of IMEX-methods [54, 112], we use the robust trapezoidal rule in a convenient way,

$$g_{j+1/2}^{n+1} = \frac{1}{2}\left(g_j^n + g_{j+1}^n\right) + \frac{1}{8}\left[(g_x)_j^n - (g_x)_{j+1}^n\right]$$
$$-\frac{\Delta t}{\Delta x}\left[f(u_{j+1}^{n+1/2}) - f(u_j^{n+1/2}))\right] + \frac{\Delta t}{2\,\epsilon}\left[q(u_j^{n+1/2}) + q(u_{j+1}^{n+1/2})\right], \tag{4.6}$$

where $g_j^{n+1/2} \equiv g(u(x_j, t + \Delta t/2))$ is determined (again) by (4.3). We stress at this point that even though we need a *prediction* to $g_{j+1/2}^{n+1}$ no additional computation is needed at this time since all quantities that appears in (4.6) are already available to use. Thus, equations (4.3), (4.4) and (4.6) define our new scheme. Notice that in the equation (4.4), we must use some method for finding roots in each point the mesh, to find the variable u. For this purpose, we prefer to use the Newton method because it is easy to implement and it has order two of accuracy.

4.1.1 Numerical scheme for a compositional model for oil recovery

In the previous chapter we show that the general system (3.1) of steam and nitrogen injection may write in general form as [35, 93],

$$\frac{\partial}{\partial t}G_1(\mathcal{V}) + \frac{\partial}{\partial x}\Big(uF_1(\mathcal{V})\Big) = \frac{1}{\epsilon}\mathcal{Q}(\mathcal{V}), \tag{4.7}$$

$$\frac{\partial}{\partial t}G_2(\mathcal{V}) + \frac{\partial}{\partial x}\Big(uF_2(\mathcal{V})\Big) = 0, \tag{4.8}$$

where (4.8) denotes the conservation of energy and (4.7) denotes the balance of each component (chemical species) in the system, for each phase (gaseous, liquid or oleic). Therefore, the total mass of chemical species is conserved. The independent unknowns are the volumetric flow rate $u \in \mathbb{R}$ (in the literature of transport in porous medium it is called *Darcy speed*) and the variables $\mathcal{V} \in \mathbb{R}^m$. The quantity ϵ is the time scale related to the mass phase transfer per unit volume that are activated in non-equilibrium regions. The mass transfer is very fast and reversible [35, 93, 90].

We can not implement directly the scheme (4.4) in the form of the systems because the Jacobian matrix of G is singular. For simplicity we assume that system (4.7)-(4.8) is a 2×2, i.e., the unknowns variables are $u, \mathcal{V} \in \mathbb{R}$. We divide differential problems. First, we approximate the unknown variable $\mathcal{V}$, of balance system ((4.7), using the numerical scheme (4.4)-(4.6) for all j in each time step $m+1$. In this manner, just need to approximate the variable u in the time $m+1$ for all j.

Note that all eigenvalues are positive then form the equation (4.8),

$$\frac{(G_2)_j^{m+1} - (G_2)_j^m}{\Delta t} + \frac{\partial}{\partial x}\left(u(F_2)\right) = 0. \tag{4.9}$$

Thus, after a bit of calculation one writes (4.9) as follows,

$$u_j^{n+1}(F_2)_j^{n+1} - u_{j-1}^{n+1}(F_2)_{j-1}^{n+1} = -\frac{\Delta x}{\Delta t}\left((G_2)_j^{n+1} - (G_2)_j^n\right). \tag{4.10}$$

Now, let $[G_i]_j = (G_i)_j^{n+1} - (G_i)_j^n$ and rewrite (4.10) as,

$$u_j^{n+1}(F_i)_j^{n+1} - u_{j-1}^{n+1}(F_i)_{j-1}^{n+1} = -\frac{\Delta x}{\Delta t}\left([G_i]_j\right). \tag{4.11}$$

Thus, if $[G_i]_j \neq 0$ and after some more calculation, we might write (4.11) as:

$$u_j^{n+1} = \frac{u_{j-1}^{n+1}\Big([G_2]_j(F_1)_{j-1}^{n+1} - [G_1]_j(F_2)_{j-1}^{n+1}\Big)}{[G_2]_j(F_1)_j^{n+1} - [G_1]_j(F_2)_j^{n+1}}. \tag{4.12}$$

Thus, we find an explicit expression to the Darcy velocity to be used along with the unsplitting finite volume scheme for the approximation of the temperature-saturation transport system.

4.2 Numerical experiments with applications to stiff differential models with relaxation

In this section we use the our numerical scheme for approximate some numerical examples. The first example is a simple system of 2×2 equations, we can compare the numerical approximations with analytical solution in the equilibrium for a Riemann problem. The second example is a Riemann problem for the model (3.15)-(3.18), in which we contrasted the numerical solution for the balance system with the numerical solution in the equilibrium situation (3.27).

4.2.1 A simple example

We study the system hyperbolic balance law with stiff relaxation term given by,

$$\frac{\partial}{\partial t}\begin{pmatrix} u^2 \\ v^2 \end{pmatrix} + \frac{\partial}{\partial x}\begin{pmatrix} v \\ u^3 \end{pmatrix} = \frac{1}{\epsilon}\begin{pmatrix} 0 \\ u - v \end{pmatrix}. \tag{4.13}$$

We denote the matrices B and A as the *Jacobian of accumulation vector* and the *flux vector*, respectively, given by,

$$B = \begin{bmatrix} 2u & 0 \\ 0 & 2v \end{bmatrix}, \qquad A = \begin{bmatrix} 0 & 1 \\ 3u^2 & 0 \end{bmatrix}. \tag{4.14}$$

Thus, the eigenvalue of system (4.13) are,

$$\lambda = \pm\frac{1}{2}\sqrt{\frac{3u}{v}}, \tag{4.15}$$

hence this is strict hyperbolic and genuinely non-linear. Notice that if u and v are positive, the system (4.13) in equilibrium, i.e. $v \to u$ is determined by,

$$\frac{\partial}{\partial t}u^2 + \frac{\partial}{\partial x}u = 0. \tag{4.16}$$

If we fixed the point u^- the speed of the system in equilibrium (4.16) is determined by,

$$\sigma(u)(u^2 - (u^-)^2) = u - u^-, \qquad \sigma(u) = \frac{1}{u + u^-}. \tag{4.17}$$

We study the Riemann problem with initial conditions,

$$(u_0, v_0) = \begin{cases} (2, 1), & \text{if } x < 0, \\ (3/2, 3/2), & \text{if } x \geq 0. \end{cases}$$

For this condition we have that sub-characteristic property is fulfilled (see [103]). Further, we observe that the problem (4.16) with initial condition $(u^-, u^+) = (2, 1)$ has a admissible shock with speed $\sigma = 1/3$, them the solution for the Riemann problem in the equilibrium is,

$$u(x, t) = \begin{cases} 2 \text{ if } x < t\sigma, \\ 1 \text{ if } x \geq t\sigma. \end{cases} \tag{4.18}$$

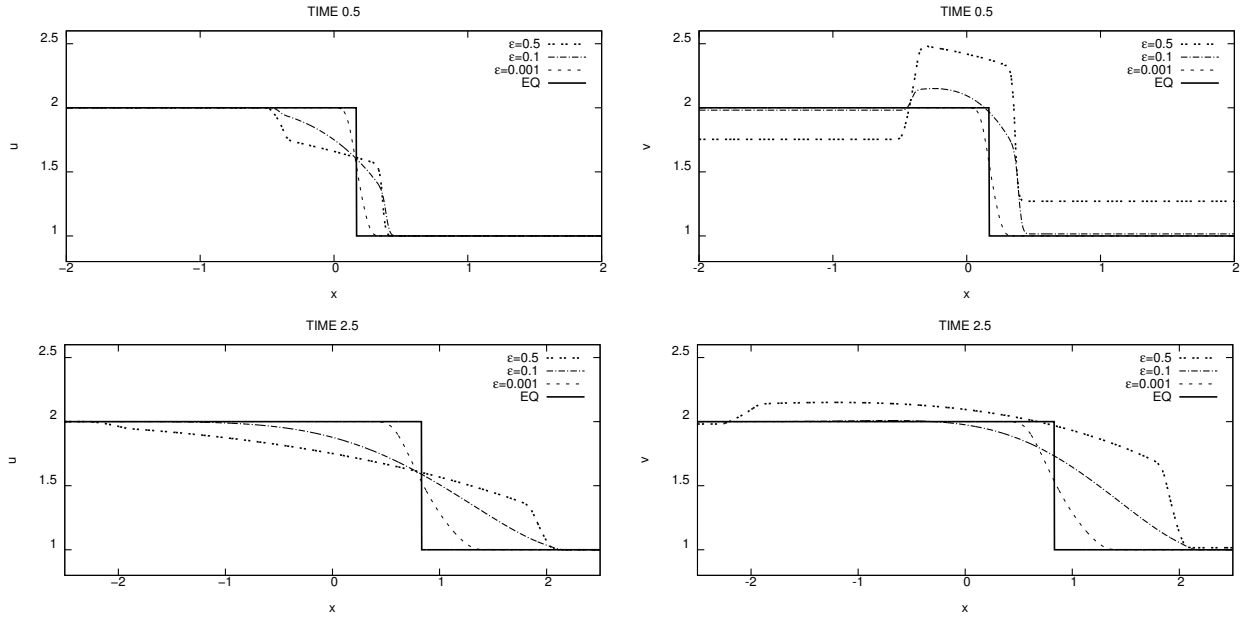

Figure 4.1: In the top (button) shows the profile wave for the variable u (v), with 500 points in the mesh for time $t = 0.5$ ($t = 2.5$) and $\epsilon = 0.5, 0.1, 0.001$ and solution in equilibrium.

In Figure 4.2.1, we present the numerical solutions for $\epsilon = 0.5$, 0.1, 0.05 and 0.001 and at time 0.5 in a computational grid with 500 cells. From these numerical experiments we have some numerical evidence that $v \to u$ when $\epsilon \to 0$, as it would be expected. Of course, this is not a proof, but just only a preliminary numerical experiment that show us some numerical evidence that we are computing qualitatively the expected behaviour from the previous analysis and no more than this. A convergence proof is to be pursued as a continuation of this work.

In this numerical experiment, we have used the Newton's method in order to solve the pertinent nonlinear system at each step of time. We have performed many different numerical tests with distinct tolerances to the Newton's method in order to select *optimal* parameters to achieve qualitative good numerical solutions with efficiency. For instance, we have used 10^{-6} as a tolerance to check residual error in each time step.

4.2.2 A Riemann problem for an injection of steam and nitrogen in a porous medium

We will study the numerical steam and nitrogen injection problem in porous media given by system (3.15)-(3.18). Here, we choose the source term based on the discussion held section 3.2.1.4 as the simple term

$$q_{g,a\to w} = \frac{1}{\epsilon}\left(\frac{\rho_{gw}}{\rho_{gW}} - \psi_{gw}\right), \tag{4.19}$$

where ϵ is the relaxation time scale far from the thermodynamic equilibrium. Thus, under the thermodynamic equilibrium, i.e., when the limit $\epsilon \to 0$ we obtain the physical phase tp given by the system (3.27), see [93, 94]. Moreover, this function works as an attractor in the sense that states far from equilibrium tp tends to tp when $\epsilon \longrightarrow 0$. Indeed, it is also possible to obtain

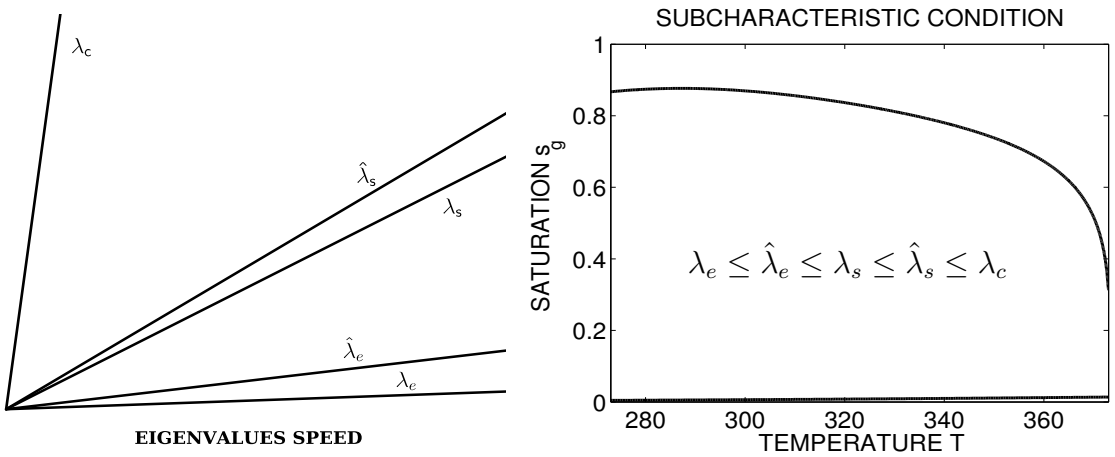

Figure 4.2: On left picture shows the eigenvalues speed and the right picture shows the region where the condition (4.22) is satisfied, when the solution projected into the plane $s_g \times T$.

this condition when $t \longrightarrow \infty$.

The system (3.27) has two eigenvalues (see [90]),

$$\hat{\lambda}_e = \frac{u}{\varphi}\frac{f_g\Upsilon + H'_w\rho_W}{s_g\Upsilon + \rho_W(H'_w + \hat{H}'_r)} \quad \text{and} \quad \hat{\lambda}_s = \frac{u}{\varphi}\frac{\partial f_g}{\partial s_g}, \tag{4.20}$$

with

$$\Upsilon = \rho_W(\gamma' - (\rho'_{gn}/\rho gn)\gamma) - H_w(\rho'_{gw} - (\rho'_{gn}/\rho_{gn})(\rho_{gw} - \rho_W)).$$

Notice that the eigenvalues of the balance law (3.15)-(3.18) satisfied the property,

$$\lambda_s \to \hat{\lambda}_s \text{ and } \lambda_e \to \hat{\lambda}_e \text{ when } \quad \epsilon \to 0. \tag{4.21}$$

Additionally in the region shows in the figure 4.2.2 satisfy the inequality

$$\lambda_e \leq \hat{\lambda}_e \leq \lambda_s \leq \hat{\lambda}_s \leq \lambda_c, \tag{4.22}$$

which is a kind of *subcharacteristic condition*, see [101, 102, 103].

In a system 2×2 the subcharacteristic condition is enough to prove the convergence of hyperbolic relaxation system, but in a system with a higher number of equations this proposition is an open problem [102]. However, in a first attempt to understand the relaxation comportment, we choose the Riemann condition that satisfies the property (4.22). Then the Riemann conditions are

$$\text{with } \begin{cases}(s_g, T, u)^L = (0.2, 320, 1)\\ (s_g, T, u)^R = (0.6, 360, \cdot)\end{cases}, \quad \text{without } \begin{cases}(s_g, T, \psi_{gw}, u)^L = (0.1, 320, 0.10489, 1)\\ (s_g, T, \psi_{gw}, u)^R = (0.6, 360, 0.61013, \cdot)\end{cases}. \tag{4.23}$$

Note that the initial conditions for the Riemann solution with thermodynamic equilibrium does not cross any coincidence or bifurcation loci (see Figure 3.1). Thus, the obtained solutions must satisfy the admissibility criteria (3.3.3).

Thus, we do a simple analysis for different values of ϵ, which generates different profile in the case without thermodynamic equilibrium and these results are compared with the profiles under the thermodynamic equilibrium for each variable.

We could do a study of all Riemann data, but we will need a more detailed analysis and it must be conducted in future works. Thus, we found an interesting behaviour linked to the relaxation term, which is the existence of a non-monotonic travelling decaying profile over initial conditions (4.23).

With thermodynamic equilibrium. We solve the system (3.27) for the above Riemann states. In the Figs. 4.3.b and 4.3.c, the solution consists of first a thermal rarefaction wave from $(s_L = 0.1, T_L = 320, u_L = 1)$ to an intermediary state $(s^* = 0.123697, T_R = 360, u^* = 1.904713)$. The thermal wave in the equilibrium is slower than the non-equilibrium ones. It is seen that due to the balance between equilibrium and non-equilibrium forces the thermal wave travel faster to overcome the equilibrium forces, see Fig. 4.3.b. After the thermal wave there is a constant state followed by a Buckley-Leverett wave, which is an isothermal wave with constant Darcy speed, Fig. 4.3.c. In classical isothermal problems u is constant. Here we notice that when the temperature increases, the steam expands then part of this expansion energy pushes the fluid, thus the Darcy speed increases, in Fig. 4.3.d. In Fig. 4.3.e, we represent the wave sequence in the plane TS. Notice here, $\psi_{gw} = \rho_{gw}/\rho_{gW}$. Note that in the figure 4.4(b) the solution has a qualitatively similar behaviour with the analytic solution (see Figure 3.1).

Without thermodynamic equilibrium. We solve the system (3.15)-(3.18), for different values of ϵ with same above Riemann data. Notice in the Fig. 4.3.a, that for ϵ values tending to 0 the variable ψ_{gw} tends to the equilibrium, and for $\epsilon \geq 0.5$ the solution exhibits a non-monotonic travelling wave with Buckley-Leverett speed. Notice that in the thermal wave the saturation in model under thermodynamic equilibrium regime varies slower than in the non-equilibrium regime. However, after the manifold equilibrium is reached the Buckley-Leverett saturation in the equilibrium regime is faster.

We believe this behaviour is associated to the fact that the part of the energy (in the case the hydrodynamic energy) is used to balance the relaxation forces. In other hand it is remarkable that the wave sequence for the saturation and temperature does not change much when ϵ varies, see Figs. 4.3.e and 4.3.f. One can see that they are very similar (see the superimposed equilibrium "blue" solution on equilibrium). Notice that this behaviour is expected because the relaxation term acts to lead the fluid to the manifold equilibrium, i.e., force ψ_{gw} to become function of temperature T. However, the speed u strongly depends on ϵ (because u strongly depends on ψ_{gw}) and for large ϵ values the waves travels slower than the corresponding waves in the equilibrium case, in other hand when ϵ tends to zero, u increases, however, but is smaller than in the equilibrium case. We believe that this behaviour is associated to the fact the part of the energy for this speed is used in the relaxation behaviour to leads the system to equilibrium.

An interesting feature appearing in the non-equilibrium solution is the existence of an inverted top for large values of ϵ in the variable ψ_{gw}, as we can notice from Fig. 4.3.a, moreover, we can see that u decreases in this wave. We believe this behaviour is due to the fact the part of the kinetic energy is used to balance relaxation forces to reach the equilibrium manifold. One can prove that this structure is a travelling decaying profile. This is a remarkable structure and it seems that is recurrent on some class of relaxation problems.

We now turn our attention to describe other numerical experiments for balance laws problems with very stiff relaxation terms by using the new scheme (4.4)-(4.6).

A pictorial illustration of solution paths for to configurations of phase transition is depicted

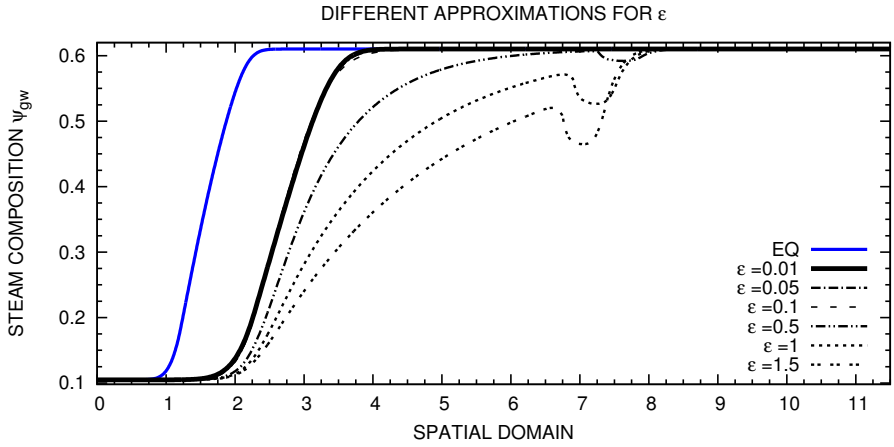

(a)

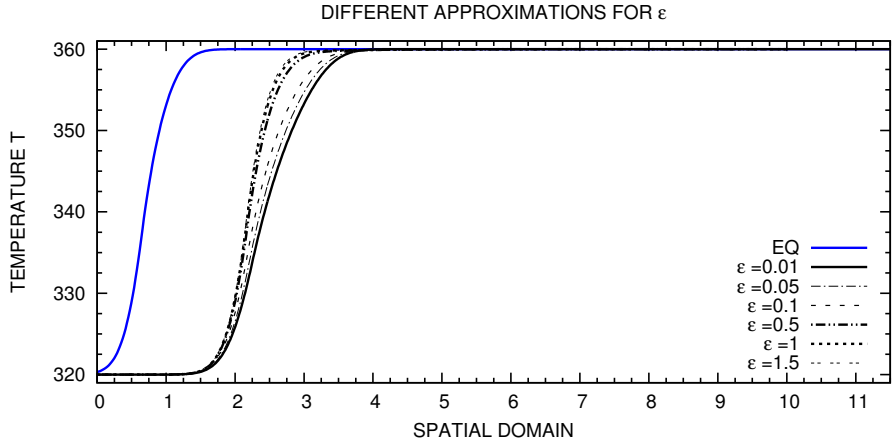

(b)

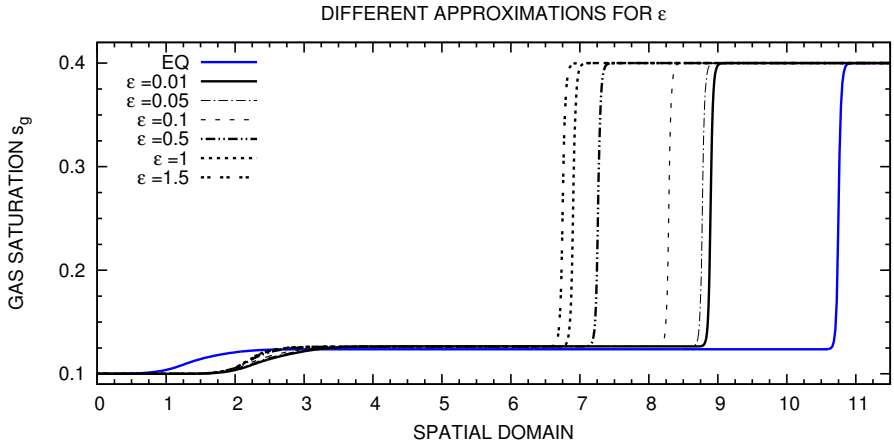

(c)

Figure 4.3: Numerical plots are shown to illustrate the behaviour of the approximate wave solutions for a Riemann problem for an injection of steam and nitrogen in a porous medium. The final time simulation is $t = 1$.

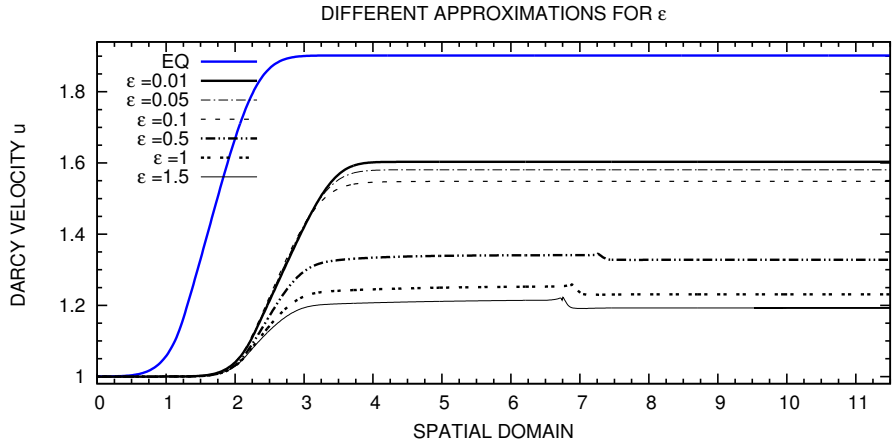

(a)

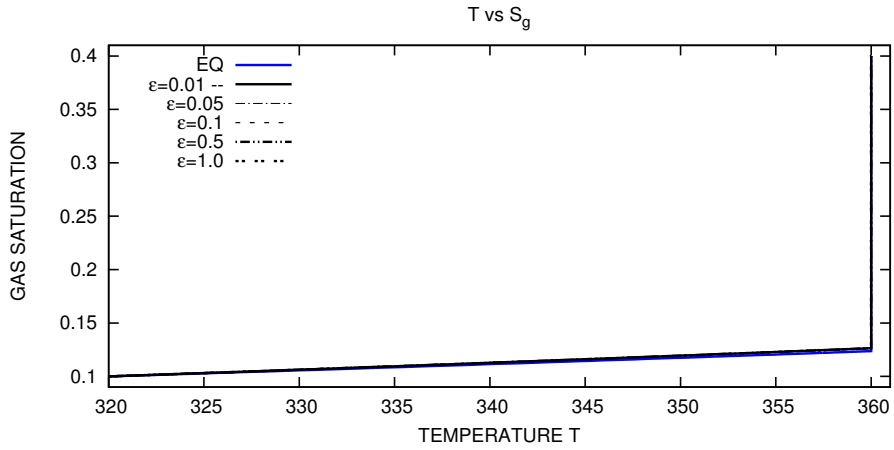

(b)

Figure 4.4: Numerical plots are shown to illustrate the behaviour of the approximate wave solutions for a Riemann problem for an injection of steam and nitrogen in a porous medium. The final time simulation is $t = 1$.

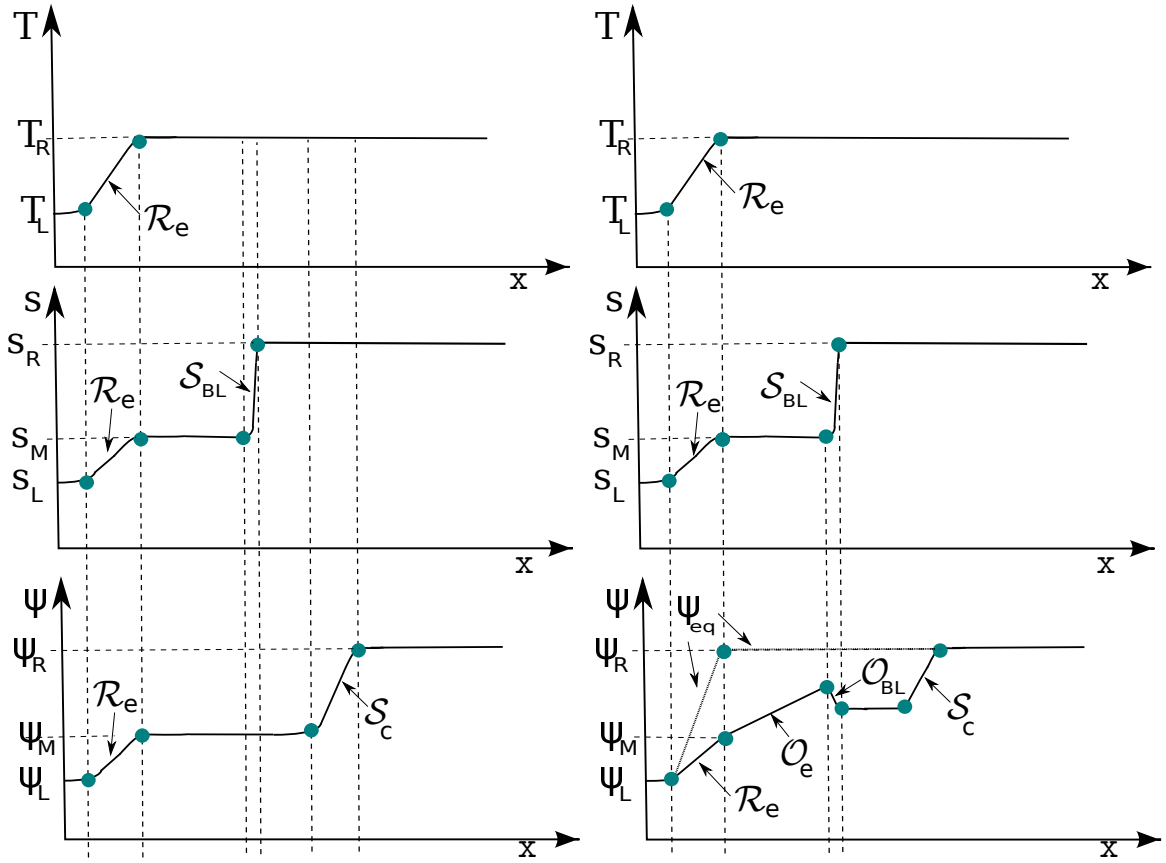

Figure 4.5: A pictorial illustration of solution paths a Riemann problem related to system (3.15)-(3.18) in an injection of steam and nitrogen in a porous medium.

in Figure 4.5: on the left column we have the system (3.27) in the *equilibrium manifold*, or the *thermodynamic equilibrium* and on the right column we have system (3.15)-(3.18) with relaxation. Again, in this moment a natural questions is: How different are both solutions obtained by means of these two approaches? In this regard, a more stringent – and more fundamental – question is: How is the behaviour of such solutions during the relaxation process and how is its limit?

In the picture 4.3, we notice that functions s_g, T profile wave without equilibrium thermodynamic was contracted but when $\epsilon \to 0$ the profile expand, we hope this behaviour because the relation of the eigenvalues (4.22). Further, as we show in the Figure 4.5 the ψ_{gw} profile wave is influenced by the λ_c (see S_c), this influence is attenuate according as $\epsilon \to 0$.

In addition, in what follows in this section, we study the behaviour of a decaying travelling profile supported by balance laws with relaxation attenuating terms. We assume Riemann data and we utilize the waves speed of the system to analyse the qualitative behaviour of travelling decaying profile. We show that for a fixed ϵ the profile tends to equilibrium surface when time increases. We corroborate our analysis with some numerical simulations. For completeness and the reader's convenience, we will provide in the next section in a self-contained fashion, all needed formulas as well as some numerical experiments, although some of them we have already mentioned previously in this chapter.

4.2.3 Mathematical analysis

We are interested in drawing the qualitative behaviour of one particular Riemann solution. We choose Riemann data on the equilibrium sheet, i.e., for states on *tp* satisfying (3.27). Then we consider the particular Riemann data (4.23)-b. In E.0.1, it was shown that it is not necessary to prescribe the Riemann Darcy speed on the right side u_R, such that u_R is obtained from the Riemann solution, see Proposition E.0.1. Here we describe our analysis in this solution. In the previous sections, we use the function $q_{a,w\to g}$ given by (4.19).

To analyse the solution, we need to study the wave speeds appearing in the solution. The system (3.14)-(3.17) has three different eigenvalues λ_s, λ_c and λ_e, with their respectively eigenvectors, see proposition 3.3.1. The eigenpair (λ_e, r_e) is called *evaporation wave*. Associated to this waves we have shocks (denoted as $\mathcal{S}_e$) and rarefactions (denoted as $\mathcal{R}_e$) and the eigenvector $\vec{r}_e$.

Our strategy to study this problem is as follows,

1. First, we obtain the Riemann solution for the left and right Riemann data below prescribe, disregarding the relaxation term $q_{a,w\to g}$, i.e., we consider the system (3.14)-(3.17) setting $q_{a,w\to g} = 0$, see Figure 4.6.

2. Second, we study all waves appearing in the solution and we perform a separated analysis for each wave to study the long time behaviour.

To obtain the Riemann solution we use the *geometrical compatibility*, i.e., the waves go from the slowest to fastest one. Here we have three wave groups with different speeds. In the region considered for the Riemann data, it was shown in this work that the speed of the wave associated to evaporation family is the slowest one, after that there is a Buckley Leverett shock $\mathcal{S}_{BL}$ and then a contact discontinuity $\mathcal{S}_c$. The Riemann solution comprises first of an $\mathcal{R}_e$. The temperature changes only on this wave see Figure 4.6, the rarefaction is obtained from the L state to the state $M = (s_M, T_M, (\psi_{gw})_M)$ in $\mathcal{R}_e$, in which $T_M = T_R = 360$, see Figure 4.6(a). In this state M we have $\lambda_e(M) < \lambda_s(M)$, thus there is a constant state. As the gas saturation changes only on the evaporation wave and on the Buckley-Leverett wave, in this manner the saturation s_g changes from s_M to s_R, then this Buckley-Leverret wave leads M to the state $(s_R, T_R, (\psi_{gw})_M)$. As only s_g varies, we can project all analysis in the plane (s_g, f_g). From Oleinik construction using convex hull, there is a Buckley-Leverett shock connecting M to $(s_R, T_R, (\psi_{gw})_M)$ with speed $\sigma^s = \dfrac{u}{\varphi}\dfrac{(f_g(s_R, T_R) - f_g(s_M, T_R))}{s_R - s_M}$.

Since it is possible to verify that $\sigma^s < \lambda_c(s_R, T_R, (\psi_{gw})_M)$, there is a constant state and finally there is a contact discontinuity connecting $(s_R, T_R, (\psi_{gw})_M)$ to right state R. This solution is summarized in Figure (4.5)-a.

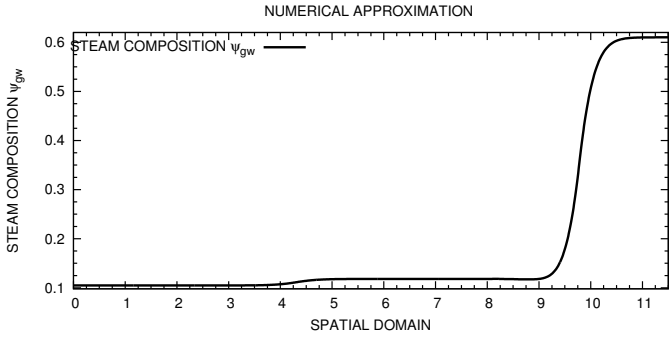

(a)

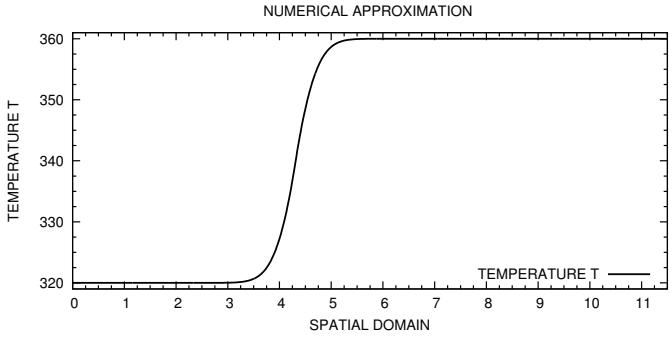

(b)

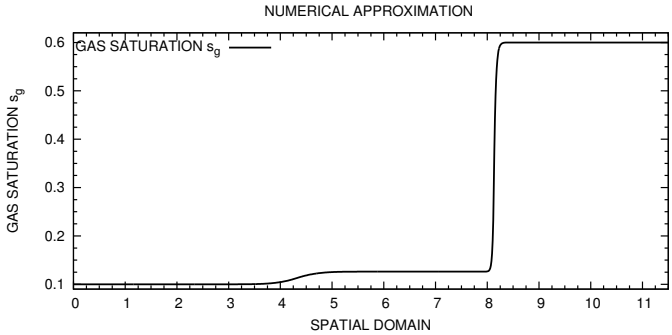

(c)

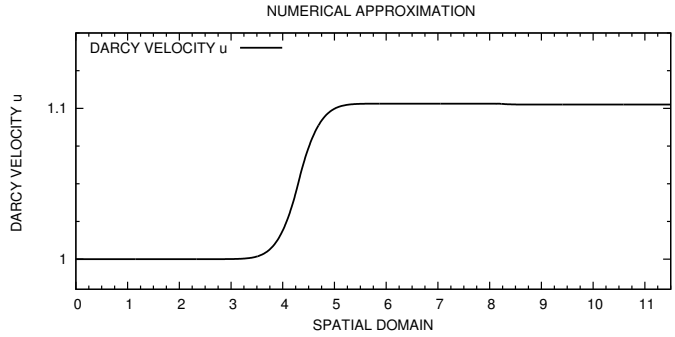

(d)

Figure 4.6: Numerical plots are shown to illustrate the behaviour of the approximate wave solutions for a Riemann problem for balance law (3.14)-(3.17) setting $q_{a,w\to g} = 0$, in time $t = 1$.

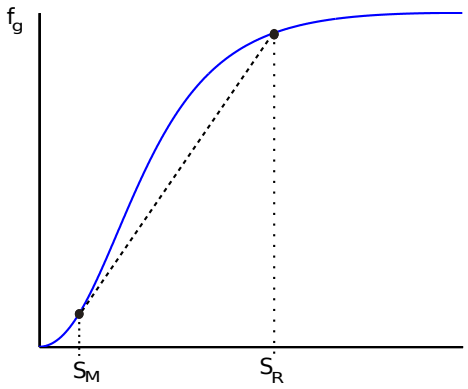

Figure 4.7: Shock connecting s_M to s_R in the plane (s_g, f_g).

Now, we are able to analyse the decaying behaviour of this solution. Our strategy here is to split the analysis for each wave. The first wave in the Riemann solution is a $\mathcal{R}_e$. This waves leads an equilibrium state to a non-equilibrium state M. Notice that the equilibrium will reach when $\psi_{gw} = \rho_{gW}(T_R)/\rho_{gw}(T_R)$.

If we consider the relaxation term, we conjecture, due to several facts, that the only variable changing is ψ_{gw}. This conjecture dues to several facts. The first one is because of the form of $q_{a,w\to g}$ that depends only on ψ_{gw} and on a constant number $\rho_{gW}(T_R)/\rho_{gw}(T_R)$. Moreover, there are two conservation laws: one for the mass of water and other for energy. Since the temperature is constant after T_R, we can disregard the energy equation and we have only two equations. Then in the state between the waves $\mathcal{R}_e$ and $\mathcal{S}_{BL}$, since s_g and T are constant, the main evolution equation reduces to:

$$\varphi\rho_{gW}s_M\frac{\partial\psi_{gw}}{\partial t} + u\rho_{gW}f_g\frac{\partial\psi_{gw}}{\partial x} = \frac{\mathcal{A}}{\epsilon}\frac{\psi_{gW}(T_R)}{\psi_{gw}(T_R)} - \psi_{gw} \longrightarrow \frac{\partial\psi_{gw}}{\partial t} + \frac{uf_g}{\varphi s_M}\frac{\partial\psi_{gw}}{\partial x} = \frac{\mathcal{A}}{\varphi s_M\rho_{gW}\epsilon} \quad (4.24)$$

where $\mathcal{A} \equiv \frac{\psi_{gW}(T_R)}{\psi_{gw}(T_R)} - \psi_{gw}$ $f_g = f_g(s_M, T_R)$, $\rho_{gW} = \rho_{gW}(T_R)$. Here, we are disregarding variations in the variable u since we are interested only in the projection of the solution in the space (T, s_g, ψ_{gw}). Notice that we have only an approximation of the original system. However, this splitting strategy is also used for the numerical system. This analysis is corroborated by the numerical solution in this way.

The solution of (4.24), via characteristic waves, is:

$$\psi_{gw} = \frac{\rho_{gW}(T_R)}{\rho_{gw}(T_R)} + \left(\psi^*_{gw} - \frac{\rho_{gW}(T_R)}{\rho_{gw}(T_R)}\right) exp\left(-\frac{1}{\varphi s_M\rho_{gW}\epsilon}t\right), \quad (4.25)$$

on each characteristic of form $x - \dfrac{uf_g}{\varphi s_M}t = constant$. Here we are taking as initial condition any constant state for ψ^*_{gw}, since we are interested only in the qualitative behaviour. Notice that for large times (or small ϵ) ψ_{gw} tends to the equilibrium, independently on ψ^*_{gw}. We call this wave $\mathcal{O}_\urcorner$, see Figure (4.5)-b.

Notice that if there was no Buckley-Leverett between the states on the wave $\mathcal{O}_e$ to the equilibrium state $\psi_{gw}(T_R) = \rho_{gW}(T_R)/\rho_{gw}(T_R)$ the decaying behaviour would not change. However, the Buckley-Leverett shocks interfere in the wave sequence introducing another behaviour. Here

we need to separate our analysis by assuming that T is constant, then we disregard the energy equation. We also fix u constant (in the splitting spirit of analysis). Then we have two equations. An equation for mass conservation of water (3.15) and an equation with relaxation term 3.14.

Here we draw some interesting comments. The first of all is associated with the equation for mass conservation of water. In the modelling of system (3.14)-(3.17) we disregard diffusive effects, however, in the shocks they are important in order to select shocks with viscous profile. Numerically this viscous profile is even more evident, such that the diffusive term can be relatively large when compared with physical ones. For the equation for mass conservation this Buckley-Leverett shock $\mathcal{S}_e$ exhibits a travelling profile supported by the diffusive terms that we disregard. This travelling profiles travels in the coordinate system $\eta = x - v^s t$. Several authors consider the existence of travelling profiles supported by relaxation terms (see e.g., [43]). On this way, on this coordinate system by assuming that $s_g(x,t) = s_g(\eta)$ and on this travelling profile that $\psi_{gw} = \psi_{gw}(\eta)$, from the Eq. (3.14), after we apply the chain rule, we obtain:

$$\psi gw\left(\mathcal{D}\right)\frac{ds_g}{d\eta} + \left(\mathcal{E}\right)\frac{d\psi_{gw}}{d\eta} = \frac{-q_{a,w\to g}}{\epsilon\rho_{gW}} \longrightarrow \frac{d\psi_{gw}}{d\eta} = \frac{\frac{q_{a,w\to g}}{\epsilon\rho_{gW}} - \psi gw\left(\mathcal{D}\right)\frac{ds_g}{d\eta}}{\left(\mathcal{E}\right)}, \tag{4.26}$$

where $\mathcal{D} \equiv -v^s + \frac{u}{\varphi}\frac{\partial f_g}{\partial s_g}$ and $\mathcal{E} \equiv \frac{uf_g}{\varphi} - v^s s_g$. We are interested only on the qualitative behaviour. Notice in this wave that $\dfrac{ds_g}{d\eta} > 0$, because s_g increases in this wave; we also can see, from geometrical inspection, that $v^s > \dfrac{u}{\varphi}\dfrac{\partial f_g}{\partial s_g}$. Indeed, notice that the second term in the last inequality is the Buckley-Leverett eigenvalue, that represents the speed of a rarefaction wave. From the Figure 4.7 we can see that v^s is faster than λ_{BL} in S_M. From the same picture, we can see that the denominator of (4.26.b) is negative. Moreover, if we have the qualitative behaviour satisfying $\dfrac{\psi_{gw}}{d\eta} < 0$, we have a decreasing wave as we see in Figure 4.5, which in turn was obtained by a numerical scheme [12]. Notice also here $-q_{a,w\to g} > 0$, because $\rho_{gW}(T)/\rho_{gw}(T) > \psi_{gw}$, since since the denominator is negative it also corroborates for the existence of the profile described in the figure 4.5. On the other hand, if for some state we have that $\dfrac{\psi_{gw}}{d\eta} > 0$, we would have ψ_{gw} increasing, and in this case the wave is stable because ψ_{gw} tends to the equilibrium profile where $q_{a,w\to g} = 0$.

We remark that this wave is not a travelling wave in the sense that it connects two two equilibrium. Here the existence of this profile is due to the fact that the saturation wave crosses the decaying wave $\mathcal{O}_e$.

After the saturation wave crosses the profile, we obtain again a constant state for T_R and s_R with a system of form (4.24) where we substitute s_M by s_R and $f_g = f_g(S_R, T_R)$. The solution is obtained in the similar way by using (4.25). Then we have another decaying wave of form $\mathcal{O}_e$. This wave occurs to the contact discontinuity $\mathcal{S}_c$ to the right state R.

The above qualitative analysis corroborates the numerical solutions and show, at least for this particular Riemann problem, that the solution is stable and tends to the equilibrium profile. We intend to use this methodology for solving the complete Riemann problem for states on the *tp* region and perform similar analysis to justify the existence of equilibrium and decaying profiles

Chapter 5

Concluding remarks and perspectives for the future

5.1 Concluding remarks

In this thesis, concerned the above mentioned questions, we considered two mathematical related models, but with distinct physical meaning: i) the Euler system with high friction and gravity and ii) the thermal flow in porous media. Indeed, the Euler system with a high friction region the system is reduced to a parabolic equation, or the porous media equation, and thus there are close connections between these models see [33, 107]. However, due to the complexity inherent to this class of models, there are few analytical solutions of such phenomena. Therefore, it was also developed a new unsplitting finite volume method, which in turn is locally conservative by (formal) construction. Indeed, this method was able to corroborate the non-monotonic solutions as well as to reproduce qualitatively correct solutions of the Euler models with high friction regime, recently published in the literature [38, 39, 49, 54, 61, 70, 73].

Concerning the Euler system with high friction and gravity, we studied the existence of non-monotone travelling wave solutions and its properties for an isothermal Euler system with relaxation. This equation describe the perfect gas flow linked to a more general model that describe Euler equations with gravity and large friction relaxation terms. Indeed, we also list our finds in what follows: *i*) In order to confront our results, we first applied a mollification technique as an effective analytical regularization method for solving an ill-posed problem for an associated reduced system for the Euler model under consideration, which in turn is solved by using the method of characteristics, *ii*) Next, we also developed a cheap unsplitting finite volume central differencing scheme that reproduces the same travelling wave asymptotic structure as that of the Euler solutions of the continuous system at the discrete level. The method is locally conservative by construction and relatively easy to understand/implement and not time consuming, and *iii*) The new numerical scheme is also used to reproduce consistent solutions for the more general Euler equations with gravity and friction recently published in literature: Bouchut [33], Dumbser [61], Chalons [38, 39], Coquel [49], see our corresponding computations in Chapter 1 and in Chapter 2, which in turn we explain our findings in more details, along with a representative set of numerical examples to describe an interplay of theory and numerics with disciplinary models and applications. Finally, this is a trial to add one more contribution in order to tackle the above mentioned class of differential equation. A

possible further continuation of this research is the application of the new findings to account non equilibrium effects in models of three-phase flow in porous media and for thermal injection problems as those found in the modelling of many groundwater flow and solute transport problems in groundwater aquifer systems as well as in oil recovery problems in porous media.

Concerning the thermal flow in porous media, we were able to modify the finite volume approach in order to developed a new cheap unsplitting scheme to account the delicate nonlinear balance between numerical approximations of the hyperbolic flux function and the source term linked to a physical and mathematical modelling for a nitrogen and steam injection in porous media. This is the described in details in the Chapter 3. We used such numerical methodology to a study a Riemann problem for an injection of steam and nitrogen in a porous medium under and without thermodynamic equilibrium. Furthermore, in order to verify our implementation, we also studied again the Euler equations with gravity and friction and a prototype shallow-water flow in an inclined channel with friction. Moreover, we applied the proposed numerical scheme as methodology tool to the study of distinct approaches for thermal modelling of flow in porous media, namely, steam and nitrogen injection problems. For the underlying problems, we discussed the computed numerical solutions to the same initial Riemann data with respect to an equilibrium manifold, under and without thermodynamic equilibrium. An interesting behaviour has appeared for relaxation term $\epsilon \geq 0.5$, which is the existence of a non-monotonic travelling wave. Another interesting feature is that the wave sequence in the state space ST is very similar. We believe that this behaviour is associated to the fact that the relaxation term leads the steam composition ψ_{gw} to an equilibrium state, without modify the temperature and saturation. For future work, this methodology will be applied for other problems of same class to study the similarities and differences in the mathematical behaviour of the solutions linked to more general stiff balance laws. Again, we believe that the natural questions are still valid upon such studies: How different are the both solutions obtained by means of these two approaches? In this regard, a more stringent – and more fundamental – question is: How is the behaviour of such solutions during the relaxation process and how is its limit?

From the previous discussion, we point out that in the thermodynamic model (3.14)-(3.17) the capillary pressure is considered as constant variable (constant function), which is unrealistic in general, it is possible to address the issue of relaxation modelling in significant models from a mathematical viewpoint keeping some aspects of the underlying physics. A more realistic model for the injection of steam and nitrogen problems is achieved by considering a nonlinear capillary pressure models, which depend upon the state variable as such saturation, temperature the the remaining pertinent primary variable of state. Thus, such more general model to the injection of steam and nitrogen problems – still in one-space dimension – lead to a pressure velocity model that dictates the Darcy velocity. This means that now are a unable to find an analogue explicit formula to the Darcy velocity as in (4.11), or (4.12). Thus, we have to use the a suitable numerical strategy that captures the underlying physical properties of each equation. Therefore, we may use an extended version of the unsplitting approximate algorithm for relaxation balance laws to approximate the hyperbolic balance system and we will build a numerical scheme based in a hybrid and mixed finite elements for solving the pertinent parabolic equation in order to approximate simultaneously the pair pressure and Darcy's velocity. We point out that the reader should not look here to this moment for a rigorous analysis nor for implementation details, but for formal construction of the numerical procedure to be implemented further later on. Indeed, the numerical solution of the coupled, nonlinear, governing system (D.7)-(D.6) is achieved by an operator splitting technique. Thus, we separate (D.7)-(D.6) in parts,

the pressure-velocity (D.6) and the temperature-saturation transport (D.7) in the spirit of IMPES approach (implicit in pressure, explicit in temperature-saturation). Why not fully implicit method for (D.7)-(D.6)? Roughly speaking, a fully implicit scheme leads to a large, strongly nonlinear algebraic system, whose solution is rather complicated and expensive to use. Moreover for advection, or convection, a nonlinear implicit discretization is hard to solve (difficulties in the resolution of large gradients due to the first order operator) and possible high computational cost (reduced CFL stability constraints). It is crucial to say that we are aware that operator splitting may not always be the right answer. Most of the refinements depend on further knowledge of properties of the underlying sub-problems. Finally, the proposed numerical strategy is fully based on the above arguments along with our current understanding of the stiff relaxation process to this class of differential problems at hand.

5.2 Perspectives for future work

As previously announced, the focus of this thesis is twofold: *i*) the mathematical study with applications of models of hyperbolic balance laws with stiff source terms and *ii*) the design and implementation of approximation algorithms to support the mathematical analysis with the help of computer simulation linked to item *i*).

With respect to item *i*) we would like the reiterate our viewpoint concerning the fundamental aspects of the limit behaviour of hyperbolic systems of conservation laws with stiff relaxation terms to the local systems of conservation laws as the relaxation time tends to zero, which in turn motivates our list of issues for a further research:

- Stability and singular limits of zero relaxation time. Relaxation is important in many physical situations. For example, it arises in kinetic theory [37], gases not in local thermodynamic equilibrium [86, 128], elasticity with memory [51, 75, 115], multiphase and phase transition [48, 66, 69, 76, 93, 94], and linear and nonlinear waves [131]. Such models are also very relevant for compositional models in petroleum science (see [94, 106] and the references cited therein).

- Indeed, although the mathematical theory of nonlinear balance law with relaxation has presented significant progress on well-posedness linked to extended thermodynamics and kinetic theory, a complete understanding for systems larger than 2 by 2 (the case 2 by 2, for some hypothesis is well understood, see [103]) about how solutions evolve from a given initial datum and their regularity and asymptotic behaviour remains elusive, mainly for weak solutions of hyperbolic systems.

- Another important application of the relaxation modelling is in problems with fast phase transitions. The most common phase transition models are obtained by assuming that there are different phases and, which in turn, in each phase the evolution equation is a modelled by a hyperbolic system of conservation laws, subject to a natural equilibrium constraint. Often, the initial data are given on different phases and the solution is obtained as a sequence of waves connecting these different phases. The solutions associated to this kind of problems, in many times, exhibit non uniqueness even for the classical role of entropy admissibility criteria as such Lax's or Liu's entropy conditions. It is worth pointing out that such occurrence of non uniqueness is, many times, associated to the distinct forms which it is possible to connect waves from different phases. Many relevant

questions have appeared on this subject in order to overcome this non uniqueness, which are very often answered by using purely mathematical criteria, without physical meaning (i.e., in many problems the uniqueness is obtained only by using artificial conditions to obtain the uniqueness). On the other hand, we believe that we can give a good contribution to answer this question by using relaxation systems of balance equations. This should be further investigated in a more deep details in a solid basis.

- Another perspective is the application of the outer expansion technique to the steam and nitrogen injection problems in porous medium. In this case, we will first assume the equilibrium hypothesis. We expect to be able to corroborate our analysis along with the relaxation approach in order to get some insight upon the behaviour of associated solution waves. We believe that it is possible to perform similar analysis used to the Euler system, i.e. we know that in the steam and nitrogen injection problems, the solution is composed by groups with simple waves (i.e., rarefaction, shock and constant wave). Thus we expect find the solution in the equilibrium of the injection problem using the same analysis introduced in the works [90, 93, 94]. In this way, we might split the solution wave in simple waves and then make an analysis with respect to each simple wave with a suitable outer expansion. For the rarefaction wave, we will use the same outer expansion approach proposed by Lambert in [92]. In the case shock wave we expect to use a suitable self-similar solution wave $v(x,t) = v(x+\eta t)$; this approach is heavily based of a diffusive regularization of the balance law to allows to seek for a viscous profile. Therefore, the principal issue is to find the outer expansion of order zero. Thus, the next step is to find the higher order expansions in order to obtain some rigorous convergence proof.

- In this current work, we consider a new insight to the same physical model, namely, the modelling of the equilibrium manifold by means of a relaxation parameter linked to the underlying balance law model. For concreteness, in this work we revisit a phase transition model for the injection of steam and nitrogen into a porous media with water. This physical phenomena was first considered and analysed in [93, 94], which in turn the associated 3 by 3 system of balance laws was taken under a thermodynamic equilibrium, where these equilibria composed an equilibria stratified variety. For such model, and under this assumption for each physical phase, the authors studied cases where initial Riemann data are given in the same phase and in the different phases related to the equilibrium manifold, and then the corresponding Riemann solutions for phase transitions were analysed and constructed. Indeed, in this novel framework we were able to analyse a particular Riemann initial data, where we take two different states in the same physical phase with under this relaxed condition. We point out that this analysis was done for a single physical phase. However, the technique used here can be generalized for two or more phases, as the 4 by 4 model (3.14)-(3.17) depicted in Chapter 3. We stress out that in spite of this we do not obtain the complete Riemann solution, we obtain the main structures to obtain this solution (see Appendix B and Appendix C), which we intend to complete as a future work.

With respect to item *ii*) we mention the following two points to be considered in future work:

- In this chapter we make use of a locally conservative finite volume approach in order to developed a cheap unsplitting scheme to account the delicate nonlinear balance between

numerical approximations of the hyperbolic flux function and the source term linked to steady solutions for balance law problems. The method is conservative by construction and relatively easy to understand and implement in order to design a locally conservative scheme to account the balance between numerical approximations of the hyperbolic flux function and the source term linked to steady solutions. The scheme is based on central differencing schemes see [110, 47, 2] or [85], which in turn exhibits some desirable stability and entropy properties good for approximation of hyperbolic conversation laws and balance laws [21, 22, 24, 32, 68, 70, 123]

- For this model problem at hand, however, a proof of stability and convergence of approximate solutions remains elusive. There are several other methods to construct approximate solutions to balance law models as discussed here. Some are naturally derived from physical considerations, others lead to more efficient numerical algorithms; see also [113] and the references cited therein. Indeed, for balance laws, we mention [32, 70] for a modern description of numerical methods for relaxation systems of conservation laws. No matter what is the approximation algorithm, the same natural questions arise (see [70]). Does the total variation of the approximate solutions remain uniformly bounded for all times $t > 0$? In general, the source term might not be decreasing and some semi-implicit and fully implicit scheme are not applicable, at least in a straightforward manner. Additionally, it is possible to design well-balanced schemes which is also asymptotically consistent for a particular system of parabolic equations [32, 70], but the resulting scheme is stable under a very restrictive CFL condition. Another issue is: Do the approximate solutions depend continuously on the initial data, in the L_1 norm? As the approximation parameters (in discrete space and in discrete time) tend to zero, do the approximate solutions converge to the unique entropy weak solution of the hyperbolic Cauchy problem with relaxation? All such questions must be addressed carefully as a possible continuation with respect to the underlying work. Of particular interest on this matter, is the approximate functional space associated to the underlying constructive numerical scheme.

- From the previous discussion, we point out that in the thermodynamic model (3.14)-(3.17) the capillary pressure is considered as constant variable (constant function), which in turn it is unrealistic in general. Although such assumption is unrealistic in general, it is possible to address the issue of relaxation modelling in significant models from a mathematical viewpoint keeping some aspects of the underlying physics. A more realistic model for the injection of steam and nitrogen problems is achieved by considering a non linear capillary pressure models, which depend upon the state variable as such saturation, temperature the the remaining pertinent primary variable of state. Thus, such more general model to the injection of steam and nitrogen problems – still in one-space dimension – lead to a pressure velocity model that dictates the Darcy velocity. This means that it is now impossible to find an analogue explicit formula to the Darcy velocity as in (4.11), or (4.12). Thus, we were able to give a formal construction of a suitable numerical strategy aiming to capture the underlying physical properties of each equation. Moreover, we use an extended version of the unsplitting approximate algorithm for system (3.14)-(3.17) for solving the pertinent parabolic equation in order to approximate simultaneously the pair pressure and Darcy's velocity. We separate (D.7)-(D.6) in parts, the pressure-velocity (D.6) and the temperature-saturation transport (D.7) in the spirit of IMPES approach (implicit in pressure, explicit in temperature-saturation). Roughly speaking, at each time

step, the balance transport problem (D.7) and the pressure-velocity problem (D.6) are sequentially solved.

- Apparently the overall procedure is quite simple to implement in multi-dimensions. This relies on the fact the our novel unsplitting approximate algorithm is based on the structure of the non oscillatory central difference scheme of Nessyahu and Tadmor [110], in which the resolution of Riemann problems at the cell interfaces is bypassed thanks to the use of the staggered Lax-Friedrichs scheme (see [85]). We mention that a high-order, non oscillatory unsplitting central scheme for balance laws might be constructed based on a high-order *Essentially Non-Oscillatory schemes* (ENO) or *Uniformly Non-Oscillatory* (UNO) reconstruction step. These schemes were shown to enjoy the desired properties for conservation laws and balance law problems; see [6, 21, 22, 24, 30, 32, 70, 85, 123].

We are aware that these questions will not be answered in unique work. Clearly, a solid starting point is a thorough study of the one-dimensional case for a concrete problem, which is done in this thesis. We believe we have a very interesting (and promising) field of work ahead of us, which we intend to continue studying in order to better understand this important question that remains elusive.

Appendix A

An analysis of the qualitative behaviour of the non-monotone travelling wave of the reduced Euler system

Here, we give the proof of proposition 2.1.1, which discussed the qualitative behaviour of the non-monotone travelling wave of a reduced Euler system.

A.1 Proof of proposition 2.1.1

Proposition A.1.1. *The system* (2.1) *over open set, for fixed* τ *the energy* E_τ *is bounded around the shock curve, and* E_τ *tends to the equilibrium solution* E *when* $\epsilon \longrightarrow 0$. *Moreover, if* ϵ *is fixed and* $\tau \longrightarrow 0$ *then* $(m_\tau)_x$ *tends to* $(m_r - m_m)\delta_{st}$ *(*δ_{st} *stand for Dirac delta) when* m_m *and* m_r *are the intermediary and right states for* m, *respectively.*

Proof of the Proposition: From Eq. (2.10), we find the characteristic curves $(x(t), t) \in \Omega$, when $\Omega = [a, b] \times (0, T]$, by the system define the following functions along on characteristic curves $(x(t), t)$:

$$\begin{aligned} &f_1(x(t),t) = \beta\frac{m_\tau}{\rho_\tau}, \quad f_3(x(t),t) = \frac{a^2\rho_\tau}{\gamma-1} + \frac{1}{2}\frac{m_\tau^2}{\rho_\tau}, \\ &f_4(x(t),t) = a^2(m_\tau)_x. \end{aligned} \tag{A.1}$$

thus Eq. (2.10) is written as:

$$\frac{dE}{dt} + E\left(f_1(x(t),t) + \frac{1}{\epsilon}\right) = \frac{1}{\epsilon}(f_3(x(t),t))) - f_4(x(t),t)). \tag{A.2}$$

Since Eq. $(A.2)$ is a first order linear equation, the integrant factor is written as:

$$\begin{aligned} I(t) &= \exp\left(\int_0^t \left[f_1(x(\xi),\xi) + \frac{1}{\epsilon}\right] d\xi\right), \\ &= \exp\left(\frac{t}{\epsilon}\right) \exp\left(\int_0^t f_1(x(\xi),\xi) d\xi\right). \end{aligned} \tag{A.3}$$

Notice $I(t) > 0$ and increasing function, since $f_1(x,t) > 0$ is positive, then

$$E = \frac{1}{I(t)}\left[\int_0^t \frac{1}{\epsilon}\left(f_3(x(\theta),\theta)I(\theta)\right)d\theta - \int_0^t f_4(x(\theta),\theta)I(\theta)d\theta\right]$$

$$\leq \frac{1}{I(t)}\left|\frac{1}{\epsilon}\int_0^t f_3(x(\theta),\theta)I(\theta)d\theta\right| + \frac{1}{I(t)}\left|\int_0^t f_4(x(\theta),\theta)I(\theta)d\theta\right|.$$

Since ρ_τ, m_τ are bounded in Ω then f_3 is bounded, let $M = \max_{\Omega}|f_3(x(\theta),\theta)|$, from the first integral of the right hand side of the above inequality we get,

$$\frac{1}{I(t)}\left|\frac{1}{\epsilon}\int_0^t f_3(x(\theta),\theta)I(\theta)d\theta\right| \leq \frac{M}{\epsilon}\int_0^t \exp\left(\frac{\theta}{\epsilon}\right)\exp\left(\int_0^\theta f_1(x(\xi),\xi)d\xi\right)d\theta. \tag{A.4}$$

Now, $f_1(x(\xi),\xi)$ is increasing for all $\xi > 0$, then reads,

$$\exp\left(\int_0^\theta f_1(x(\xi),\xi)d\xi\right) \leq \exp\left(\int_0^t f_1(x(\xi),\xi)d\xi\right), \tag{A.5}$$

and thus,

$$\left|\frac{1}{\epsilon}\int_0^t f_3(x(\theta),\theta)I(\theta)d\theta\right| \leq M\exp\left(\int_0^t f_1(x(\xi),\xi)d\xi\right)\left(\exp\left(\frac{t}{\epsilon}\right)-1\right). \tag{A.6}$$

Finally we get,

$$\frac{1}{I(t)}\left|\frac{1}{\epsilon}\int_0^t f_3(x(\theta),\theta)I(\theta)\right| \leq M\left(1-\exp\left(-\frac{t}{\epsilon}\right)\right).$$

We turn now our attention to the remaining integral,

$$\begin{aligned}&\frac{1}{I(t)}\left(\int_0^t f_4(x(\theta),\theta)I(\theta)d\theta\right) \leq \frac{1}{I(t)}\left[\frac{1}{\epsilon}\exp\left(\int_0^t f_1(x(\xi),\xi)d\xi\right)\int_0^t f_4(x(\theta),\theta)\exp\left(\frac{\theta}{\epsilon}\right)d\theta\right]\\ &\leq \frac{1}{\exp\left(\frac{t}{\epsilon}\right)}\int_0^t f_4(x(\theta),\theta)\exp\left(\frac{\theta}{\epsilon}\right)d\theta.\end{aligned} \tag{A.7}$$

Thus,

$$\frac{1}{I(t)}\left|\int_0^t f_4(x(\theta),\theta)I(\theta)d\theta\right| \leq \frac{1}{\exp\left(\frac{t}{\epsilon}\right)}\int_0^t |f_4(x(\theta),\theta)|\exp\left(\frac{\theta}{\epsilon}\right)d\theta. \tag{A.8}$$

Notice that $|f_4(x(\theta),\theta)| \leq \hat{M}$ is bounded and then,

$$\frac{1}{I(t)}\left|\int_0^t f_4(x(\theta),\theta)I(\theta)d\theta\right| \leq \hat{M}\left(\frac{1}{\exp\left(\frac{t}{\epsilon}\right)}\int_0^t \exp\left(\frac{\theta}{\epsilon}\right)d\theta\right) \leq \hat{M}\epsilon\left(1-\exp\left(\frac{\theta}{\epsilon}\right)\right).$$

This result quite is consistent since for fixed τ_x, functions are C^∞ then bounded, and $\epsilon \to 0$ the jump, that depends on ϵ, vanishes.

We will shown that $(m_\tau)_x = \delta_{st}$ converge to a Dirac Delta located at the shock profile. To do so, we prove that $(m_\tau)_x$ converges to identity approximating. From Eq. (2.7), we can write $(m_\tau)_x(x,t)$ as:

$$(m_\tau)_x(x,t) = \frac{1}{\sqrt{\pi\tau}} \int_{\mathbb{R}} R \frac{-2(x-y)}{\tau} exp\left(-\frac{(x-y)^2}{\tau}\right) m(y,t)\, dy. \tag{A.9}$$

We are interested in the analysis of the structure near the shock speed. By using properties $exp(-(x-y)^2/\tau)$, notice that for a $A = A(t)$ to the shock curve, $m(x,t) = m_m$ and for states from shock to $+\infty$, $m(x,t) = m_r$, then previous integral can be written as:

$$(m_\tau)_x(x,t) = \frac{1}{\sqrt{\pi\tau}}\Big(\int_A^{st} \frac{-2(x-y)}{\tau} exp\left(-\frac{(x-y)^2}{\tau}\right) m(y,t)dy +$$
$$\int_{st}^{\infty} \frac{-2(x-y)}{\tau} exp\left(-\frac{(x-y)^2}{\tau}\right) m(y,t)dy\Big) + \kappa_\tau,$$

$$(m_\tau)_x(x,t) = \frac{1}{\sqrt{\pi\tau}}\Big(\int_A^{st} \frac{-2(x-y)}{\tau} exp\left(-\frac{(x-y)^2}{\tau}\right) m_m dy +$$
$$+ \int_{st}^{\infty} \frac{-2(x-y)}{\tau} exp\left(-\frac{(x-y)^2}{\tau}\right) m_r dy\Big) + \kappa_\tau,$$

$$(m_\tau)_x(x,t) = \frac{1}{\sqrt{\pi\tau}} \left(m_m exp\left(-\frac{u^2}{\tau}\right)\Big|_{x-A}^{x-st} + m_r exp\left(-\frac{u^2}{\tau}\right)\Big|_{x-st}^{-\infty} \right) + \kappa_\tau,$$

$$(m_\tau)_x(x,t) = \frac{1}{\sqrt{\pi\tau}} \left((m_r - m_m) exp\left(-\frac{(st-x)^2}{\tau}\right)\right) + \frac{1}{\sqrt{\pi\tau}} \left(exp\left(-\frac{(A-x)^2}{\tau}\right)\right) + \kappa_\tau,$$

such that for $A \neq x$ $\dfrac{1}{\sqrt{\pi\tau}} \left(exp\left(-\dfrac{(A-x)^2}{\tau}\right)\right) \longrightarrow 0$ and $\kappa_\tau \longrightarrow 0$, when $\tau \longrightarrow 0$. From *approximating identity*, see [52], we can see that $(m_\tau)_x(x,t)$ converges to $(m_r - m_m)\delta_{st}$ when $\tau \longrightarrow 0$. Notice that, from parameter β, we have two possibilities:

(i) the curve $x = st$ crosses some characteristic curves, for small β;

(ii) some characteristic curves cross $x = st$, for large β;

In both cases, if the characteristic curve does not reach the shock curve $x = st$,

$$\frac{1}{I(t)} \left(\int_0^t f_4(x(\theta),\theta) I(\theta) d\theta \right) = 0$$

and for characteristic reached by the shock curve $x = st$,

$$\left| \frac{1}{I(t)} \left(\int_0^t f_4(x(\theta),\theta) I(\theta) d\theta \right) \right| \leq (m_r - m_m). \quad \blacksquare$$

Appendix B

Calculations for the eingenpairs linked to thermodynamic balance law system

In what follows, we show the pertinent calculations for the eingenpairs linked to thermodynamic balance law system (3.14)-(3.17).

B.1 Eingenpairs for the thermodynamic balance law system (3.14)-(3.17)

Consider the thermodynamic balance law system,

$$\frac{\partial}{\partial t}(\varphi\rho_W s_w) + \frac{\partial}{\partial x}(u\rho_W f_w) = q_{g\to a,w}, \tag{B.1}$$

$$\frac{\partial}{\partial t}(\varphi\psi_{gw}\rho_{gW} s_g) + \frac{\partial}{\partial x}(u\psi_{gw}\rho_{gW} f_g) = -q_{g\to a,w}, \tag{B.2}$$

$$\frac{\partial}{\partial t}(\varphi\rho_{gN}\psi_{gn} s_g) + \frac{\partial}{\partial x}(u\rho_{gN}\psi_{gn} f_g) = 0, \tag{B.3}$$

$$\frac{\partial}{\partial t}\Big(\varphi(\hat{H}_r + s_w H_w + s_g H_g)\Big) + \frac{\partial}{\partial x}\Big(u(f_w H_w + f_g H_g)\Big) = 0. \tag{B.4}$$

To obtain the eingenpairs we solve:

$$A\vec{r} = \lambda B\vec{r} \quad \textit{with characteristic polynomial} \quad det(A - \lambda B) = 0, \tag{B.5}$$

where the matrices B and A are the derivatives of $G(V)$ and $uF(V)$ with respect to the variables (V, u). In [90] the authors proved that each eigenvalue for a $n \times n$ system has the form $\lambda = u\sigma(V)$ and eigenvectors $\vec{r} = (\gamma_1(V), \gamma_2(V), \cdots, \gamma_{n-1}(V), u\gamma_n(V)$. In addition, it is proved that the solution can be projected on the Ω space of states V.

Note that φ and ρ_w are constants. The functions $\rho_{gN}, \rho_{gW}, \hat{H}_r$ and H_w only dependent of that variable $\{T\}$, the function f_g depends on the variables $\{s_g, T\}$ and the function H_g depends on the $\{T, \psi_{gw}\}$. Let $\gamma = H_g - H_w$. We use the following notation, $\rho'_{gN}, \rho'_{gW}, \hat{H}'_r, H'_w, H'_g$ and γ' for the derivative with respect the variable T

Thus, A is

$$\begin{bmatrix} -u\dfrac{\partial f_g}{\partial s_g}\rho_W & -u\dfrac{\partial f_g}{\partial T}\rho_W & 0 & (1-f_g)\rho_W \\ u\dfrac{\partial f_g}{\partial s_g}\psi_{gw}\rho_{gW} & u\dfrac{\partial f_g}{\partial T}\psi_{gw}\rho_{gW} + uf_g\psi_{gw}\rho'_{gW} & uf_g\rho_{gW} & f_g\psi_{gw}\rho_{gW} \\ u\dfrac{\partial f_g}{\partial s_g}(1-\psi_{gw})\rho_{gN} & u\dfrac{\partial f_g}{\partial T}(1-\psi_{gw})\rho_{gN} + uf_g(1-\psi_{gw})\rho'_{gN} & -uf_g\rho_{gN} & f_g(1-\psi_{gw})\rho_{gN} \\ u\dfrac{\partial f_g}{\partial s_g}\gamma & u\dfrac{\partial f_g}{\partial T}\gamma + u\Big(H'_w + f_g\gamma'\Big) & uf_g\dfrac{\partial H_g}{\partial \psi_{gw}} & H_w + f_g\gamma \end{bmatrix}, \tag{B.6}$$

and the matrix B is determined as

$$\begin{bmatrix} -\varphi\rho_W & 0 & 0 & 0 \\ \varphi\psi_{gw}\rho_{gW} & \varphi\psi_{gw}\rho'_{gW}s_g & \varphi\rho_{gW}s_g & 0 \\ \varphi(1-\psi_{gw})\rho_{gN} & \varphi(1-\psi_{gw})\rho'_{gN}s_g & -\varphi\rho_{gN}s_g & 0 \\ \varphi\gamma & \varphi(H'_g - H'_w)s_g + \varphi(\hat{H}'_r + H'_w) & \varphi\dfrac{\partial H_g}{\partial \psi_{gw}}s_g & 0 \end{bmatrix}. \tag{B.7}$$

We need to solve characteristic equation

$$\det(A - \lambda B) = 0, \tag{B.8}$$

for to find the general eigenvalues of the system ((3.14)-(3.17)), so the determinant of the equation (B.8) is

$$
\begin{vmatrix}
-(u\dfrac{\partial f_g}{\partial s_g}-\lambda\varphi)\rho_W & -u\dfrac{\partial f_g}{\partial T}\rho_W & 0 & (1-f_g)\rho_W \\
\Big(u\dfrac{\partial f_g}{\partial s_g}-\lambda\varphi\Big)\psi_{gw}\rho_{gW} & u\dfrac{\partial f_g}{\partial T}\psi_{gw}\rho_{gW}+(uf_g-\lambda\varphi s_g)\psi_{gw}\rho'_{gW} & \Big(uf_g-\lambda\varphi s_g\Big)\rho_{gW} & f_g\psi_{gw}\rho_{gW} \\
\Big(u\dfrac{\partial f_g}{\partial s_g}-\lambda\varphi\Big)\Big((1-\psi_{gw})\rho_{gN}\Big) & u\dfrac{\partial f_g}{\partial T}(1-\psi_{gw})\rho_{gN}+(uf_g-\lambda\varphi s_g)(1-\psi_{gw})\rho'_{gN} & -\Big(uf_g-\lambda\varphi s_g\Big)\rho_{gN} & f_g\Big((1-\psi_{gw})\rho_{gN}\Big) \\
\Big(u\dfrac{\partial f_g}{\partial s_g}-\lambda\varphi\Big)\gamma & u\dfrac{\partial f_g}{\partial T}\gamma+uH'_w+(uf_g-\lambda\varphi s_g)\gamma'-\lambda\varphi(\hat{H}'_r+H'_w) & \Big(uf_g-\lambda\varphi s_g\Big)\dfrac{\partial H_g}{\partial\psi_{gw}} & H_w+f_g\gamma
\end{vmatrix}, \tag{B.9}
$$

can factorize the terms $u\dfrac{\partial f_g}{\partial s_g} - \lambda\varphi$ and $uf_g - \lambda\varphi s_g$, then we obtain the eigenpairs (eingevalues and eigenvectors) $\lambda_s = \frac{u}{\varphi}\dfrac{\partial f_g}{\partial s_g}$ and $\vec{r}_s = (1,0,0,0)$; and $\lambda_c = \frac{uf_g}{\varphi s_g}$ and $\vec{r}_c = (0,0,1,0)$. To obtain the third eigenvalue, (B.9) is rewritten as

$$\begin{vmatrix} -\rho_W & -u\dfrac{\partial f_g}{\partial T}\rho_W & 0 & (1-f_g)\rho_W \\ \psi_{gw}\rho_{gW} & u\dfrac{\partial f_g}{\partial T}\psi_{gw}\rho_{gW} + (uf_g - \lambda\varphi s_g)\psi_{gw}\rho'_{gW} & \rho_{gW} & f_g\psi_{gw}\rho_{gW} \\ (1-\psi_{gw})\rho_{gN} & u\dfrac{\partial f_g}{\partial T}(1-\psi_{gw})\rho_{gN} + (uf_g - \lambda\varphi s_g)(1-\psi_{gw})\rho'_{gN} & -\rho_{gN} & f_g\Big((1-\psi_{gw})\rho_{gN}\Big) \\ \gamma & u\dfrac{\partial f_g}{\partial T}\gamma + uH'_w + (uf_g - \lambda\varphi s_g)\gamma' - \lambda\varphi(\hat{H}'_r + H'_w) & \dfrac{\partial H_g}{\partial \psi_{gw}} & H_w + f_g\gamma \end{vmatrix}. \tag{B.10}$$

Note that if we multiply the first column by $-u\dfrac{\partial f_g}{\partial T}$, add to the second column, then multiply the first column by $-f_g$ and add to fourth column, we obtain the following determinant:

$$\begin{vmatrix} -\rho_W & 0 & 0 & \rho_W \\ \psi_{gw}\rho_{gW} & (uf_g - \lambda\varphi s_g)\psi_{gw}\rho'_{gW} & \rho_{gW} & 0 \\ (1-\psi_{gw})\rho_{gN} & (uf_g - \lambda\varphi s_g)(1-\psi_{gw})\rho'_{gN} & -\rho_{gN} & 0 \\ \gamma & uH'_w + (uf_g - \lambda\varphi s_g)\gamma' - \lambda\varphi(\hat{H}'_r + H'_w) & \dfrac{\partial H_g}{\partial \psi_{gw}} & H_w \end{vmatrix}. \tag{B.11}$$

Now we sum the fourth column with the first column

$$\begin{vmatrix} 0 & 0 & 0 & \rho_W \\ \psi_{gw}\rho_{gW} & (uf_g - \lambda\varphi s_g)\psi_{gw}\rho'_{gW} & \rho_{gW} & 0 \\ (1-\psi_{gw})\rho_{gN} & (uf_g - \lambda\varphi s_g)(1-\psi_{gw})\rho'_{gN} & -\rho_{gN} & 0 \\ \gamma + H_w & uH'_w + (uf_g - \lambda\varphi s_g)\gamma' - \lambda\varphi(\hat{H}'_r + H'_w) & \dfrac{\partial H_g}{\partial \psi_{gw}} & H_w \end{vmatrix}, \tag{B.12}$$

we define $\theta = (uf_g - \lambda\varphi s_g)$, thus (B.12) is rewritten as

$$\rho_W \begin{vmatrix} \psi_{gw}\rho_{gW} & \theta\psi_{gw}\rho'_{gW} & \rho_{gW} \\ (1-\psi_{gw})\rho_{gN} & \theta(1-\psi_{gw})\rho'_{gN} & -\rho_{gN} \\ H_g & uH'_w + \theta\gamma' - \lambda\varphi(\hat{H}'_r + H'_w) & \dfrac{\partial H_g}{\partial \psi_{gw}} \end{vmatrix} = 0. \tag{B.13}$$

We calculate the determinant using the determinant expansion rule by minor in the third row

$$\begin{aligned} H_g \begin{vmatrix} \theta\psi_{gw}\rho'_{gW} & \rho_{gW} \\ \theta(1-\psi_{gw})\rho'_{gN} & -\rho_{gN} \end{vmatrix} - \Big(uH'_w + \theta\gamma' - \lambda\varphi(\hat{H}'_r + H'_w)\Big) \begin{vmatrix} \psi_{gw}\rho_{gW} & \rho_{gW} \\ (1-\psi_{gw})\rho_{gN} & -\rho_{gN} \end{vmatrix} \\ + \frac{\partial H_g}{\partial \psi_{gw}} \begin{vmatrix} \psi_{gw}\rho_{gW} & \theta\psi_{gw}\rho'_{gW} \\ (1-\psi_{gw})\rho_{gN} & \theta(1-\psi_{gw})\rho'_{gN} \end{vmatrix} = 0, \end{aligned} \tag{B.14}$$

$$\begin{aligned} H_g\theta \begin{vmatrix} \psi_{gw}\rho'_{gW} & \rho_{gW} \\ (1-\psi_{gw})\rho'_{gN} & -\rho_{gN} \end{vmatrix} - \Big(uH'_w + \theta\gamma' - \lambda\varphi(\hat{H}'_r + H'_w)\Big)\rho_{gW}\rho_{gN} \begin{vmatrix} \psi_{gw} & 1 \\ (1-\psi_{gw}) & -1 \end{vmatrix} \\ + \frac{\partial H_g}{\partial \psi_{gw}}(1-\psi_{gw})\theta\psi_{gw} \begin{vmatrix} \rho_{gW} & \rho'_{gW} \\ \rho_{gN} & \rho'_{gN} \end{vmatrix} = 0. \end{aligned} \tag{B.15}$$

Let

$$A = \begin{vmatrix} \psi_{gw}\rho'_{gW} & \rho_{gW} \\ (1-\psi_{gw})\rho'_{gN} & -\rho_{gN} \end{vmatrix} = -\rho_{gN}\psi_{gw}\rho'_{gW} - \rho_{gW}(1-\psi_{gw})\rho'_{gN} \\ = \psi_{gw}(\rho_{gW}\rho'_{gN} - \rho_{gN}\rho'_{gW}) - \rho_{gW}\rho'_{gN} = \psi_{gw}C - \rho_{gW}\rho'_{gN} \tag{B.16}$$

$$B = \begin{vmatrix} \psi_{gw} & 1 \\ (1-\psi_{gw}) & -1 \end{vmatrix} = -\psi_{gw} - (1-\psi_{gw}) = -1 \tag{B.17}$$

$$C = \begin{vmatrix} \rho_{gW} & \rho'_{gW} \\ \rho_{gN} & \rho'_{gN} \end{vmatrix} = \rho_{gW}\rho'_{gN} - \rho_{gN}\rho'_{gW}, \tag{B.18}$$

Thus we can rewritten the equation (B.25) as

$$H_g\theta\Big(\psi_{gw}C - \rho_{gW}\rho'_{gN}\Big) + \Big(uH'_w + \theta\gamma' - \lambda\varphi(\hat{H}'_r + H'_w)\Big)\rho_{gW}\rho_{gN} + \frac{\partial H_g}{\partial \psi_{gw}}(1-\psi_{gw})\theta\psi_{gw}C = 0, \tag{B.19}$$

$$\theta\Big(H_g(\psi_{gw}C - \rho_{gW}\rho'_{gN}) + \frac{\partial H_g}{\partial \psi_{gw}}(1-\psi_{gw})\psi_{gw}C + \gamma'\rho_{gW}\rho_{gN}\Big) + \Big(uH'_w - \lambda\varphi(\hat{H}'_r + H'_w)\Big)\rho_{gW}\rho_{gN} = 0. \tag{B.20}$$

Defining,

$$\Pi = H_g(\psi_{gw}C - \rho_{gW}\rho'_{gN}) + \frac{\partial H_g}{\partial \psi_{gw}}(1-\psi_{gw})\psi_{gw}C + \gamma'\rho_{gW}\rho_{gN}. \tag{B.21}$$

Moreover, notice that if $\rho_{gW} = M_W/T$ e $\rho_{gN} = M_N/T$, then $C = 0$. The eigenvalue is written as:

$$(uf_g - \lambda\varphi s_g)\Pi + uH'_w\rho_{gW}\rho_{gN} - \lambda\varphi(\hat{H}'_r + H'_w)\rho_{gW}\rho_{gN} = 0. \tag{B.22}$$

$$\lambda = \frac{u}{\varphi}\frac{f_g\Pi + H'_w\rho_{gW}\rho_{gN}}{s_g\Pi + (\hat{H}'_r + H'_w)\rho_{gW}\rho_{gN}}, \tag{B.23}$$

$$\Pi = -H_g(\rho_{gW}\rho'_{gN}) + \gamma'\rho_{gW}\rho_{gN}. \tag{B.24}$$

We now turn our attention to the calculation of the eigenvectors associated to the evaporation process. We define the following notation $\hat{\lambda_e} = \frac{1}{\varphi}\frac{f_g\Pi + H'_w\rho_{gW}\rho_{gN}}{s_g\Pi + \left(\hat{H}'_r + H'_w\right)\rho_{gW}\rho_{gN}}$, thus we rewrite the equation (B.9) as

$$\begin{pmatrix} -u(\frac{\partial f_g}{\partial s_g}-\hat{\lambda}_e\varphi)\rho_W & -u\frac{\partial f_g}{\partial T}\rho_W & 0 & (1-f_g)\rho_W \\ u\Big(\frac{\partial f_g}{\partial s_g}-\hat{\lambda}_e\varphi\Big)\psi_{gw}\rho_{gW} & u\left[\frac{\partial f_g}{\partial T}\psi_{gw}\rho_{gW}+(f_g-\hat{\lambda}_e\varphi s_g)\psi_{gw}\rho'_{gW}\right] & u\Big(f_g-\hat{\lambda}_e\varphi s_g\Big)\rho_{gW} & f_g\psi_{gw}\rho_{gW} \\ u\Big(\frac{\partial f_g}{\partial s_g}-\hat{\lambda}_e\varphi\Big)\Big((1-\psi_{gw})\rho_{gN}\Big) & u\left[\frac{\partial f_g}{\partial T}(1-\psi_{gw})\rho_{gN}+(f_g-\hat{\lambda}_e\varphi s_g)(1-\psi_{gw})\rho'_{gN}\right] & -u\Big(f_g-\hat{\lambda}_e\varphi s_g\Big)\rho_{gN} & f_g\Big((1-\psi_{gw})\rho_{gN}\Big) \\ u\Big(\frac{\partial f_g}{\partial s_g}-\hat{\lambda}_e\varphi\Big)\gamma & u\left[\frac{\partial f_g}{\partial T}\gamma+H'_w+(uf_g-\hat{\lambda}_e\varphi s_g)\gamma'-\hat{\lambda}_e\varphi(\hat{H}'_r+H'_w)\right] & u\Big(f_g-\hat{\lambda}_e\varphi s_g\Big)\frac{\partial H_g}{\partial\psi_{gw}} & H_w+f_g\gamma \end{pmatrix}. \tag{B.25}$$

To calculate the right e-eigenvector we add the first with the second row, later we use the Gaussian elimination in (B.25) on first and third elements of the first column yields,

$$\begin{pmatrix} 0 & -u\frac{\partial f_g}{\partial T}\psi_{gw}\rho'_{gW}\rho_W & u\Big(f_g-\hat{\lambda}_e\varphi s_g\Big)\rho_{gW}\rho_W & \psi_{gw}\rho_{gW}\rho_W \\ u\Big(\frac{\partial f_g}{\partial s_g}-\hat{\lambda}_e\varphi\Big)(\psi_{gw}\rho_{gW}-\rho_W) & u\left[\frac{\partial f_g}{\partial T}(\psi_{gw}\rho_{gW}-\rho_W)+(f_g-\hat{\lambda}_e\varphi s_g)\psi_{gw}\rho'_{gW}\right] & u\Big(f_g-\hat{\lambda}_e\varphi s_g\Big)\rho_{gW} & f_g\psi_{gw}\rho_{gW}+(1-f_g)\rho_W \\ 0 & 0 & -u\Big(f_g-\hat{\lambda}_e\varphi s_g\Big)\rho_{gN}\rho_{gW} & 0 \\ u\Big(\frac{\partial f_g}{\partial s_g}-\hat{\lambda}_e\varphi\Big)\gamma & u\left[\frac{\partial f_g}{\partial T}\gamma+H'_w+(uf_g-\hat{\lambda}_e\varphi s_g)\gamma'-\hat{\lambda}_e\varphi(\hat{H}'_r+H'_w)\right] & u\Big(f_g-\hat{\lambda}_e\varphi s_g\Big)\frac{\partial H_g}{\partial\psi_{gw}} & H_w+f_g\gamma \end{pmatrix}, \tag{B.26}$$

so, we rewrite the previous matrix as

$$J=\begin{pmatrix} 0 & ud_{12}(V) & ud_{13}(V) & d_{14}(V) \\ ul_{21}(V) & ul_{22}(V) & ul_{23}(V) & l_{24}(V) \\ 0 & 0 & ud_{33}(V) & 0 \\ ul_{41}(V) & ul_{42}(V) & ul_{43}(V) & l_{44}(V) \end{pmatrix}. \tag{B.27}$$

Note that we changed the nomenclature and all elements d_{ij} and l_{ij}, for $i,j=1,..4$, only depends of the variables set $\{s_g,T,\psi\}$. For example, the element in the first column and second row in matrix (B.26) is rewritten as

$$d_{12}=-\frac{\partial f_g}{\partial T}\psi_{gw}\rho'_{gW}\rho_W.$$

Let $r_e = (r_1, r_2, r_3, r_4)^T$ be the evaporation eigenvector, so we have $Jr_e = 0$. If we multiply the third row with r_e, it yields the equation $ud_{33}r_3 = 0$, obtaining $r_3 = 0$. The element

$$l_{24} = f_g\psi_{gw}\rho_{gW} + (1 - f_g)\rho_W$$

vanishes when $\psi = 0$ and $s_g = 1$, i.e., the system is fully saturated with nitrogen. We assume that $l_{24} \neq 0$. We can multiply the second row of the matrix (B.27) with the eigenvector r_e obtaining

$$ul_{21}r_1 + ul_{22}r_2 + l_{24}r_4 = 0, \tag{B.28}$$

$$r_4 = \frac{-u}{l_{24}}(l_{21}r_1 + l_{22}r_2). \tag{B.29}$$

Now, we multiply the first row with r_e

$$ud_{12}r_2 + d_{14}r_4 = 0,$$

we substituting r_4 into the previous equation yielding

$$(d_{12}l_{24} - d_{14}l_{22})r_2 = d_{14}l_{21}r_1.$$

So the evaporation eigenvector in the case where $s_g \neq 1$ and $\psi_{gw} \neq 0$ is

$$r_e = (d_{12}l_{24} - d_{14}l_{22}, d_{14}l_{21}, 0, -ul_{21}d_{12})\,. \tag{B.30}$$

We can summarize these calculations as:

Proposition B.1.1. *The system* (B.1)-(B.4) *has three positives eigenvalues*

$$\lambda_s = \frac{u}{\varphi}\frac{\partial f_g}{\partial s_g}, \quad \textit{and} \quad \vec{r_s} = (1, 0, 0, 0), \tag{B.31}$$

$$\lambda_c = \frac{uf_g}{\varphi s_g} \quad \textit{and} \quad \vec{r_c} = (0, 0, 1, 0),$$

$$\lambda_e = \frac{u}{\varphi}\frac{f_g\Pi + H'_w\rho_{gW}\rho_{gN}}{s_g\Pi + (\hat{H}'_r + H'_w)\rho_{gW}\rho_{gN}} \quad \textit{and} \quad \vec{r_e}.$$

Appendix C

Physical quantities, the equations of state and the laws of thermodynamics

In the appendix we give a list of the physical quantities, the equations of state and the laws of thermodynamics to facilitate the reading and comprehension this these.

C.1 Primary and secondary variables and properties of fluids in injection problems

Consider the Darcy's velocity for water and steam phases,

$$u_w = -\frac{kk_{rw}}{\mu_w}\frac{\partial p_w}{\partial x} \qquad u_g = -\frac{kk_{rg}}{\mu_g}\frac{\partial p_g}{\partial x}. \tag{C.1}$$

The fractional flow for water and steam are define by:

$$f_w = \frac{k_{rw}/\mu_w}{k_{rw}/\mu_w + k_{rg}/\mu_g} \quad f_g = \frac{k_{rg}/\mu_g}{k_{rw}/\mu_w + k_{rg}/\mu_g}. \tag{C.2}$$

The relative permeability functions k_rw and k_rg are

$$k_{rw} = 0.5s_w^2, \qquad k_{rg} = 0.95s_g^2. \tag{C.3}$$

Water saturation pressure is

$$\begin{aligned} p_{sat} = 10^3\big(&- 0.175776 \cdot 10^3 + 2.29272T - 0.0113953T^2 + 0.26278 \cdot 10^{-4}T^3 \\ &- 0.2737264 \cdot 10^{-7}T^4 + 1.13816 \cdot 10^{-11}T^5\big)^2. \end{aligned} \tag{C.4}$$

Steam enthalpies and nitrogen enthalpies are, respectively

$$\begin{aligned} h_{gw} = &-0.49688 \cdot 10^{-8}T^6 + 0.126913 \cdot 10^{-4}T^5 - 0.0133437T^4 \\ &+ 7.3742T^3 - 2258.37T^2 + 365317.0T - 23268318.16, \end{aligned} \tag{C.5}$$

$$h_{gn} = -0.476 \cdot 10^{-7}T^3 + 0.0935T^2 + 975T - 293700.6842. \tag{C.6}$$

Rock enthalpy

$$H_r = \frac{(1.0 - \varphi)}{\varphi} C_r (T - \hat{T}), \tag{C.7}$$

where $\hat{T} = 293$.

Gas effective Entalphy in equilibrium

$$H_g = \rho_{gw} h_{gw} + \rho_{gn} h_{gn}. \tag{C.8}$$

Gas effective Entalphy out equilibrium

$$H_g = \Psi_{gw} \rho_{gw} h_{gw} + \Psi_{gn} \rho_{gn} h_{gn}. \tag{C.9}$$

Water effective Entalphy

$$H_w = 4229295.572T - 1239183603. \tag{C.10}$$

Water viscosity

$$\mu_w = -0.0123274 + \frac{27.1038}{T} - \frac{23527.5}{T^2} + \frac{11014250}{T^3} - \frac{2173420000}{T^4} + \frac{1.86935 \cdot 10^{11}}{T^5}. \tag{C.11}$$

Steam viscosity

$$\mu_g = 0.00164376(0.002679887445T)^6. \tag{C.12}$$

Steam and Nitrogen densities

$$\rho_{gw} = \frac{M_w p^{sat}}{RT}, \qquad \rho_{gn} = \frac{M_n (p_{at} - p^{sat})}{RT}. \tag{C.13}$$

Pure Steam and Nitrogen densities

$$\rho_{gW}(T) = \frac{M_w p_{at}}{RT}, \qquad \rho_{gN}(T) = \frac{M_n p_{at}}{RT}. \tag{C.14}$$

Mass transfer between liquid and gaseous water

$$q_g = \frac{\rho_{gw}}{\rho_{gW}} - \Psi_{gw} \tag{C.15}$$

Table 2, Summary of physical input parameters and variables

Physical quantity	*Symbol*	*Value*	*Unit*
Water, steam fractional functions	$f_w, f_g.$	Eq (C.2)	$[m^3/m^3]$
Porous rock permeability	k	$1.0 \times 10^{-12}.$	$[m^3]$
Water, steam relative permeabilities	k_{rw}, k_{rg}	Eq. (C.3) .	$[m^3/m^3]$
Pressure	p_{at}	$1.0135 \times 10^5.$	[Pa]
Water saturation pressure	p^{sat}	Eq. (C.4)	[Pa]
Water, steam phase velocity	u_w, u_g	Eq. (C.1) .	$[m^3/(m^2s)]$
Total Darcy velocity	u	$u_w + u_g.$	$[m^3/(m^2s)]$
Effective Rock heat capacity	C_r	$2.029 \times 10^6.$	$[J/(m^3K)]$
Steam and nitrogen enthalpies	h_{gw}, h_{gn}	Eqs. $(C.5)$, $(C.6.b)$.	$[J/m^3]$
Rock enthalpy	H_r	Eq. (C.7)	$[J/m^3]$
Gas Effective Entalphy	H_g	Eqs. (C.8)-(C.9)	$[J/m^3]$
Water Entalphy	H_w	Eq. (C.10)	$[J/m^3]$
Water, steam saturations	s_w, s_g	Dependent variables.	$[m^3/m^3]$
Temperature	T	Dependent variable.	[K]
Water, steam viscosity	μ_w, μ_g	Eqs. (C.11) , (C.12).	[Pa s]
Steam and nitrogen densities	ρ_{gw}, ρ_{gn}	Eqs. (C.13) .	$[kg/m^3]$
Water density	ρ_W	998.2	$[kg/m^3]$
The pure phase densities	ρ_{gW}, ρ_{gN}	Eqs. (C.14) .	
Nitrogen and water molar masses	M_n,M_w	0.28, 0.18	[kg/mol]
Universal gas constant	R	8.31	[J/mol/K]
Rock porosity (constant)	φ	0.38.	$[m^3/m^3]$
Mass transfer between lq and wa	q_g	Eq. (C.15)	

Appendix D

An approximation of the pressure-velocity problem by hybrid mixed finite elements linked to a thermodynamic balance law system

From the previous discussion, we point out that in the thermodynamic model (3.14)-(3.17) that the capillary pressure is considered as a constant variable (constant function), which turn it is unrealistic in general. Although such assumption is unrealistic, it is allow us to address the issue of relaxation modelling in significant models from a mathematical viewpoint, and keeping some aspects of the underlying physics. A more realistic model for the injection of steam and nitrogen problems is achieved by considering a nonlinear capillary pressure models, which depend upon the state variable such as saturation, temperature and the remaining pertinent primary variable of state. Thus, this much more general model for the injection of steam and nitrogen problems – still in one-space dimension – leads to a pressure-velocity model that dictates the Darcy's velocity. This means that now are a unable to find an analogue explicit formula to the Darcy's velocity as in (4.11), or (4.12).

D.1 A thermodynamic balance law system coupled with a pressure-velocity problem to the Darcy's equation

By following [90], a thermodynamic balance law system coupled with a *variable* pressure-velocity problem for the Darcy's equation for a more general model to the injection of steam and nitrogen problems might be given by as,

$$\frac{\partial}{\partial t}(\varphi\rho_W s_w) + \frac{\partial}{\partial x}(u\rho_W f_w) = q_{g\to a,w}, \tag{D.1}$$

$$\frac{\partial}{\partial t}(\varphi(\rho_{gW} s_g + \rho_W s_w)) + \frac{\partial}{\partial x}(u(\rho_{gW} f_g + \rho_W f_w)) = 0, \tag{D.2}$$

$$\frac{\partial}{\partial t}(\varphi\rho_{gN} s_g) + \frac{\partial}{\partial x}(u\rho_{gN} f_g) = 0 \tag{D.3}$$

$$\varphi\frac{\partial}{\partial t}\Big(\varphi(\hat{H}_r + s_w H_w + s_g H_g)\Big) + \frac{\partial}{\partial x}\Big(u(f_w H_w + f_g H_g)\Big) = 0, \tag{D.4}$$

subject to the equation

$$u = -k\Big(\frac{k_{rw}}{\mu_w} + \frac{k_{rg}}{\mu_g}\Big)\frac{\partial}{\partial x}p. \tag{D.5}$$

In this manner, we have a new system with the variables (s_g, T, ψ_{gw}, p), where p is pressure. In this way, we may combine the equations (D.2) and (D.5) to obtain the parabolic equation for the pressure-velocity Darcy problem,

$$c(p, s_g, T, \psi_{gw})\frac{\partial p}{\partial t} - \frac{\partial}{\partial x}\left(a(p, s_w, T, \psi_{gw})\frac{\partial}{\partial x}p\right) = f(p, s_w, T, \psi_{gw}), \tag{D.6}$$

and with remaining equations of the previous system we get to a balance hyperbolic system

$$\frac{\partial}{\partial t}G(\mathcal{V}) + \frac{\partial}{\partial x}(uF(\mathcal{V})) = Q(\mathcal{V}). \tag{D.7}$$

The system (D.6)-(D.7) is the combination of two equations with two distinct nature, i.e., a pressure-velocity system (of parabolic nature) and a transport system (of hyperbolic balance law nature). We will use the splitting operator to approximate separately each differential equation. We separate (D.7)-(D.6) in parts: the pressure-velocity (D.6) and the Temperature-saturation transport (D.7) in the spirit of IMPES approach (implicit in pressure, explicit in Temperature-saturation). Roughly speaking, at each time step, the balance transport problem (D.7) and the pressure-velocity problem (D.6) are sequentially solved.

Thus, we have to use the a suitable numerical strategy that captures the underlying physical properties of each equation. Therefore, we may use an extended version of the unsplitting approximate algorithm for relaxation balance laws (1.1.2) to approximate the hyperbolic balance system and we will build a numerical scheme based in a hybrid mixed finite elements for solving the pertinent parabolic equation in order to approximate simultaneously the pair pressure and Darcy's velocity.

The unsplitting algorithm for relaxation balance laws was previously introduced and discussed. We now turn to a brief discussion of the hybrid mixed finite element formulation (HMFEM); see [65] or [34, 44, 57]. We propose a HMFEM formulation, along with Robin type boundary conditions (see [28, 29, 45, 60, 56, 45, 117]) to be used to transmit information between subdomains, for the spatial approximation combined with a backward Euler in time, intended for efficiently computing of the pressure-velocity problem Darcy equation (D.6).

The mixed and hybrid finite element method is an established tool for the numerical approximation of problems arising in many physical fields: hydrostatic stress, heat conduction, fluid mechanics, solid mechanics, flow in porous media, just to name a few list of applications [44]. Here we will follow some ideas introduced and discussed in the manuscripts [29, 28, 57, 88] motivated by the successful development of domain decomposition methods combined with mixed hybrid finite element methods for the numerical approximation of nonlinear parabolic partial differential equations and related equations as well as for the numerical solution of the convection-diffusion equations. We point out that the reader should not look here this moment for a rigorous analysis nor for implementation details, but for formal construction of the numerical procedure to be implemented further later on.

D.2 A computational physics-based operator splitting modelling for the thermal equations

The numerical solution of the coupled, nonlinear, governing system (D.7)-(D.6) is achieved by an operator splitting technique. Thus, we separate (D.7)-(D.6) in parts, the pressure-velocity (D.6) and the Temperature-saturation transport (D.7) in the IMPES (implicit in pressure, explicit in Temperature-saturation) approach framework. Why not a fully implicit method for (D.7)-(D.6)? Roughly speaking, a fully implicit scheme leads to a large, strongly nonlinear algebraic system, whose solution is rather complicated and expensive to use [44]. Moreover for advection, or convection, a nonlinear implicit discretization is hard to solve (difficulties in the resolution of large gradients due to the first ordem operator) and possible high computational cost (reduced CFL stability constraints).

Operator splitting techniques for the approximation of solutions of systems of partial differential equations arising in many fields of application have a long history and have been developed with various objectives in mind, see, e.g., [2, 15, 16, 46, 67, 84, 109] and the references cited therein. The earliest of these procedures were introduced to reduce each time step of a multidimensional transient problem to a cycle of one-dimensional calculations. The operator splitting based on separating the underlying physical processes and treating each such process appropriately. Thus, instead of solving the governing differential equations original, results from the basic conservation laws supplemented by constitutive relations (or other fundamental equations), we rewrite the equations in such a way as to exhibit clearly each physical process. We separate (D.7)-(D.6) in parts, the pressure-velocity (D.6) and the temperature-saturation transport and the pressure-velocity problem (D.6) are sequentially solved.

It is crucial to say that we are aware that operator splitting may not always be the right answer. The extent to which operator splitting will give an effective overall method depends on the coupling of different elementary operators and the dynamics of the evolution problem. It needs a detailed knowledge of the behaviour of the solutions to make rather powerful methods. Most of the refinements depend on further knowledge of properties of the underlying subproblems. Finally, to the best of our knowledge, we do not have a right answer upon the best, or optimal, numerical strategy to tackle the nonlinear model problem (D.7)-(D.6). Clearly, the proposed numerical strategy is fully based on the above arguments along with our current understanding of the stiff relaxation process to this class of differential problems at hand.

Thus, for the model problem (D.7)-(D.6) we introduce two time steps: Δt_c (subjected to some dynamical condition of the type Courant-Friedrichs-Levy) for the balance problem related to the convective transport of the pair (s_g, T, ψ_{gw}) and Δt_p, for the calculation of the pressure-velocity pair (p, u). To simplify the description of the time evolution fractional algorithm, we will consider that for each time step we have an unique value during the simulation, i.e., $\Delta t \equiv \Delta t_c = \Delta t_p$. We are setting up to calculate (D.7)-(D.6), but a more general model taking into account diffusive effects and other boundary conditions can be treated by our techniques [2, 15, 16].

D.3 An approximation of the pressure-velocity model by hybrid mixed finite element

We will describe the mixed methods to approximate the pressure-velocity system (D.6). The mixed finite element is a generalization the finite element method and employs two different spaces. Moreover, the mixed finite element is also developed to approximate, simultaneously, the total velocity and the pressure in order to give a high order approximation of both variables. Also, it is well known that the mixed finite element method conserves mass locally. Indeed, in this work we adopt the Hybrid Mixed Finite Element discretization approach in $H(div)$ spaces of Raviart-Thomas [114] (see also [65, 118]), motivated by its successful application in three-phase flow problems [1, 14, 15, 16, 17, 18, 20, 19] as well as its previous and successfully performance in numerical approximation and simulation of two-phase oil-water flow within the tradition established by Jim Douglas, Jr., Richard Ewing, Thomas F. Russell and Mary F. Wheeler in the joint work [55, 63, 64, 119, 130] and more recently in the works [15, 16, 56, 58, 59]. In this series of studies, hybrid mixed finite elements were identified as most appropriate for the calculation of velocity fields even in the presence of high variability of the geologic rock properties, namely, porosity and permeability. Moreover, it is worth mentioning that the hybrid mixed finite element approach has a rigorous mathematical foundation for numerical approximation of both elliptic and parabolic partial differential equations [25, 27, 34, 65, 114, 118]. In the context of this current study, after an application of the operator splitting approach, the parabolic (as well as the associated elliptic) problem is then fully identified to account the flow velocity, or Darcy's law (see e.g., [2, 65, 114, 118]).

The basic idea is as follows: First, perform a locally conservative discretization along with the other associated approximations into the hybrid mixed formulation; second, derive a related linear system with good mathematical properties, such as symmetric and positive definite as well as with good condition number. Finally, reproduce the locally conservative nature in the discrete level as is its corresponding counterparts in the continuum.

D.3.1 Mixed methods for nonlinear parabolic problems

Thanks to the operator splitting approach designed in Section D.2 we will be able to rewrite system (D.7)-(D.6) in order to identify the following non linear parabolic problem [2, 45]:

$$\begin{aligned} & c(p)\frac{\partial p}{\partial t} - \frac{\partial}{\partial x}(a(p)\frac{\partial}{\partial x}p) = f(p), \quad \text{in } \Omega \times J, \\ & g(s_w, T, p)\frac{\partial p}{\partial x}(0,t) = inrate_L, \\ & p(L,0) = 0 \text{ and } p(x,0) = p_0, \quad \text{in } x \in \Omega, \end{aligned} \tag{D.8}$$

where $c(p) = c(x,t,p)$, $a(p) = a(x,t,p)$, $f(p) = f(x,t,p)$, $J = (0,T]$ $(T > 0)$, and $\Omega \subset \mathbb{R}$. At this moment we stress that we have performed a formal analysis in order to verify all needed hypothesis to adapt our model parabolic problem (D.8) to that described in [2, 45]. For this fact to be hold, it was sufficient review the works [90, 92, 93, 94] to the steam and nitrogen injection problem in order to analyze the issue of regularity of the differential equations restrict to that

constitutive relations related to the Appendix C. Thus, all the basic required assumptions are then strictly satisfied as follows.

For the description of the procedure, we might assume that the coefficients $c(p)$, $a(p)$, and $f(p)$ are *globally Lipschitz continuous* in p. i.e., for some constants C_ξ they satisfy

$$|\xi(p_1) - \xi(p_2)| \leq C_\xi |p_1 - p_2|, \qquad p_1, p_2 \in \mathbb{R}, \xi = c, a, f. \tag{D.9}$$

We assume that (D.8) admits a unique solution. As usual in the mixed finite element approach, e.g., [2, 25, 27, 34, 65, 114, 118, 129], let the spaces,

$$H^1(\Omega) = \left\{ v \in L^2(\Omega) : \frac{dv}{dx} \in L^2(\Omega) \right\},$$

$$V = \left\{ J, v \in H^1(\Omega) : v(0,t) = g_0(t) \right\}, \qquad W = \{J, w \in L^2(\Omega)\}. \tag{D.10}$$

After we introduce the variable

$$u = -a(p)\frac{\partial p}{\partial x}, \tag{D.11}$$

the equations (D.8) can be rewrite in the form,

$$c(p)\frac{\partial p}{\partial t} + \frac{\partial}{\partial x}u = f(p). \tag{D.12}$$

We then multiply the equation (D.11) by any function $v \in V$ and integration over Ω follow by the application of integration by parts to the right-hand side and reads,

$$(a^{-1}(p)u, v) - \left(p, \frac{\partial v}{\partial x}\right) = 0. \tag{D.13}$$

Following the same procedure to (D.12), for any function $w \in W$, reads,

$$\left(c(p)\frac{\partial p}{\partial t} + \frac{\partial}{\partial x}u, w\right) = \left(f(p), w\right). \tag{D.14}$$

By considering (D.11)-(D.14), we notice that (D.8) can be rewrite as a convenient mixed variational formulation,

Find $u \in V$ and $p \in W$ such that:

$$\begin{aligned} &(a^{-1}(p)u, v) - (\frac{\partial}{\partial x}v, p) = 0 && v \in V, \\ &\left(c(p)\frac{\partial p}{\partial t}, w\right) + (\frac{\partial}{\partial x}u, w) = (f(p), w) && w \in W, \end{aligned} \tag{D.15}$$

with $p(\cdot, 0) = p_0$.

Thus, the basic idea is to formulate these weak forms first globally (as above) and then locally (as below) over the computational domain. Then, we construct the mixed finite element method for solving (D.8) through the definition of the local mixed finite element spaces $V_h \subset V$ and $W_h \subset W$ as follows,

$$\begin{aligned} V_h &= \{v : v \text{ is a continuous function on } \Omega \text{ and linear on each subinterval } \Omega_i\}, \\ W_h &= \{w : w \text{ is a continuous function on } \Omega\}, \end{aligned}$$

where M is a positive integer and $a = x_1 < x_2 < \cdots < x_m = b$ is a partition of Ω into a set of subintervals $\Omega_{i-1} = (x_{i-1}, x_i)$ with length $h_i = x_i - x_{i-1}$, $i = 2.3, ..., M$ and $h = max\{h_i, 2 \leq i \leq M\}$. Finally, the (local) mixed finite element method for (D.8) is given by,

Find $u_h \in V_h$ and $p \in W_h$ such that:

$$\begin{aligned} &(a^{-1}(p_h)u_h, v) - (\frac{\partial v}{\partial x}, p_h) = 0 \qquad\qquad v \in V_h, \\ &\left(c(p_h)\frac{\partial p_h}{\partial t}, w\right) + (\frac{\partial u_h}{\partial x}, w) = (f(p_h), w) \quad w \in W_h. \end{aligned} \tag{D.16}$$

We notice that $p_h(\cdot, 0)$ can be any appropriate projection of p_0 in W_h (see, e.g., [34, 65, 114, 118]), its L^2-projection in W_h:

$$(p_h(\cdot, 0) - p_0, w) = 0, \qquad w \in W_h.$$

We now introduce the basis functions $\varphi_i \in V_h$, $i = 1, 2, ..., M$,

$$\varphi_i(x) = \begin{cases} 1, & \text{if } i = j, \\ 0, & \text{if } i \neq j. \end{cases} \tag{D.17}$$

as well as the functions $\psi_i \in V_h$, $i = 1, ..., M-1$,

$$\psi_i(x) = \begin{cases} 1, & \text{if } x_i \in \Omega_i, \\ 0, & \text{otherwise.} \end{cases} \tag{D.18}$$

We point out that the functions ψ_i are the *characteristic* functions [34, 65, 114, 118] in the mixed formulation. Now, the functions $v \in V_h$ and $w \in W_h$ have unique representations (see., e.g., [34, 45, 65, 114, 118]),

$$v(x) = \sum_{i=1}^{M} v_i\varphi_i(x), \qquad w(x) = \sum_{i=1}^{M-1} w_i\varphi_i(x), \qquad a \leq x \leq b, \tag{D.19}$$

where $v_i = v(x_i)$ and $w_i = w|_{I_i}$. We can replace the functions v and w into (D.16),

$$\begin{aligned} &(a^{-1}(p_h)u_h, \varphi_i) - (\tfrac{\partial \varphi_i}{\partial x}, p_h) = 0, \qquad\qquad i = 1, 2, ..., M, \\ &\left(c(p_h)\tfrac{\partial p_h}{\partial t}, \psi_j\right) + (\tfrac{\partial u_h}{\partial x}, \psi_j) = (f(p_h), \psi_j), \qquad j = 1, 2, ..., M-1. \end{aligned} \tag{D.20}$$

Set

$$u_h(x) = \sum_{i=1}^{M} u_i\varphi_i(x) \qquad u_i = u_h(x_i), \tag{D.21}$$

and substitute

$$p_h(x) = \sum_{k=1}^{M-1} p_k\psi_k(x) \qquad p_k = p_h|_{\Omega_k}. \tag{D.22}$$

Next, connect (D.21) and (D.22) into equation (D.20) to give,

$$\begin{aligned} &a^{-1}(p_h)\sum_{i=1}^{M} u_i(\varphi_i(x), \varphi_j(x)) - \sum_{k=1}^{M-1} p_k\left(\frac{\partial \varphi_i(x)}{\partial x}, \psi_k(x)\right) = 0, \\ &c(p_h)\sum_{k=1}^{M-1}\left(\frac{\partial p_k}{\partial t}\psi_k(x), \psi_j(x)\right) + \sum_{i=1}^{M} u_i\left(\frac{\partial \varphi_i(x)}{\partial x}, \psi_j(x)\right) = (f(p_h), \psi_j(x)). \end{aligned} \tag{D.23}$$

We now can define the matrices and vectors as follows,

$$\mathbf{A}(\mathbf{p}) = (a_{ij})_{i,j=1,2,...,M}, \quad \mathbf{B} = (b_{jk})_{j=1,2,...,M,k=1,2,...,M-1}, \quad \mathbf{C}(\mathbf{p}) = (c_{j,k})_{j=1,2,...,M,k=1,2,...,M-1},$$
$$\mathbf{U} = (u_i)_{i=1,2,...,M} \qquad \mathbf{p} = (p_{ij})_{i,j=1,2,...,M-1}, \qquad \mathbf{f}(\mathbf{p}) = (f_i)_{i=1,2,...,M}$$

and $\dfrac{d\mathbf{p}}{dt} = \left(\left(\dfrac{\partial p_k}{\partial t}\right)_k\right)_{k=1,2,...,M-1}$, where,

$$a_{ij} = a^{-1}(p_h)(\varphi_i(x), \varphi_j(x)), \quad b_{jk} = -\left(\frac{\partial \varphi_i(x)}{\partial x}, \psi_k(x)\right),$$
$$f_i = (f(p_h), \psi_j(x)), \qquad c_{j,k} = c(p_h)(\psi_k(x), \psi_j(x)).$$

Along with the above definitions we can write the problem (D.20) in the matrix form as follows,

$$\begin{aligned} &\mathbf{A}(\mathbf{p})\mathbf{U} + \mathbf{B}\mathbf{p} = 0, && t \in J, \\ &\mathbf{C}(\mathbf{p})\frac{d\mathbf{p}}{dt} - \mathbf{B}^T\mathbf{U} = \mathbf{f}(\mathbf{p}), && t \in J. \end{aligned} \tag{D.24}$$

We point out that if the coefficient $c(p)$ is bounded below by a positive constant, the non linear system of ODEs generate by (D.24) has a unique solution for small time [45]; i.e., under an appropriate Courant-Friedrichs-Lewy stability condition (CFL condition).

Again, thanks to the operator splitting procedure depicted in Section D.2 we can perform distinct (local) linearizations to the nonlinear parabolic problem (D.24) in mixed form for its numerical approximation [2, 16, 15, 84, 109]. Therefore, we could combine the mixed finite element approximation in space with different explicit (e.g., Forward Euler) or implicit (Backwards Euler) in time, thereby arise different strategies to approximate the parabolic problem. We believe that which could be one important development in further work (D.24).

We will now briefly explain in the following subsections some possible alternatives we have in mind in order to achieve a full approximation algorithm for solving the the overall parabolic system (D.24).

First, remember that we separate in parts, the pressure-velocity sub-problem (with a parabolic character) and the temperature-saturation transport (with a balance law character). Essentially, at each time step, we will apply IMPES approach (implicit in pressure, explicit in temperature-saturation), i.e., at each time step, the balance transport problem and the pressure-velocity problem are sequentially solved. However, we are dealing with a nonlinear system of balance in which its properties are not well known and thus we belive be advisable to avoid the operator splitting approach to the pertinent *balance law operator*, which in turn we still use the unsplitting approach for solving the hyperbolic conservation laws with relaxation source terms to account the delicate nonlinear balance between numerical approximations of the hyperbolic flux function and the stiff relaxation source term linked to steady solutions for balance law problems.

D.3.1.1 Linearization Approaches

The nonlinear system (D.23) can be linearized by allowing the nonlinearities to stay frozen one time step behind from the current time level. Thus the backward Euler method for the discrete parabolic system (D.23), associated to the full coupled system (D.7)-(D.6), takes the form:

Find $p_h^n \in V_h, n = 1, 2, ..., N$, such that:

$$\begin{aligned} a^{-1}(p_h^{n-1}) \sum_{i=1}^{M} u_i(\varphi_i(x), \varphi_j(x)) - \sum_{k=1}^{M-1} p_k^{n-1} \left(\frac{\partial \varphi_i(x)}{\partial x}, \psi_k(x) \right) = 0, \\ c(p_h^{n-1}) \sum_{k=1}^{M-1} \left(\frac{p_h^n - p_h^{n-1}}{\Delta t^n} \psi_k(x), \psi_j(x) \right) + \sum_{i=1}^{M} u_i \left(\frac{\partial \varphi_i(x)}{\partial x}, \psi_j(x) \right) = (f(p_h^{n-1}), \psi_j(x)). \end{aligned} \tag{D.25}$$

In compact matrix form it is given by,

$$\begin{cases} \mathbf{A}(\mathbf{p}^{n-1})\mathbf{U} + \mathbf{B}\mathbf{p}^{n-1} = 0, & t \in J, \\ \mathbf{C}(\mathbf{p}^{n-1}) \dfrac{\mathbf{p}^n - \mathbf{p}^{n-1}}{\Delta t^n} - \mathbf{B}^T\mathbf{U} = \mathbf{f}(\mathbf{p}^{n-1}), & t \in J, \\ \mathbf{D}\mathbf{p}(0) = \mathbf{p}_0. \end{cases} \tag{D.26}$$

We point out that (D.26) is a system of linear equations for $\mathbf{p}$, which in turn can be solved by means of robust iterative solver with preconditioner (e.g., based on algebraic domain decomposition) or any robust direct solvers [120, 124]; the proper choice depend inherently upon the size of the computational domain as well as the mesh size.

D.3.1.1.1 Implicit Time Approximations

We now consider a fully *implicit time approximation* scheme for (D.23), again associated to the full coupled balance law system (D.7)-(D.6) and final discrete equations takes the following form:

Find $p_n^h \in V_h, n = 1, 2, ..., N$, such that:

$$\begin{aligned} a^{-1}(p_h^n) \sum_{i=1}^{M} u_i(\varphi_i(x), \varphi_j(x)) - \sum_{k=1}^{M-1} p_k^n \left(\frac{\partial \varphi_i(x)}{\partial x}, \psi_k(x) \right) = 0, \\ c(p_h^n) \sum_{k=1}^{M-1} \left(\frac{p_h^n - p_h^{n-1}}{\Delta t^n} \psi_k(x), \psi_j(x) \right) + \sum_{i=1}^{M} u_i \left(\frac{\partial \varphi_i(x)}{\partial x}, \psi_j(x) \right) = (f(p_h^n), \psi_j(x)). \end{aligned} \tag{D.27}$$

We might write (D.27) in compact matrix formulation as:

$$\begin{cases} \mathbf{A}(\mathbf{p}^n)\mathbf{U} + \mathbf{B}\mathbf{p}^n = 0, & t \in J, \\ \mathbf{C}(\mathbf{p}^n) \dfrac{\mathbf{p}^n - \mathbf{p}^{n-1}}{\Delta t^n} - \mathbf{B}^T\mathbf{U} = \mathbf{f}(\mathbf{p}^n), & t \in J, \\ \mathbf{D}\mathbf{p}(0) = \mathbf{p}_0. \end{cases} \tag{D.28}$$

Of course, system (D.28) is now a set of fully non linear equations in the $\mathbf{p}$ variable, which must be solved at each time step by means of Newton-like procedures [45, 87, 111, 116]. For instance, let us consider Newton's formulation. So, the first equation of (D.28) can be rewritten as,

$$\begin{aligned} &\mathbf{A}(\mathbf{p}^n)\mathbf{U} + \mathbf{B}\mathbf{p}^n = 0, && t \in J, \\ &\frac{1}{\Delta t^n}\mathbf{C}(\mathbf{p}^n)\mathbf{p}^n = \mathbf{B}^T\mathbf{U} + \mathbf{f}(\mathbf{p}^n) + \frac{1}{\Delta t^n}\mathbf{C}(\mathbf{p}^n)\mathbf{p}^{n-1}, && t \in J, \\ &\mathbf{D}\mathbf{p}(0) = \mathbf{p}_0. \end{aligned} \tag{D.29}$$

Then we can write equation (D.29) as,

$$\mathbf{F}(\mathbf{p}^n, \mathbf{U}) = 0. \tag{D.30}$$

Newton's method for (D.30) can now be defined as,

$$\begin{aligned} \text{Set } \mathbf{v}^0 &= (\mathbf{p}^{n-1}, \mathbf{U}^*), \text{ where } \mathbf{A}(\mathbf{p}^{n-1})\mathbf{U}^* + \mathbf{B}\mathbf{p}^{n-1} = 0, \\ \text{Iterate } \mathbf{v}^k &= \mathbf{v}^{k-1} + \mathbf{d}^k, \qquad k = 1, 2, ..., \end{aligned}$$

along with $\mathbf{G}$ being the Jacobian matrix of the vector function $\mathbf{F}$ which in turn $\mathbf{d}^k$ solves the system,

$$\mathbf{G}(\mathbf{v}^{k-1})\mathbf{d}^k = -\mathbf{F}(\mathbf{v}^{k-1}). \tag{D.31}$$

If the matrix $\mathbf{G}(\mathbf{p}^n, \mathbf{U}^n)$ is nonsingular and the second partial derivatives of $\mathbf{F}$ are bounded, then Newton's method converges quadratically in a neighborhood of $[\mathbf{p}^n.\mathbf{U}^n]$; see, e.g., [45, 87, 111, 116]. The main drawback with Newton's method is to get a sufficiently good initial guess. Once it is obtained, Newton's method converges with very few iterations. This method is a very powerful iteration method for strongly non linear problems. It is on the choice of the initial "guess" to the Newton method that a benefit of the operator splitting approach manifest itself. For instance, after solving the purely hyperbolic balance laws system in system (D.7)-(D.6) from time level t^n to t^{n+1} we can use the solution with combined convection and relaxation as both [2] the initial condition and approximation for the initial guess to the linearized discrete parabolic system (D.29).

There are many variants of Newton's method available in the literature that come along with the finite element method (see, e.g., [34, 44, 111, 116].

D.3.1.1.2 Explicit Time Approximations

Finally, it is also possible to perform the application of the forward Euler explicit integration technique to (D.23) in a standard way (but now under severe CFL stability condition) as it would be expected from the nonlinearities of the nonlinear differential parabolic problem.

Find $p_h^n \in V_h, n = 1, 2, ..., N$, such that:

$$\begin{aligned} a^{-1}(p_h^{n-1}) \sum_{i=1}^{M} u_i(\varphi_i(x), \varphi_j(x)) - \sum_{k=1}^{M-1} p_k^{n-1} \left(\frac{\partial \varphi_i(x)}{\partial x}, \psi_k(x) \right) = 0, \\ c(p_h^n) \sum_{k=1}^{M-1} \left(\frac{p_h^n - p_h^{n-1}}{\Delta t^n} \psi_k(x), \psi_j(x) \right) + \sum_{i=1}^{M} u_i \left(\frac{\partial \varphi_i(x)}{\partial x}, \psi_j(x) \right) = (f(p_h^{n-1}), \psi_j(x)). \end{aligned} \tag{D.32}$$

Again, we write sytem (D.32) in matrix form as:

$$\begin{cases} \mathbf{A}(\mathbf{p}^{n-1})\mathbf{U} + \mathbf{B}\mathbf{p}^{n-1} = 0, & t \in J, \\ \mathbf{C}(\mathbf{p}^n)\dfrac{\mathbf{p}^n - \mathbf{p}^{n-1}}{\Delta t^n} - \mathbf{B}^T\mathbf{U} = \mathbf{f}(\mathbf{p}^{n-1}), & t \in J, \\ \mathbf{D}\mathbf{p}(0) = \mathbf{p}_0. \end{cases} \tag{D.33}$$

We point out that the only non linearity appears in matrix C of system (D.33). As before, this system can be solved by Newton's method [111, 116].

Appendix E

The secondary variable u

In [90] the author proof for the system (3.1) of $n \times n$ over the hypothesis of local thermodynamic equilibrium the author the Reiamnn problem the variable u^- is secondary, i.e., in the initial conditions is not necessary write the term u^+ because it is rewrite using the variables $\mathcal{V}$ and u. We in this appendix prove the fact neglect the hypothesis of local thermodynamic equilibrium.

Proposition E.0.1. *Let the system* (3.1) *general*

$$\frac{\partial}{\partial t}(\boldsymbol{G}(\mathcal{V})) + \frac{\partial}{\partial x}(u\boldsymbol{F}(\mathcal{V})) = \frac{1}{\epsilon}\boldsymbol{Q}(\mathcal{V}) \tag{E.1}$$

$$\frac{\partial}{\partial t}(G_n(\mathcal{V})) + \frac{\partial}{\partial x}(uF_n(\mathcal{V})) = 0 \tag{E.2}$$

where $\mathcal{V} = (V_1, V_2, ..., V_{n-1}) : \Omega \to \mathbb{R}^n$ *is vectorial function and* u *is the Darcy's speed, the functions* $\boldsymbol{G}(\mathcal{V}) := (G_1(\mathcal{V}), G_2(\mathcal{V}), ..., G_{n-1}(\mathcal{V}))^T : \Omega \to \mathbb{R}^{n-1}$, $\boldsymbol{F}(\mathcal{V}) := (F_1(\mathcal{V}), F_2(\mathcal{V}), ..., F_{n-1}(\mathcal{V}))^T : \Omega \to \mathbb{R}^{n-1}$ *and* $\boldsymbol{Q}(\mathcal{V}) := (Q_1(\mathcal{V}), Q_2(\mathcal{V}), ..., Q_{n-1}(\mathcal{V}))^T : \Omega \to \mathbb{R}^{n-1}$ *also are* $\mathcal{C}^2$. *The functions* $G_n(\mathcal{V}) : \Omega \to \mathbb{R}$, $F_n(\mathcal{V}) : \Omega \to \mathbb{R}$ *are* $\mathcal{C}^2$ *function and* F_n *is never vanishes in* Ω. *Let following Riemann problem for* (E.1)

$$\begin{cases} (\mathcal{V}^-, u^-) \text{ if } x \leq 0 \\ (\mathcal{V}^+, \ \cdot \ ) \text{ if } x > 0 \end{cases} \tag{E.3}$$

with $u^- > 0$ *then the solution for* (E.1) *is not depend of* u^+

Proof of the Proposition:

We divide the proof in three parts according the solution profile as: i) when the solution is a function smooth, ii) when the solution is discontinuous, iii)when exist of travelling wave.

i) We suppose that the solution is smooth, thus we can differentiate the system (E.1)-(E.1) with respect to their variable, obtaining a system

$$\mathcal{B}\frac{\partial \mathcal{V}}{\partial t} + \mathcal{A}\frac{\partial \mathcal{V}}{\partial x} = \frac{1}{\epsilon}Q(\mathcal{V}), \tag{E.4}$$

where

$$\mathcal{B} = \begin{pmatrix} \hat{B} & 0 \\ b & 0 \end{pmatrix}, \qquad \mathcal{A} = \begin{pmatrix} u\hat{A} & \mathbf{F} \\ ua & F_n \end{pmatrix}, \tag{E.5}$$

with

$$\hat{B} = \begin{pmatrix} \frac{\partial G_1}{\partial V_1} & \frac{\partial G_1}{\partial V_2} & \cdots & \frac{\partial G_1}{\partial V_{n-1}} \\ \frac{\partial G_2}{\partial V_1} & \frac{\partial G_2}{\partial V_2} & \cdots & \frac{\partial G_2}{\partial V_{n-1}} \\ \vdots & \vdots & \ddots & \vdots \\ \frac{\partial G_{n-1}}{\partial V_1} & \frac{\partial G_{n-1}}{\partial V_2} & \cdots & \frac{\partial G_{n-1}}{\partial V_{n-1}} \end{pmatrix}, \qquad \hat{A} = \begin{pmatrix} \frac{\partial F_1}{\partial V_1} & \frac{\partial F_1}{\partial V_2} & \cdots & \frac{\partial F_1}{\partial V_{n-1}} \\ \frac{\partial F_2}{\partial V_1} & \frac{\partial F_2}{\partial V_2} & \cdots & \frac{\partial F_2}{\partial V_{n-1}} \\ \vdots & \vdots & \ddots & \vdots \\ \frac{\partial F_{n-1}}{\partial V_1} & \frac{\partial F_{n-1}}{\partial V_2} & \cdots & \frac{\partial F_{n-1}}{\partial V_{n-1}} \end{pmatrix},$$

$$b = \frac{\partial G_n}{\partial V_n}, \qquad a = \frac{\partial F_n}{\partial V_n}, \qquad Q(\mathcal{V}) = (\mathbf{Q}(\mathcal{V}), 0)^T.$$

We can suppose that $\hat{B}$ is nonsingular in Ω. Let the following $n \times n$ nonsingular matrix

$$\overline{B} = \begin{pmatrix} \hat{B}^{-1} & 0 \\ 0 & 1 \end{pmatrix}.$$

Thus, we multiply the equation (E.4) by $\overline{B}$ yield

$$\begin{pmatrix} I & 0 \\ b & 0 \end{pmatrix} \frac{\partial}{\partial t} \begin{pmatrix} \mathcal{V} \\ u \end{pmatrix} + \begin{pmatrix} \hat{B}^{-1}\hat{A} & \mathbf{F} \\ ua & F_n \end{pmatrix} \frac{\partial}{\partial x} \begin{pmatrix} \mathcal{V} \\ u \end{pmatrix} = \frac{1}{\epsilon} \begin{pmatrix} \hat{B}^{-1}\mathbf{Q} \\ 0 \end{pmatrix} \tag{E.6}$$

we can rewrite the before system as

$$\mathcal{V}_t + u\hat{B}^{-1}\hat{A}V_x + \mathbf{F}u_x = \frac{1}{\epsilon}\hat{B}^{-1}\mathbf{Q}(\mathcal{V}), \tag{E.7}$$

$$b\mathcal{V}_t + ua\mathcal{V}_x + F_n u_x = 0. \tag{E.8}$$

We supposed that $F_n \neq 0$. Thereby, we obtain from the equation (E.8)

$$u_x = \frac{-1}{F_n}(b\mathcal{V}_t + ua\mathcal{V}_x),$$

substituting u_x in the Eq. (E.7) yield

$$(F_n - b)\mathcal{V}_t + u(F_2\hat{B}^{-1}\hat{A} - b)\mathcal{V}_x = \frac{F_n}{\epsilon}\hat{B}^{-1}\mathbf{Q}. \tag{E.9}$$

Note that the Eq. (E.8) determine a ordinary differential equation in terms of u with t fixed. Thus, the Eq. (E.8) can be written as

$$u_x + p(\mathcal{V}, \mathcal{V}_x)u = q(\mathcal{V}, \mathcal{V}_t) \tag{E.10}$$

where

$$p(\mathcal{V}, \mathcal{V}_x) = a\frac{\mathcal{V}_x}{F_n(\mathcal{V})}, \qquad qp(\mathcal{V}, \mathcal{V}_t) = -b\frac{\mathcal{V}_t}{F_n(\mathcal{V})}.$$

We find the solution of the equation (E.10) fixed a time t, then u is determined by

$$\begin{aligned} u(x,t) =& e^{-H}\left[u_0 + \int_{x_0}^{x} q(\mathcal{V}(s,t), \mathcal{V}_t(s,t))e^{H}ds\right], \\ H =& \int_{x_0}^{x} p(\mathcal{V}(\omega,t), \mathcal{V}_x(\omega,t))d\omega. \end{aligned} \tag{E.11}$$

Then with the previous equation we finish the first part of the proof.

ii) We supposed that the solution is discontinuous then its has a shock and satisfies the Rankine-Hugoniout condition, that is equal to the case conservation law, thereby this case the proof is in [90].

iii) We supposed that the solution is a travelling waves, thus we use the the viscosity criterion, then the solution $[\mathcal{V}, u]^T$ is a admissible provided it is the $\eta \downarrow 0$ limit solution $[\mathcal{V}_\eta, u_\eta]^T$ to a system

$$\frac{\partial}{\partial t}G(\mathcal{V}) + \frac{\partial}{\partial x}\Big(uF(\mathcal{V})\Big) = \epsilon^{-1}Q(\mathcal{V}) + \eta\frac{\partial}{\partial x}\left(B(\mathcal{V}, u)\right)\frac{\partial}{\partial x}\mathbf{V}, \tag{E.12}$$

where $\mathbf{V} = [\mathcal{V}, u]^T$, namely functions of the single variable $x - \sigma t$. We seek a family of solutions in the form

$$\mathbf{V}_\eta(x, t) = \mathbf{W}\left(\frac{x - \sigma t}{\eta}\right), \tag{E.13}$$

with $\mathbf{W} = [W, w]^T$. We choose the matrix B as

$$B = \begin{pmatrix} \hat{B} & 0 \\ b(\mathcal{V}) & 0 \end{pmatrix}, \tag{E.14}$$

where $\hat{B}$ is non singular and its elements are smooth function in $\mathcal{V}$, the function b is smooth function and does not vanish. Thus, we can write the system (E.12) as

$$-\sigma\dot{\mathbf{G}}(W) + (u\mathbf{F}(W))^{\cdot} = \frac{1}{\epsilon}\mathbf{Q}(W) + \eta[B(W)\dot{W}]^{\cdot} \tag{E.15}$$

$$-\sigma\dot{G}_n(W) + (uF_n(W))^{\cdot} = \eta[B(W)\dot{W}]^{\cdot}. \tag{E.16}$$

Note that equation (E.16) is a ordinary differential equation over the $\tau = (x - \sigma)/\eta$. We are interested in solution in which $\dot{\mathcal{V}}$ vanishes at $\mathcal{V} = \mathcal{V}^-$ and so, upon integration (E.16) once with respect to τ

$$b(\mathcal{V})\dot{\mathcal{V}} = (uF_n(\mathcal{V})) - (u^-F_n(\mathcal{V}^-)) - \sigma((G_n(\mathcal{V})) - (G_n(\mathcal{V}^-))),$$

thus we obtain u as

$$\begin{aligned} uF_n(\mathcal{V}) &= (u^-F_n(\mathcal{V}^-)) + \sigma((G_n(\mathcal{V})) - (G_n(\mathcal{V}^-))) + b(\mathcal{V})\dot{\mathcal{V}}, \\ u &= \Big((u^-F_n(\mathcal{V}^-)) + \sigma((G_n(\mathcal{V})) - (G_n(\mathcal{V}^-))) + b(\mathcal{V})\dot{\mathcal{V}}\Big)/F_n(\mathcal{V}). \end{aligned} \tag{E.17}$$

We find u in term of $\{\mathcal{V}^-, u^-, \mathcal{V}\}$, then we can replace u in the equation (E.15) and upon integration once with respect to τ we obtain that is no necessary u^+ thereby we find the proof.

Bibliography

[1] E. Abreu. "Numerical simulation of three-phase flow in heterogeneous media with spatially varying nonlinear hyperbolic-parabolic flux functions". In: *AIMS on Applied Mathematics*. Ed. by F Ancona, A Bressan, P Marcati, and A. Marson. Vol. 8. Proceedings of the Fourteenth International Conference on Hyperbolic Problems held in Padova, 2012, pp. 233–240.

[2] E. Abreu. "Numerical modelling of three-phase immiscible flow in heterogeneous porous media with gravitational effects". In: *Mathematics and Computers in Simulation* 97 (2014), pp. 234–259.

[3] E. Abreu, A. Bustos, P. Ferraz, and W. Lambert. "A computational multiscale approach for ncompressible two-phase flow in heterogeneous porous media including relative permeability hysteresis". In: *MAMERN VI-2015: Proceedings of the 6th International Conference on Approximation Methods and Numerical Modelling in Environment and Natural*. Ed. by E Amaziane, D Ahusborde, M. J. Ibáñez Pérez, R Romero-Zaliz, and D Sbibih. Editorial Universidad de Granada, Campus Universitario de Cartuja. Granada, 2015, pp. 349–366.

[4] E. Abreu, A. Bustos, and W. Lambert. "A mathematical and numerical study of a 3×3 system of isothermal Euler equations with relaxation". In: *29º Colóquio Brasileiro de Matemática* (2013).

[5] E. Abreu, A. Bustos, and W. Lambert. "Study the outer expansion and the scheme numerical for the 3×3 system of isothermal Euler equations with relaxation". In: **VII ENAMA**, *Encontro Nacional de Análise Matemática e Aplicações* (2013).

[6] E. Abreu, A. Bustos, and W. Lambert. "A Conservative finite volume scheme for balance laws: application to Euler equations with stiff source terms". In: *Fifteenth International Conference on Hyperbolic Problems: Theory Numerics and Applications- HYP2014* (2014), 25 pages.

[7] E. Abreu, A. Bustos, and W. Lambert. "A mathematical and computational study for hyperbolic conservation laws with stiff source terms". In: *VIII Pan-American Workshop Applied and Computational Mathematics* (2014).

[8] E. Abreu, A. Bustos, and W. Lambert. "Análise de existência e comportamento de onda viajante para equações de Euler com relaxação". In: *XXXV Congresso nacional de matemática aplicada e computacional* (2014).

[9] E. Abreu, A. Bustos, and W. Lambert. "A conservative unsplitting scheme for nonlinear balance laws: application to Euler system with stiff relaxation source terms". In: *8th International Congress on Industrial and Applied Mathematics* (2015).

[10] E. Abreu, A. Bustos, and W. Lambert. “A unsplitting finite volume method for models with stiff relaxation source terms”. In: *Preparation* (2015).

[11] E. Abreu, A. Bustos, and W. Lambert. “Asymptotic behaviour of a decaying solution of relaxation system modelling thermal flow in porous media”. In: *Preparation* (2015).

[12] E. Abreu, A. Bustos, and W. Lambert. “Non-monotonic travelling wave and computational solutions for gas dynamics Euler equations with stiff relaxation source terms”. In: *Computers & Mathematics with application* (Accepted).

[13] E. Abreu, A. Bustos, and W. Lambert. “An approximate algorithm for solving steam and nitrogen injection models in a porous medium transport problem”. In: *30o Colóquio no Instituto Nacional de Matemática Pura e Aplicada (IMPA)* (July 26-31, of 2015).

[14] E. Abreu and D. Conceição. “Numerical Modeling of Degenerate Equations in Porous Media Flow”. In: *Journal of Scientific Computing* 55.3 (2013), pp. 688–717.

[15] E. Abreu, J. Douglas Jr, F. Furtado, D. Marchesin, and F. Pereira. “Three-phase immiscible displacement in heterogeneous petroleum reservoirs”. In: *Mathematics and computers in simulation* 73.1 (2006), pp. 2–20.

[16] E. Abreu, J. Douglas Jr, F. Furtado, and F. Pereira. “Operator splitting based on physics for flow in porous media”. In: *International Journal of Computational Science* 2.3 (2008), pp. 315–335.

[17] E. Abreu, F. Furtado, F. Pereira, and G. Souza. “Numerical Modeling of Two-phase Flow With Hysteresis in Heterogeneous Porous Media”. In: *Rio Oil & Gas*. IBP1685. 2008, pp. 8–15.

[18] E. Abreu and F. Pereira. “Desenvolvimento de Novas estratégias Para a Recuperação Avançada de Hidrocarbonetos em Reservatórios de Petróleo”. In: *Boletim Técnico da Produção de Petróleo (PETROBRAS-CENPES)* 2 (2007), pp. 83–106.

[19] E. Abreu, F. Pereira, and S. Ribeiro. “Central schemes for porous media flows”. In: *Computational & Applied Mathematics* 28.1 (2009), pp. 87–110.

[20] E. Abreu and R. Seixas. “Exploiting OpenMP Efficiency for Multiphase Flow Simulation in Heterogeneous Porous Media”. In: 30^o Iberian-Latin-American Congress on Comp. Methods in Engineering. 2008.

[21] A. Adimurthi, S. MISHRA, and G. Gowda. “Optimal entropy solutions for conservation laws with discontinuous flux-functions”. In: *Journal of Hyperbolic Differential Equations* 2.04 (2005), pp. 783–837.

[22] C. Agrell and N. Risebro. “Convergence of a relaxation scheme for a $2\times$ 2 triangular system of conservation laws”. In: *International journal of numerical analysis and modeling* 11.1 (2014), pp. 148–171.

[23] D. Amadori and L. Gosse. “Stringent error estimates for one-dimensional, space-dependent $2\times$ 2 relaxation systems”. In: *Annales de l’Institut Henri Poincare (C) Non Linear Analysis*. Elsevier. 2015.

[24] B. Andreianov and D. Mitrović. “Entropy conditions for scalar conservation laws with discontinuous flux revisited”. In: *Annales de l’Institut Henri Poincare (C) Non Linear Analysis*. Elsevier. 2014.

[25] D. Arnold, F. Brezzi, B. Cockburn, and D. Marini. "Unified analysis of discontinuous Galerkin methods for elliptic problems". In: *SIAM journal on numerical analysis* 39.5 (2002), pp. 1749–1779.

[26] A. Azevedo, A. Souza, F. Furtado, D. Marchesin, and B. Plohr. "The solution by the wave curve method of three-phase flow in virgin reservoirs". In: *Transport in porous media* 83.1 (2010), pp. 99–125.

[27] Nicola Bellomo, Franco Brezzi, and Gianmarco Manzini. "Recent techniques for PDE discretizations on polyhedral meshes". In: *Mathematical Models and Methods in Applied Sciences* 24.08 (2014), pp. 1453–1455.

[28] J. Benamou and B. Desprès. "A domain decomposition method for the Helmholtz equation and related optimal control problems". In: *Journal of Computational Physics* 136.1 (1997), pp. 68–82.

[29] J. Benamou and B. Desprès. "A mixed hybrid finite element/volume approach for a pseudo-parabolic linked to two-phase flow in porous media with dynamic effects in the capillary pressures". In: *MAMERN VI-2015: 6th International Conference on Approximation Methods and Numerical Modelling in Environment and Natural Resources Pau (France)* (2015), p. 21.

[30] S. Berres, R. Bürger, and K. Karlsen. "Central schemes and systems of conservation laws with discontinuous coefficients modeling gravity separation of polydisperse suspensions". In: *Journal of Computational and Applied Mathematics* 164 (2004), pp. 53–80.

[31] C. Berthon, P. LeFloch, and R. Turpault. "Late-time/stiff-relaxation asymptotic-preserving approximations of hyperbolic equations". In: *Mathematics of Computation* 82.282 (2013), pp. 831–860.

[32] F. Bouchut. *Nonlinear stability of finite volume methods for hyperbolic conservation laws: And well-balanced schemes for sources*. Springer Science & Business Media, 2004.

[33] F. Bouchut, H. Ounaissa, and B. Perthame. "Upwinding of the source term at interfaces for Euler equations with high friction". In: *Computers and Mathematics with Applications* 53.3 (2007), pp. 361–375.

[34] S. Brenner and R. Scott. *The mathematical theory of finite element methods*. Vol. 15. Springer Science & Business Media, 2008.

[35] J. Bruining and D. Marchesin. "Analysis of nitrogen and steam injection in a porous medium with water". In: *Transport in Porous Media* 62.3 (2006), pp. 251–281.

[36] J. Bruining, D. Marchesin, and CJ. Van Duijn. "Steam injection into water-saturated porous rock". In: *Computational & Applied Mathematics* 22.3 (2003), pp. 359–395.

[37] C. Cercignani. *The Boltzmann equation*. Springer, 1988.

[38] C. Chalons, F. Coquel, E. Godlewski, P. Raviart, and N. Seguin. "Godunov-type schemes for hyperbolic systems with parameter-dependent source: the case of Euler system with friction". In: *Mathematical Models and Methods in Applied Sciences* 20.11 (2010), pp. 2109–2166.

[39] C. Chalons, M. Girardin, and S. Kokh. "Large time step and asymptotic preserving numerical schemes for the gas dynamics equations with source terms". In: *SIAM Journal on Scientific Computing* 35.6 (2013), A2874–A2902.

[40] T. Chang, G. Chen, and S. Yang. “On the 2-D Riemann problem for the compressible Euler equations. I. Interaction of shocks and rarefaction waves”. In: *Discrete and Continuous Dynamical Systems* 1 (1995), pp. 555–584.

[41] S. Chapman and T. Cowling. *The mathematical theory of non-uniform gases: an account of the kinetic theory of viscosity, thermal conduction and diffusion in gases*. Cambridge university press, 1970.

[42] G. Chen, C. Levermore, and T. Liu. “Hyperbolic conservation laws with stiff relaxation terms and entropy”. In: *Communications on Pure and Applied Mathematics* 47.6 (1994), pp. 787–830.

[43] G. Chen and A. Tzavaras. “Remarks on the Contributions of Constantine M. Dafermos to the Subject of Conservation Laws”. In: *Acta Mathematica Scientia* 32.1 (2012), pp. 3–14.

[44] Z. Chen. *Finite element methods and their applications*. Springer Science & Business Media, 2005.

[45] Z. Chen and J. Douglas Jr. “Approximation of coefficients in hybrid and mixed methods for nonlinear parabolic problems”. In: *Mat. Aplic. Comp* 10 (1991), pp. 137–160.

[46] A. Chertock, C. Doering, E. Kashdan, and A. Kurganov. “A fast explicit operator splitting method for passive scalar advection”. In: *Journal of Scientific Computing* 45.1-3 (2010), pp. 200–214.

[47] I. Christov and B. Popov. “New non-oscillatory central schemes on unstructured triangulations for hyperbolic systems of conservation laws”. In: *Journal of Computational Physics* 227.11 (2008), pp. 5736–5757.

[48] R. Colombo and A. Corli. “Continuous dependence in conservation laws with phase transitions”. In: *SIAM Journal on Mathematical Analysis* 31.1 (1999), pp. 34–62.

[49] F. Coquel and E. Godlewski. “Asymptotic preserving scheme for Euler system with large friction”. In: *Journal of Scientific Computing* 48.1-3 (2011), pp. 164–172.

[50] J. Da Mota, W. Dantas, E. Gomes, and D. Marchesin. “Combustion fronts in petroleum reservoirs”. In: (1995).

[51] C. Dafermos. *Contemporary issues in the dynamic behavior of continuous media*. Lefschetz Center for Dynamical Systems and Center for Control Sciences, Division of Applied Mathematics, 1985.

[52] C. Dafermos. *Hyperbolic conservation laws in continuum physics, volume 325 of Grundlehren der Mathematischen Wissenschaften [Fundamental Principles of Mathematical Sciences]*. 2005.

[53] C. Dafermos. “Hyperbolic systems of balance laws with weak dissipation”. In: *Journal of Hyperbolic Differential Equations* 3.03 (2006), pp. 505–527.

[54] R. Donat, I. Higueras, and A. Martinez-Gavara. “On stability issues for IMEX schemes applied to 1D scalar hyperbolic equations with stiff reaction terms”. In: *Mathematics of Computation* 80.276 (2011), pp. 2097–2126.

[55] J. Douglas Jr. “Numerical methods for the flow of miscible fluids in porous media”. In: *Numerical methods in coupled systems* (1984), pp. 405–439.

[56] J. Douglas Jr, F. Furtado, and F. Pereira. "On the numerical simulation of waterflooding of heterogeneous petroleum reservoirs". In: *Computational Geosciences* 1.2 (1997), pp. 155–190.

[57] J. Douglas Jr, P. Leme, J. Roberts, and J. Wang. "A parallel iterative procedure applicable to the approximate solution of second order partial differential equations by mixed finite element methods". In: *Numerische Mathematik* 65.1 (1993), pp. 95–108.

[58] J. Douglas Jr, F. Pereira, and L. Yeh. "A locally conservative Eulerian–Lagrangian numerical method and its application to nonlinear transport in porous media". In: *Computational Geosciences* 4.1 (2000), pp. 1–40.

[59] J. Douglas Jr, F. Pereira, and L. Yeh. "A locally conservative Eulerian-Lagrangian method for flow in a porous medium of a mixture of two components having different densities". In: *Numerical Treatment of Multiphase Flows in Porous Media*. Springer, 2000, pp. 138–155.

[60] J. Douglas Jr and T. Russell. "Numerical methods for convection-dominated diffusion problems based on combining the method of characteristics with finite element or finite difference procedures". In: *SIAM Journal on Numerical Analysis* 19.5 (1982), pp. 871–885.

[61] M. Dumbser, C. Enaux, and E. Toro. "Finite volume schemes of very high order of accuracy for stiff hyperbolic balance laws". In: *Journal of Computational Physics* 227.8 (2008), pp. 3971–4001.

[62] L. Evans. *Partial Differential Equations*. 2nd ed. American Mathematical Soc, 2010.

[63] R. Ewing, T. Russell, and M. Wheeler. "Convergence analysis of an approximation of miscible displacement in porous media by mixed finite elements and a modified method of characteristics". In: *Computer Methods in Applied Mechanics and Engineering* 47.1 (1984), pp. 73–92.

[64] R. Ewing, M. Wheeler, et al. "The approximation of the pressure by a mixed method in the simulation of miscible displacement". In: *ESAIM: Mathematical Modelling and Numerical Analysis-Modélisation Mathématique et Analyse Numérique* 17.1 (1983), pp. 17–33.

[65] M. Fortin and F. Brezzi. *Mixed and hybrid finite element methods*. New York: Springer-Verlag, 1991.

[66] G. Fowles, WL. Fickett, et al. "The polymorphic detonation". In: *Physics of Fluids (1958-1988)* 22.3 (1979), pp. 422–435.

[67] S. Gasda, M. Farthing, C. Kees, and C. Miller. "Adaptive split-operator methods for modeling transport phenomena in porous medium systems". In: *Advances in Water Resources* 34.10 (2011), pp. 1268–1282.

[68] S. Ghoshal. "Optimal results on TV bounds for scalar conservation laws with discontinuous flux". In: *Journal of Differential Equations* 258.3 (2015), pp. 980–1014.

[69] J. Glimm. "The continuous structure of discontinuities". In: *PDEs and Continuum Models of Phase Transitions*. Springer, 1989, pp. 175–186.

[70] L. Gosse. "Computing qualitatively correct approximations of balance laws". In: *SIMAI Springer Series* 2 (2013).

[71] L. Gosse and G. Toscani. “Asymptotic-preserving & well-balanced schemes for radiative transfer and the Rosseland approximation”. In: *Numerische Mathematik* 98.2 (2004), pp. 223–250.

[72] L. Gosse and A. Tzavaras. “Convergence of relaxation schemes to the equations of elastodynamics”. In: *Mathematics of Computation* 70.234 (2001), pp. 555–577.

[73] J. Greenberg and A. Leroux. “A well-balanced scheme for the numerical processing of source terms in hyperbolic equations”. In: *SIAM Journal on Numerical Analysis* 33.1 (1996), pp. 1–16.

[74] J. Greenberg, A. Leroux, R. Baraille, and A. Noussair. “Analysis and approximation of conservation laws with source terms”. In: *SIAM Journal on Numerical Analysis* 34.5 (1997), pp. 1980–2007.

[75] JM. Greenberg and L. Hsiao. “The Riemann problem for the system”. In: *Archive for Rational Mechanics and Analysis* 82.1 (1983), pp. 87–108.

[76] H. Hattori. “The Riemann problem for thermoelastic materials with phase change”. In: *Journal of Differential Equations* 205.1 (2004), pp. 229–252.

[77] M. Herty, J. Mohring, and V. Sachers. “A new model for gas flow in pipe networks”. In: *Mathematical Methods in the Applied Sciences* 33.7 (2010), pp. 845–855.

[78] D. Hilbert. *Grundzuge einer allgemeinen Theorie de linearen Integralgleichungen*. Teubner, 1912.

[79] E. Isaacson, D. Marchesin, and B. Plohr. “Transitional waves for conservation laws”. In: *SIAM journal on mathematical analysis* 21.4 (1990), pp. 837–866.

[80] E. Isaacson, D. Marchesin, B. Plohr, and J. Temple. “Multiphase flow models with singular Riemann problems”. In: *Mat. Apl. Comput* 11.2 (1992), pp. 147–166.

[81] M. Jackson and M. Blunt. “Elliptic regions and stable solutions for three-phase flow in porous media”. In: *Transport in porous media* 48.3 (2002), pp. 249–269.

[82] S. Jin. “Efficient asymptotic-preserving (AP) schemes for some multiscale kinetic equations”. In: *SIAM Journal on Scientific Computing* 21.2 (1999), pp. 441–454.

[83] S. Jin, L. Pareschi, and G. Toscani. “Uniformly accurate diffusive relaxation schemes for multiscale transport equations”. In: *SIAM Journal on Numerical Analysis* 38.3 (2000), pp. 913–936.

[84] K. Karlsen and N. Risebro. “Corrected operator splitting for nonlinear parabolic equations”. In: *SIAM Journal on Numerical Analysis* 37.3 (2000), pp. 980–1003.

[85] K. Karlsen and J. Towers. “Convergence of the Lax-Friedrichs scheme and stability for conservation laws with a discontinuous space-time dependent flux”. In: *Chinese Annals of Mathematics* 25.03 (2004), pp. 287–318.

[86] J. Keizer. *Statistical thermodynamics of nonequilibrium processes*. Springer Science & Business Media, 2012.

[87] C. Kelley. *Solving nonlinear equations with Newton’s method*. Vol. 1. Siam, 2003.

[88] M. Kim, E. Park, and J. Park. “Mixed finite element domain decomposition for nonlinear parabolic problems”. In: *Computers & Mathematics with Applications* 40.8 (2000), pp. 1061–1070.

[89] A. Kurganov, G. Petrova, and B. Popov. “Adaptive semidiscrete central-upwind schemes for nonconvex hyperbolic conservation laws”. In: *SIAM Journal on Scientific Computing* 29.6 (2007), pp. 2381–2401.

[90] W. Lambert. “Riemann solutions of balance system with phase change for thermal flow in porous media”. PhD thesis. PhD thesis, IMPA, 2006.

[91] W. Lambert, J. Bruining, and D. Marchesin. “Steam injection into water-saturated porous rock”. In: *Computational and Applied Mathematics* 22.3 (2005), pp. 359–395.

[92] W. Lambert and D. Marchesin. “Asymptotic rarefaction waves for balance laws with stiff sources”. In: *Acta Mathematica Scientia* 29.6 (2009), pp. 1613–1628.

[93] W. Lambert and D. Marchesin. “The Riemann problem for multiphase flows in porous media with mass transfer between phases”. In: *Journal of Hyperbolic Differential Equations* 6.04 (2009), pp. 725–751.

[94] W. Lambert, D. Marchesin, and J. Bruining. “The Riemann solution for the injection of steam and nitrogen in a porous medium”. In: *Transport in porous media* 81.3 (2010), pp. 505–526.

[95] J. Langseth, A. Tveito, and R. Winther. “On the convergence of operator splitting applied to conservation laws with source terms”. In: *SIAM journal on numerical analysis* 33.3 (1996), pp. 843–863.

[96] P. Lax. “Hyperbolic systems of conservation laws II”. In: *Communications on Pure and Applied Mathematics* 10.4 (1957), pp. 537–566.

[97] P. Lax. “Computational fluid dynamics”. In: *Journal of Scientific Computing* 31.1 (2007), pp. 185–193.

[98] P. Lax. “Mathematics and physics”. In: *Bulletin of the American Mathematical Society* 45.1 (2008), pp. 135–152.

[99] R. LeVeque. “Finite Volume Methods for Hyperbolic Problems”. In: *Meccanica* 39 (2004), pp. 88–89.

[100] R. LeVeque. *Finite difference methods for ordinary and partial differential equations: steady-state and time-dependent problems*. Vol. 98. Siam, 2007.

[101] T. Liu. “The Riemann problem for general 2× 2 conservation laws”. In: *Transactions of the American Mathematical Society* 199 (1974), pp. 89–112.

[102] T. Liu. “The Riemann problem for general systems of conservation laws”. In: *Journal of Differential Equations* 18.1 (1975), pp. 218–234.

[103] T. Liu. “Hyperbolic conservation laws with relaxation”. In: *Communications in Mathematical Physics* 108.1 (1987), pp. 153–175.

[104] A. Mailybaev. “Bifurcations of blowup in inviscid shell models of convective turbulence”. In: *Nonlinearity* 26.4 (2013), p. 1105.

[105] A. Mailybaev, D. Marchesin, and J. Bruining. “Resonance in low-temperature oxidation waves for porous media”. In: *SIAM Journal on Mathematical Analysis* 43.5 (2011), pp. 2230–2252.

[106] A. Mailybaev, D. Marchesin, and J. Bruining. “Recovery of light oil by medium temperature oxidation”. In: *Transport in porous media* 97.3 (2013), pp. 317–343.

[107] P. Marcati and A. Milani. “The one-dimensional Darcy’s law as the limit of a compressible Euler flow”. In: *Journal of Differential Equations* 84.1 (1990), pp. 129–147.

[108] D. Marchesin and B. Plohr. “Wave structure in WAG recovery”. In: 6-2 (2001), pp. 209–219.

[109] J. Natvig, H. Nordhaug, and H. Dahle. “Operator splitting methods for systems of convection-diffusion equations: nonlinear error mechanisms and correction strategies”. In: (2000).

[110] H. Nessyahu and E. Tadmor. “Non-oscillatory central differencing for hyperbolic conservation laws”. In: *Journal of computational physics* 87.2 (1990), pp. 408–463.

[111] A. Ostrowski. *Solution of equations in Euclidean and Banach spaces*. Elsevier, 1973.

[112] L. Pareschi. “Central differencing based numerical schemes for hyperbolic conservation laws with relaxation terms”. In: *SIAM Journal on Numerical Analysis* 39.4 (2001), pp. 1395–1417.

[113] A. Perez. “Lagrangian-Eulerian computational formulation to hyperbolic problems and balance laws”. PhD thesis. PhD thesis,Institute of Mathematics, Statistics and Scientific Computing, University of Campinas, 2015.

[114] P. Raviart and J. Thomas. “A mixed finite element method for 2-nd order elliptic problems”. In: *Mathematical aspects of finite element methods*. Springer, 1977, pp. 292–315.

[115] M. Renardy, W. Hrusa, and J. Nohel. “Mathematical problems in viscoelasticity”. In: *New York* (1987).

[116] W. Rheinboldt. *Methods for solving systems of nonlinear equations*. SIAM, 1998.

[117] J. Roberts and J. Thomas. “Mixed and hybrid methods”. In: *Handbook of numerical analysis* 11 (1989).

[118] J. Roberts and J. Thomas. *Mixed and Hybrid Methods in Handbook of Numerical Analysis, Vol. II (PG Ciarlet and JL Lions, eds.), Finite Element Methods (Part 1)*. 1989.

[119] T. Russell. “Time stepping along characteristics with incomplete iteration for a Galerkin approximation of miscible displacement in porous media”. In: *SIAM Journal on Numerical Analysis* 22.5 (1985), pp. 970–1013.

[120] Y. Saad. *Iterative methods for sparse linear systems*. Siam, 2003.

[121] Carsten W Schulz-Rinne, James P Collins, and Harland M Glaz. “Numerical solution of the Riemann problem for two-dimensional gas dynamics”. In: *SIAM Journal on Scientific Computing* 14.6 (1993), pp. 1394–1414.

[122] J. Silva. “Organizing structures in the Riemann solution for thermal multiphase flow in porous media.” PhD thesis. IMPA, 2011.

[123] K. Soga. “Stochastic and variational approach to the Lax-Friedrichs scheme”. In: *Mathematics of Computation* 84.292 (2015), pp. 629–651.

[124] G. Stewart. *Matrix Algorithms Volume 2: Eigensystems*. Vol. 2. Siam, 2001.

[125] A. Tzavaras. “Nonlinear analysis techniques for shear band formation at high strainrates”. In: *Applied Mechanics Reviews* 45.3S (1992), S82–S94.

[126] A. Tzavaras. “Viscosity and relaxation approximation for hyperbolic systems of conservation laws”. In: *An Introduction to Recent Developments in Theory and Numerics for Conservation Laws*. Springer, 1999, pp. 73–122.

[127] A. Tzavaras. “On the mathematical theory of fluid dynamic limits to conservation laws”. In: *Advances in mathematical fluid mechanics*. Springer, 2000, pp. 192–222.

[128] W. Vincenti and C. Kruger. “Introduction to physical gas dynamics”. In: *Introduction to physical gas dynamics, by Vincenti, Walter Guido; Kruger, Charles H. New York, Wiley [1965]* 1 (1965).

[129] M. Vohralík. “Equivalence between lowest-order mixed finite element and multi-point finite volume methods on simplicial meshes”. In: *ESAIM: Mathematical Modelling and Numerical Analysis* 40.02 (2006), pp. 367–391.

[130] M. Wheeler and C. Dawson. “An operator-splitting method for advection-diffusion-reaction problems”. In: *The Mathematics of Finite Elements and Applications VI* (1987), pp. 463–382.

[131] G. Whitham. *Linear and nonlinear waves*. Vol. 42. John Wiley & Sons, 2011.

[132] P. Woodward and P. Colella. “The numerical simulation of two-dimensional fluid flow with strong shocks”. In: *Journal of Computational Physics* 54.1 (1984), pp. 115–173.

[133] W. Yong. “Singular perturbations of first-order hyperbolic systems”. In: *Nonlinear Hyperbolic Problems: Theoretical, Applied, and Computational Aspects*. Springer, 1993, pp. 597–604.